The dynamical evolution of globular clusters

Alan P. Lightman

Center for Astrophysics, Harvard College Observatory and Smithsonian Astrophysical Observatory

Stuart L. Shapiro

Center for Radiophysics and Space Research, Cornell University

The fundamental physical ideas underlying the dynamical behavior of globular star clusters are reviewed. The results of detailed numerical experiments involving large N-body stellar systems are summarized and compared with observations. Intuitive arguments and crude, analytic derivations of many of the major results are provided. The topics treated represent, in effect, a chronological history of the dynamical life of a globular cluster—from its birth in the early universe through core contraction to a compact state, to ultimate dissolution in the galactic tidal field. The approach is nonrigorous and pedagogical rather than mathematical and the paper is intended as an introduction to recent developments in stellar dynamical theory.

CONTENTS

I. INTRODUCTION

A. What is a globular cluster?

The stars in the galaxy are not distributed uniformly. There exist the well-known concentration of visible stars towards the galactic center and a further concen-

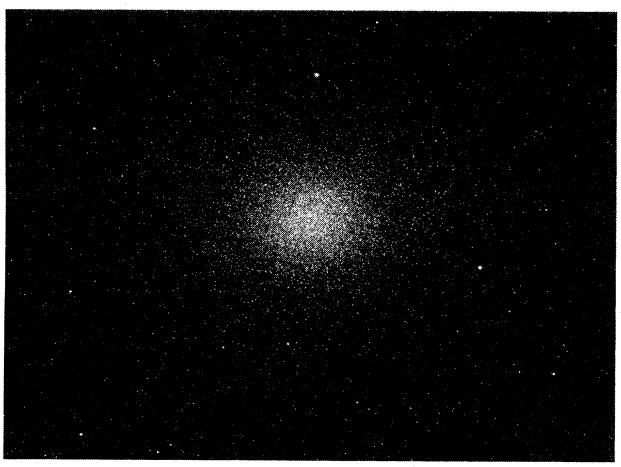

FIG. 1. The globular cluster Omega Centauri (NGC 5139), taken with the 1-m Yale reflector at Cerro Tololo Inter-American Observatory, La Serena, Chile. Date: May 20, 1974; 15-min exposure on blue sensitive emulsion. From Kitt Peak National Observatory.

tration of stars towards the galactic plane. There are also isolated star clusters whose members appear to have a stronger gravitational attraction to each other than to other stars in the general galactic field. These clusters may be divided into three categories: open or galactic clusters, associations, and globular clusters. Open clusters are weakly bound groupings of 50–100 stars, irregularly spaced and showing no particular concentration towards the (ill-defined) cluster center. They are found only in the galactic plane. Associations are small open clusters of 10–100 stars which contain O and B stars, the hottest and brightest main sequence stars (see Sec. II.A below). They are found in the gaseous spiral arms of the galaxy, where star formation is occurring. Globular clusters are the most massive star clusters, consisting of a nearly spherical distribution of 10^4–10^6 stars well concentrated towards the cluster center (see Fig. 1). Their brightest members are red giant stars which have evolved well beyond the main sequence. Globular clusters are found both in the galactic halo and in the galactic disk and are typically as far from the sun as the galactic center (10 kiloparsecs). [One parsec (abbreviated 1 pc) is approximately 3.26 light-years = 3.09×10^{18} cm.] The average globular cluster is 50–100 pc in diameter, with a core radius (at which the stellar surface density has fallen by a factor of ~2 from its central value) of several parsecs. In the nearly homogeneous core, the star density may be 10^3–10^5 stars per cubic parsec.

Historically, globular clusters were used by Harlow Shapley (1917) to map out the shape of the galaxy. There were 93 globulars then known; today there is good evidence (Arp, 1965; Harris, 1976) that the total number of globular clusters associated with our galaxy is about 200. Because they are thought to be among the oldest objects in the galaxy, globular clusters provide important clues for determining the age and process of formation of the galaxy and for verifying current theories of stellar and dynamical evolution.

B. Theme and approach

Determining the dynamical behavior of a large N-body system ($N \gg 10^3$) such as a globular cluster is a fundamental problem of modern theoretical astrophysics. Although the physical force which determines the interactions in a self-gravitating mass system is well understood—it is simply the inverse square law for gravitational attraction—its long-range character makes the overall dynamical problem a difficult one to solve. Fortunately, globular clusters have sufficiently many stars (~10^5) that statistical methods of analysis are applicable, yet they are sufficiently small that they have evolved for many relaxation timescales.

Since the pioneering development of the statistical approach to large N-body theory by Chandrasekhar (1942) and others, significant progress in dynamical theory has been achieved only in recent years, due chiefly to the advent of high-speed computers and the development of sophisticated numerical techniques. Some of the numerical calculations, together with other recent work in dynamical theory, are summarized in *The Theory of Stellar Dynamics*, IAU Symposium No. 69 (Hayli, ed., 1975). A broad summary of the numerical work is provided in the review paper by Aarseth and Lecar (1975). A review of many of the analytical methods and results is given by Haggerty and Severne (1976).

In this paper we apply the results of the detailed numerical computations, together with the underlying theory, to examine the dynamical evolution of globular clusters. Our treatment is pedagogical and nonrigorous; indeed, we have attempted, wherever possible, to supply intuitive, analytic arguments and "back of an envelope" derivations of most of the major results. Our analysis is more or less self-contained, yet it is by no means a survey of all the literature in the field. The topics are treated according to our own point of view, which gives particular (and undue) emphasis to our own recent work.

We present no systematic review of the observational features of globular clusters, but, instead, introduce the relevant observational data as is necessary. An older but excellent discussion and catalog of cluster data is given by Arp (1965). A more recent survey of the observed structure of globular clusters, together with mass estimates, is given by Peterson and King (1975) and by Peterson (1976).

Traditionally, it has been the structural symmetry, long-term stability, and simple interaction law which have inspired the theoretician to investigate the dynamical behavior of globular clusters. Recently, a new appeal has been added to these attractions: several (~7) globular clusters are now identified with powerful x-ray sources which emit between 10^{35}–10^{37} erg s^{-1} in the x-ray band from 2–10 keV. The source(s) of this emission is (are) not known with any certainty, but speculations have ranged from unusually formed binary systems, in which a normal primary supplies gas to a compact component (as in the "standard" isolated x-ray sources in the galactic field), to massive black holes formed from core collapse of the cluster. Regardless of the eventual explanation of the globular cluster x-ray emission—mundane or exotic—the phenomenon

has stimulated new interest in the dynamical evolution of globular clusters.

C. Summary

Our paper begins (Sec. II) with a rough sketch of the different types of stars found in globular clusters and the methods of determination of the ages of globular clusters. The fact that globular clusters are as old as the age of the universe ($\sim 10^{10}$ yr) and have evolved for many relaxation timescales is crucial for the remaining considerations of the paper. We end this section with a brief discussion of the primordial formation theory of globular clusters.

Next (Sec. III) we present a brief review of the underlying physical concepts and numerical methods encountered in the study of large stellar systems. Although our treatment is far from complete, it should familiarize the reader with the formalism, concepts, and calculational techniques underlying the main body of the paper.

A summary of the remainder of the paper is essentially a chronological symmary of the dynamical life of a globular cluster. The dynamical evolution of a globular cluster, as well as the evolution of other large stellar systems, can be conveniently divided into three distinct epochs. The first epoch (Sec. IV) consists of the initial stages of collapse from a primordial, bound structure to a quasiequilibrium, stellar cluster obeying the virial theorem. If star formation is virtually complete throughout the bulk of the protocluster prior to the onset of collapse, the system will undergo dissipationless collapse and "violent relaxation" which arises from collective oscillations. In the absence of rotation the resulting star system will be nearly spherical in shape and in one *dynamical* time will settle into virial equilibrium. It is during this initial collapse phase that the cluster develops an inner, high-density region, with a nearly isotropic, quasi-Maxwellian velocity distribution, and an outer halo, characterized by an anisotropic (preferentially radial) velocity distribution.

The second epoch (Sec. V) consists of the slow, secular contraction of the inner regions of the cluster and the growth of the halo. This phase is driven predominantly by the continual evaporation of high-velocity stars from the cluster. During this period, the collapsing inner regions remain nearly isothermal, thereby defining the cluster "core." Mass segregation occurs during this phase throughout the cluster: the heavier stars settle toward the cluster center while the lighter stars move preferentially outward into the halo, as two-body gravitational encounters drive the system to energy equipartition. The evaporation of stars in the high-velocity tail of the Maxwellian distribution in the inner regions of the cluster each relaxation time causes the binding energy per unit mass of the remaining core stars to increase. This process increases the central density and velocity dispersion. Stellar evaporation provides a natural mechanism by which rotating clusters may divest themselves of angular momentum and become spherical. Shock heating, which occurs when the cluster passes through the galactic disk every $\sim 10^8$ yr, may increase the evaporation rate of low-mass stars from the cluster. This quasisteady epoch lasts ~15 mean relaxation timescales for clusters with essentially one mass component and occupies $\gtrsim 99\%$ of the active lifetime of the cluster. For clusters with a significant distribution of stellar masses and sufficient mass in heavy stars, the latter may form an inner core at the cluster center, evolving initially by "heat" loss and eventually by self-evaporation as an independent subsystem. In such a case the heavy stars may terminate their intermediate phase of evolution after ~three mean relaxation timescales, well before the bulk of the cluster has undergone significant evolution.

As stellar evaporation proceeds and drives the core density to large values, physical collisions between stars may ultimately alter and dominate the subsequent dynamical evolution. As a result of stellar collisions and coalescence, massive stars are formed. In multicomponent systems this end-point evolution probably does not begin until the number of stars in the inner subsystem is $\lesssim 100$–1000 (Sec. VI). At this point the effects of binary star formation, two-body tidal dissipation, and large velocity fluctuations associated with small N systems become important. The small "singularity" formed by the heavy stars may not affect the dynamical evolution of the bulk of the cluster for many subsequent relaxation timescales. The subsequent dynamical evolution is very uncertain because of the complicating processes mentioned above and because of uncertainty in the fate of the coalescing massive stars (which produce supernovae and/or black holes). The fate of the remaining stars in the collapsed cluster may be dominated by either a central, tightly bound binary or a supermassive black hole. We explore in some detail the dynamical influence of a massive black hole at the center of a cluster core. In either case, the central object acts as an effective energy source which may ultimately expand the ambient cluster core, leading to its dissolution in the galactic tidal field.

Finally (Sec. VII) we consider observational evidence for the evolution and death of globular clusters. The recent identification of a number of x-ray sources in the cores of globular clusters may yield some clues regarding the conditions in these dense inner regions. A statistical analysis of the observed distribution of globular cluster central relaxation times suggests that any singularities formed at the centers of globular clusters have little dynamical effect on the cluster during most of its lifetime and then quickly dissolve the cluster. Detailed numerical calculations are needed to test this possibility. In addition, the statistical analysis permits an estimate of the number of clusters which have already collapsed, evaporated, and dissolved beyond recognition.

II. THE AGE AND FORMATION OF GLOBULAR CLUSTERS

A. Stellar types and the Hertzsprung–Russell diagram

We will give here an elementary discussion of the Hertzsprung–Russell diagram, an essential tool in understanding the types and ages of stars. A more detailed discussion of stellar structure and evolution can

be found in many standard texts, e.g., Clayton (1968).

Stellar brightness (energy/area/time) is measured by the magnitude scale. If a star is observed to have an apparent brightness b, then its *apparent magnitude* is defined as

$$m = -2.5 \log b + c \ , \tag{2.1}$$

where c depends on the adopted system of magnitudes and units used. For a comparison of intrinsic brightness, it is conventional to define the *absolute magnitude* of a star, M, as the magnitude the star would have if viewed from a distance of 10 pc. From the inverse square law, we may write

$$M - m = 5 - 5 \log r \ , \tag{2.2}$$

where r is the distance (in parsecs) of the star. If the detector could respond to the entire radiant spectrum, the absolute magnitude measured would be the *absolute bolometric magnitude* $M_{\rm bol}$.

Although it is difficult to measure a star's spectrum in detail, broad-band photometry, using a few filters of various colors, yields sufficient information to determine the approximate stellar surface temperature. The blue and visual (yellow) absolute magnitudes of a star are denoted by B and V, respectively, and their difference, B − V, is defined as the *color index* of the star. A one-to-one correspondence exists between the color index of a star and the location of the spectral peak of its continuum emission, from which a *color temperature* may be defined.

An early result of color photometry was the observed correlation between a star's color index and the strength of specific absorption lines. This observation led to a classification of stars into *spectral types*. In addition to other distinctive properties, each spectral type corresponds to a certain range in surface color temperature. The major spectral types and their temperature ranges are as follows: Class O, $T > 25\,000$ K; Class B, 25 000–11 000 K; Class A, 11 000–7500 K; Class F, 7500–6000 K; Class G, 6000–5000 K; Class K, 5000–3500 K; Class M, 3500–2200 K. The sun is a G star.

In the early part of this century the Danish astronomer E. Hertzsprung, and slightly later the American astronomer H. N. Russell, made the remarkable discovery that stars populate only certain portions of the color–luminosity diagram. This finding is illustrated in Fig. 2. Any graph which measures a quantity related to luminosity (e.g., luminosity, bolometric magnitude, visual magnitude, etc.) versus a quantity related to color (e.g., color index, color temperature, spectral type, etc.) is called a *Hertzsprung–Russell diagram*, or simply an H–R *diagram*.

When a large sample of all observed stars is plotted in an H–R diagram (Fig. 2), it is found that about $\gtrsim 80\%$ of the stars fall in a narrow diagonal band called the *main sequence*. The next largest class of stars, white dwarfs, represent about 10% of all stars. The primary significance of the H–R diagram is that it contains data on the evolutionary sequences of stars. From theoretical calculations of stellar evolution, it is found that stars move around in the H–R diagram as they evolve and spend most of their time in the most populated areas of the diagram. The "track" of an isolated

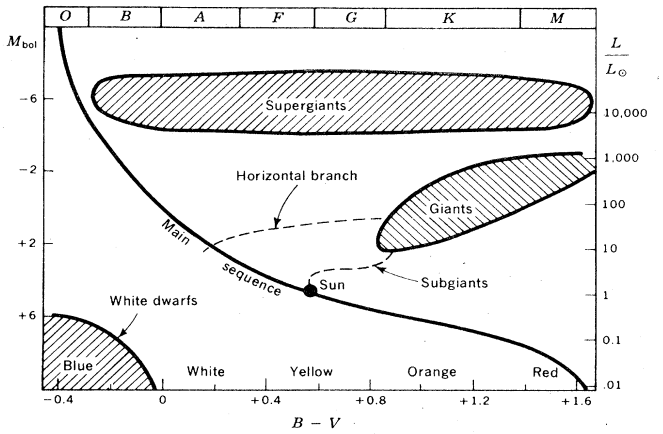

FIG. 2. A schematic representation of the heavily populated areas in the H–R diagram. A high percentage of stars lie near the main sequence. The next most populous groups are the white dwarfs and the giants. The subgiant and horizontal branches are conspicuous in those collections of stars having large numbers of giants, e.g., globular clusters. From Clayton (1968).

star is unique, given its initial chemical composition and mass. Comparison of the evolutionary calculations with the observed H–R diagram thus provides information on the initial parameters of stars, the duration of time they spend in each evolutionary phase, and their ages.

From theoretical calculations, the following simplified interpretation of the H–R diagram emerges: *Main sequence* stars are primarily those stars which convert hydrogen into helium in their interiors by nuclear fusion; this activity constitutes the first and longest phase of a star's active life. The main sequence does not represent an evolutionary track. Rather, the position on the main sequence of a newborn star is determined by its mass and chemical composition. For a given composition, more massive stars are hotter and brighter. The lifetime of a star on the main sequence is a steeply decreasing function of its initial mass m, corresponding to a steeply increasing dependence of luminosity on mass. The main sequence lifetime of a star is (Cox and Giuli, 1969) (where $M_\odot \equiv$ solar mass)

$$t_{\rm ms} \sim \begin{cases} 1.3 \times 10^{10} \text{ yr } (m/M_\odot)^{-3}, & m < 10\, M_\odot \ , \\ 1.3 \times 10^{8} \text{ yr} (m/M_\odot)^{-1}, & m > 10 M_\odot \ . \end{cases} \tag{2.3}$$

Thus, for example, stars with a mass near that of the sun remain on the main sequence for ~10 billion years, while stars of 20–30 solar masses live only a few million years on the main sequence.

Typically, 70%–80% of a star's mass is initially in the form of hydrogen, 20%–30% is in the form of helium, and 0.1%–3% is in the form of heavier elements. When 10%–20% of the hydrogen in the central active nuclear burning region has been exhausted, nuclear energy generation ceases in the core but continues in a thin shell which moves outward toward the stellar surface. The core, no longer pressure supported, contracts under its self-gravitation and heats up. The liberated gravitational energy serves to expand the outer layers of the star

while maintaining the luminosity. During this phase the star "evolves off the main sequence" and follows the *subgiant branch* of the H–R diagram upwards and to the right into the red giant region (see Fig. 2). Stars redden tremendously during this evolutionary period because of their increasing surface area (the radius can increase by a factor of ~1000).

During the relatively rapid approach to the giant branch of a $\lesssim 1\ M_\odot$ star the central region becomes sufficiently dense so that the electrons become degenerate (typical core densities and temperatures are 10^4–10^5 g cm^{-3} and $(3–7)\times 10^7$ K, respectively). When the degenerate core mass reaches about 0.5 solar masses, core temperatures are sufficiently high to ignite the triple alpha process, which converts helium into carbon in a rapid "helium flash." The released energy lifts the degeneracy of the electrons, the central region expands, the envelope contracts, and the star moves rather abruptly (e.g., ~10^5 yr for a 0.65 $M_\odot$ star) to a position on the *horizontal branch*. The horizontal branch is not entirely an evolutionary track. The position of a star on the horizontal branch is again determined by the helium core and hydrogen envelope mass and the chemical composition of the precursor star at the upper tip of the red giant region. The situation is probably complicated by (ill-understood) mass loss processes experienced by a star during its evolution on the giant branch. A massive star with $m \gtrsim 1\ M_\odot$ does not become degenerate on the subgiant branch and ignites helium non-explosively.

The subsequent evolution of stars on the horizontal branch is not entirely understood. A star may evolve back to the red giant tip of the H–R diagram several times, where it can ignite other sources of nuclear energy. Ultimately, stars exhaust their nuclear fuel and eventually cease to radiate. If the star is sufficiently massive it may explode as a supernova and/or collapse to form a black hole. Sufficiently small stellar remnants can contract to form either a white dwarf ($m \lesssim 1.4\ M_\odot$, radius $R \sim 10^9$ cm), supported against collapse by electron degeneracy pressure and shown in the lower left region of the H–R diagram, or a neutron star ($m \lesssim 3M_\odot$, radius $R \sim 10^6$ cm), supported by neutron degeneracy pressure and nuclear repulsive forces.

B. The ages of globular clusters

The primary method of estimating the ages of globular clusters involves a comparison of the observed H–R diagram for a given cluster with theoretical calculations of stellar evolution tracks for its member stars (see Iben, 1971 for a review). Stars begin evolving off the main sequence from the upper left portion of the H–R diagram, where the heaviest, most luminous stars are located. The most luminous stars in a globular cluster which still remain on the main sequence can then be used to determine the age of the cluster, if it is assumed that all of the cluster stars were formed at about the same time. For example, Fig. 3 illustrates the H–R diagram of the globular cluster M92. Note that no stars with color index bluer (lower) than about 0.4 appear on the main sequence (cf. Figs. 2 and 3).

If L_{to} is the luminosity in solar units ($L = 4\times 10^{33}$ erg s^{-1}) of a star which has just "turned off" the main sequence, and Y and Z are the initial abundances by weight of helium and all heavier elements ("metals"), respectively, then the following approximate expression for the cluster age t_g in units of 10^{10} yr may be used (Iben and Rood, 1970):

$$\log t_g \simeq 0.42 - 1.1\ \log L_{to} - 0.59(Y - 0.3) - 0.14(\log Z + 3)\,. \tag{2.4}$$

Equation (2.4) is most reliable in the range $1.2 < t_g < 1.6$, $Y < 0.3$, $-4 < \log Z < -3$, which corresponds to a range of stellar masses $0.7 \lesssim m/M_\odot \lesssim 0.9$ (Iben and Rood, 1970). The dependence on Z (typically ~10^{-3}–10^{-4} for globular cluster stars) arises mainly from the important contribution of heavy metals to the opacity. The strong dependence on Y (typically 0.20%–0.30% by mass) arises mainly from the role of primordial helium in determining the mean molecular weight of the central regions, which, in hydrostatic equilibrium, determines the temperature for nuclear burning. Demarque *et al.* (1971) have independently derived an expression for t_g from their numerical calculations, which agrees fairly well with the functional form of Eq. (2.4) but yields values of t_g approximately 20% smaller. Additional uncertainties in the actual measurements of L_{to}, Y, and Z will be discussed below. With a theoretical relationship such as Eq. (2.4), the age-dating calculations require five steps: (1) Measurements of the apparent H–R diagram and turnoff magnitude m_{to}; (2) estimates of corrections to both the observed stellar colors and magnitudes due to "interstellar reddening"; (3) measure-

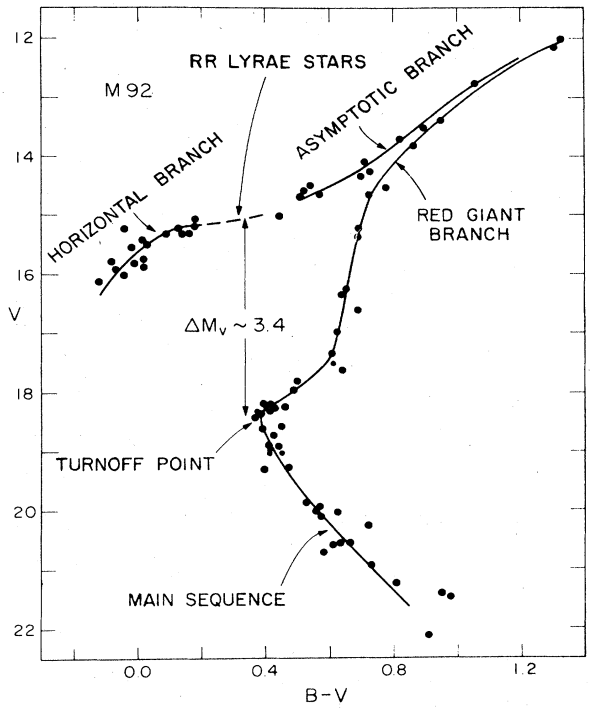

FIG. 3. Distribution in the H–R diagram diagram defined by a selection of stars in the globular M92. Note the interruption of the main sequence (cf. Fig. 2) at a B–V index of 0.4. From Iben (1971).

ment of the distance to the cluster so that L_{to} may be determined from m_{to}; (4) measurement of helium abundance Y; (5) measurement of metal abundance Z. We will discuss each of these steps in turn.

The main sequence turnoff of a cluster is defined as the magnitude where B − V is smallest (bluest) at the knee joining the main sequence and the subgiant branches. Before plotting a meaningful H–R diagram to determine the turnoff, however, the frequency-dependent interstellar absorption must be subtracted out for each individual star (i.e., intervening gas clouds may obscure portions, but not all, of the cluster). This "de-reddening" of stellar colors is accomplished by first identifying the spectral type of a star through its spectral lines and then comparing colors with a nearby star of the same spectral type for which interstellar absorption is negligible.

There are two different methods usually used to estimate the distance to a cluster. The first is by comparison of the main sequence curve in an apparent-magnitude H–R diagram of the cluster with the main sequence curve of a fiducial sample of nearby stars of known distance and luminosity (cf. Fig. 2). (Distances to nearby stars and star clusters within ~100 pc of Earth may be determined directly by various trigonometric and kinematical methods.) The relative vertical displacement of the two main sequences on the H–R diagram can be directly converted to a distance to the globular cluster. The Hyades cluster (~100 stars about ~40 pc distant) is often used as a fiducial cluster, but other fiducial main sequence curves of field stars must be constructed for low-Z stars of the type found in globular clusters (see, e.g., Sandage, 1970). One of the problems in this method of distance determination is the apparent faintness of the main sequence stars in the distant globular clusters. Another is the scarcity of fiducial stars of low Z.

The second method used to determine distances to globular clusters is measurement of the apparent magnitude of their RR Lyrae stars. These distinctive stars are horizontal branch stars which have regular (optically observed) pulsations every ~$\frac{1}{2}$ day, due to radial instabilities in their envelopes. From the early theoretical calculations of Baker (1965) and Christy (1966) and from more recent calculations (e.g., Iben, 1971) it is found that the intrinsic luminosities of RR Lyrae variables cover a relatively narrow range ~40–50 $L_\odot$. Thus RR Lyrae stars serve as reliable standard candles in distance determinations.

When the distance measurements and turnoff magnitudes are measured, it is found that the average stellar turnoff luminosity in a globular cluster is $\langle L_{to} \rangle \sim 0.45$, with an estimated error $\Delta L/L \sim 0.2$ (Sandage, 1970). For $Y \sim 0.3$, $Z \sim 10^{-3}$ the turnoff stars are in the mass range $0.7 \lesssim m/M_\odot \lesssim 0.8$ (Iben and Rood, 1970).

The majority of globular cluster stars are too cool to measure surface helium abundances through spectral lines. Instead, three indirect methods, which rely heavily on theoretical calculations, are used to measure helium abundance. The first method compares the theoretical lifetime ratios t_{HB}/t_{RG} and observed number ratios N_{HB}/N_{RG}, of horizontal branch (HB) and red giant (RG) stars. The second method compares the observed color and period of the shortest period RR Lyrae stars with theoretical calculations. A third method correlates Y with the measurable slope of the subgiant branch in the H–R diagram (e.g., Faulkner, 1972). Although t_{HB}/t_{RG} depends strongly on Y, it also depends strongly on the core mass of the horizontal branch stars, a quantity sensitive to variations in the input physics (see e.g., Iben, 1971), such as convection in HB stars and nuclear cross sections. Such problems as crowding, background effects, and proper identification introduce errors in the determination of N_{HB}/N_{RG}. In the second method, where there exists a strong theoretical dependence on the helium abundance Y of the color of the shortest period (bluest) RR Lyrae stars (e.g., Christy, 1966), the total mass of the star enters. Here mass loss, which is not well understood, can contribute uncertainties. Combining the above methods, the initial helium abundance is found to be $Y \sim 0.3 \pm 0.1$ (Sandage, 1970; Iben, 1971).

Surface metal abundances are determined by spectroscopic methods and are assumed to reflect the initial composition of the star (see discussion below). Methods discussed by Wallerstein and Helfner (1966) and adopted in recent studies (e.g., Cantera, 1975) yield values of Z ranging from 8×10^{-4} for M13 to 2×10^{-4} for extremely "metal-poor" clusters like M15 and M92, with factor of 2 errors quoted. Another method for measuring metal abundances from the relative strengths of spectral light is the Preston (1959) "ΔS" method, adopted by Butler (1975), to name one example.

Globular clusters with measured ages are given in Table I from Allen (1974), who used results from Thänert (1971) and Arp and Hartwick (1971). The rms error in the calculated ages, obtained by substitution of the above quoted errors for Y, Z, and L_{to} into Eq. (2.4) yields $\Delta t_g/t_g \sim 25\%$. It is difficult to assess the precise confidence level of Eq. (2.4) itself (see previous discussion). Despite the uncertainties, it is reasonably clear that globular clusters are among the oldest objects in the universe, which have evolved (1–2) $\times 10^{10}$ yr from the "Big Bang." The paucity of globular clusters with reliably determined ages is largely due to the difficulty of clearly defining the faint main sequence stars in each cluster. The optical emission from clusters is dominated by the less numerous but very much brighter (by a factor of ~25) red giant stars.

In addition to the above quantitative age estimates there are a number of characteristics of globulars which argue qualitatively for early formation dates. Globular clusters as a whole have relatively high spatial velocities and do not participate appreciably in the general galactic rotation. Globular clusters have high

TABLE I. Measured ages of globular clusters.[a]

	Log age in years			
	9.9	10.0	10.1	10.2
Examples:	M71	47 Tuc	M92	ω Cen
		M15	M3	
		M13	NGC 5466	
		M5		

[a] From Allen (1974).

average galactic latitudes ($\langle b\rangle \sim 14°$; Arp, 1965; Allen, 1974) and are relatively depleted in metals compared to the sun ($Z_\odot \sim 2\times 10^{-2}$; Allen, 1974). All of these properties define a class of old objects called Population II, while the opposite properties characterize a younger class of objects called Population I.

The distinction between Population I and Population II is thought to be associated with star and galaxy formation and with stellar nucleosynthesis. Nuclear burning and element formation in a star occur in the innermost regions, where temperatures and densities are highest. Old "first generation" stars, which formed with the primordial hydrogen and helium abundances characterizing the early universe, will have negligible metals in their outer layers. (It is only the outer layers of a star which are observable.) In contrast, younger stars can form out of gas which has been contaminated with the metal-laden debris from supernova explosions of earlier generation stars. Thus metal abundance can be associated with age.

It has been hypothesized that the galaxy was originally a hot, turbulent gas cloud which collapsed to its present disk shape because its thermal energy was dissipated while its angular momentum was conserved. The dissipation process presumably involved only large masses of gas; stars, once formed, have little interaction with gas or other stars. Consequently, older stars would exhibit the Population II kinematical properties previously described. Younger stars, formed from gas which had already collapsed to the galactic plane, would orbit predominantly in the plane of the galaxy. Indeed, recent studies (e.g., Peterson, 1974; Harris, 1976) indicate that globular clusters have a nearly isotropic velocity distribution. Partly as a result of their high-latitude orbits, which sweep out intracluster gas every passage through the galactic disk (typically every $\sim 10^8$ yr), little interstellar gas has been observed in globular clusters (Knapp *et al.*, 1973; Hills and Klein, 1973).

C. The formation of globular clusters

Because of their great age, the study of the formation of globular clusters is intimately involved with cosmology. Most cosmologists invoke some version of the "gravitational instability" hypothesis to explain the formation of bound systems. In this process a small density perturbation in a gas of otherwise uniform density grows if the perturbation encompasses sufficient mass that its inward self-gravitational force exceeds outward internal forces due to thermal gas or radiation pressure. Recent reviews of this problem include Peebles (1971), Weinberg (1972), and Field (1975).

The maximum mass of a perturbation stable against gravitational collapse is called the "Jeans mass" (Jeans, 1902) and can be obtained approximately by equating the gravitational and thermal energies of the perturbation. Let $\rho_m, \rho_\gamma, p, r_J$ be the matter density, radiation density, pressure, and size of the limiting perturbation, respectively. We then have, roughly,

$$G[\rho_m(1+\rho_\gamma/\rho_m)r_J^3]^2 r_J^{-1} \sim p r_J^3 \tag{2.5}$$

If we now let T_γ, T_m, p_γ, and p_m be the temperatures and pressures, respectively, of the matter (m) and radiation field (γ), we also have the additional relations $\rho_\gamma c^2 \sim a T_\gamma^4 \sim 3p_\gamma$ and $p_m \sim (\rho_m/m_H)kT_m$. Here c, a, m_H, and k are the velocity of light, radiation constant, hydrogen mass, and Boltzmann's constant, respectively.

At cosmic times sufficiently early so that all hydrogen in the universe was ionized ($T_\gamma \gtrsim 4000$ K), the matter and radiation fields were well coupled thermally, $T_\gamma = T_m$, and the dominant source of pressure was due to radiation, $p \sim p_\gamma$. After the "recombination" epoch of electrons and protons, radiation and matter decoupled and only matter pressure was effective in supporting the matter, $p \sim p_m$. Combining the above expressions with Eq. (2.5) and defining the Jeans mass $M_J = (4\pi/3)\times \rho_m r_J^3$, one may obtain the following approximate relations for M_J (cf., e.g., Weinberg, 1972):

before recombination ($T_\gamma = T_m \gtrsim 4000$ K)

$$M_J \simeq 9 M_\odot \sigma\,(1+\sigma k T_\gamma/m_H)^{-3}; \tag{2.6a}$$

after recombination ($T_\gamma, T_m \lesssim 4000$ K)

$$M_J \simeq 100 M_\odot \sigma^{1/2}(T_m/T_\gamma)^{3/2}. \tag{2.6b}$$

In Eqs. (2.6) we have used the (dimensionless) measure of photon entropy per baryon, $\sigma \equiv 4aT_\gamma^3 m_H/(3\rho_m k)$. For much of the history of the universe the radiation has expanded adiabatically (adiabatic index $\frac{4}{3}$). This fact plus baryon conservation ensures the constancy of σ, which has been measured to be roughly $\sigma \sim 10^8$–10^9 (cosmic 3

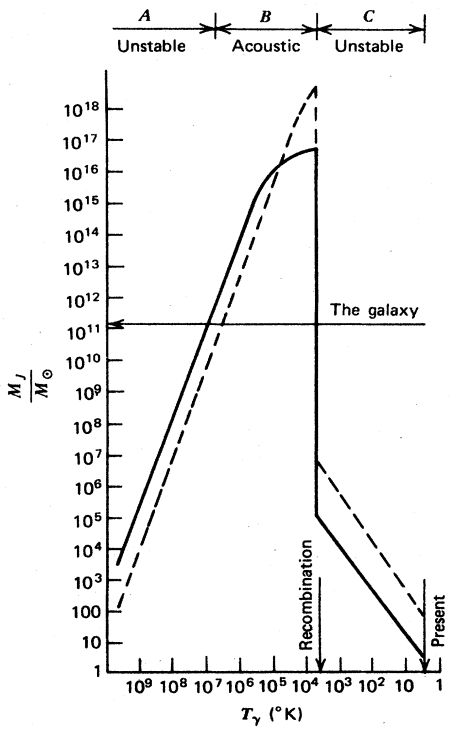

FIG. 4. Jeans mass as a function of radiation temperature. Solid line is for $\sigma = 0.8\times 10^8$, corresponding to $T_{\gamma 0} = 2.7$ K, $\rho_0 = 3\times 10^{-29}$ g/cm^3. Dashed line is for $\sigma = 2.4\times 10^9$, corresponding to $T_{\gamma 0} = 2.7$ K, $\rho_0 = 10^{-30}$ g/cm^3. The drop in Jeans mass at recombination is somewhat more gradual than shown here. From Weinberg (1972).

K radiation). After recombination, both matter and radiation followed their separate adiabatic evolution (the former with adiabatic index $\frac{5}{3}$), leading to the relation $(T_m/T_\gamma) \sim T_\gamma/4000$ K. Figure 4 shows M_J as a function of T_γ.

In most cosmological models the universe was only a tiny fraction (10^{-4}–10^{-3}) of its present age at the time of recombination. Because the Jeans mass just after recombination is so near the observed mass of globular clusters, many investigators have argued that growing condensations at the epoch of recombination should be associated with the formation of globular clusters. However, if radiation and matter depart from local thermal equilibrium with each other before recombination, the resulting dissipation can damp all acoustic perturbations of mass $\lesssim 10^{12} M_\odot$ (Silk, 1968; Weinberg, 1971; see Weinberg, 1972 for a review), thus somewhat obscuring the relevance of the Jeans mass for globular clusters. Various models of cluster formation disagree drastically in the details, in any case, and we shall only briefly mention a few such models below without attempting a critical analysis.

1. Formation of globular clusters before galaxy formation

Impressed by the apparent uniformity of globular cluster luminosities both throughout our galaxy and in other galaxies, Peebles and Dicke (1968) proposed that globular clusters formed as gravitationally bound gas clouds before the galaxies appeared. The observed nearly uniform size and mass of globulars would be a consequence of the strong radiation-drag force acting on gas just at the time of recombination and formation (see also Peebles, 1969). Van den Bergh (1975) has pointed out, however, that globular clusters do seem to differ systematically in certain traits from one galaxy to another, which may argue for a postgalaxy formation.

2. Formation of globular clusters during galaxy formation

Models of this type have been discussed first by von Weizsacker (1955) and in more detail by Eggen *et al.* (1962). In such a model a single protogalactic cloud formed globular clusters and halo field stars by subfragmentation during a brief period (~10^8 yr) in which the turbulent gas cooled and collapsed to the plane. The rapid formation of globular clusters leads to the kinematical properties observed (see above) and indicates a negligible age difference between stars in a given globular cluster.

There is a paucity of data for globular clusters outside of the galaxy. Harris and Canterna (1977) have recently presented integrated colors of four globular clusters in Fornax (a member of the "Local" group of galaxies) and six in M31 (Andromeda). They conclude that the Fornax clusters are very metal poor in comparison to clusters in our own galaxy, while those in M31 are metal rich. In the latter case, the distribution of metal-rich clusters in the halo of M31 contrasts with that of the galaxy, indicating that the sequence of cluster formation and metal enrichment of interstellar gas may not be invariant. Outside the Local group, the globulars around the giant elliptical galaxy M87 in the Virgo cluster represent the only clusters for which reliable data exist. The spatial distribution of these 4000 ± 1500 globularlike objects has recently been studied by Harris and Smith (1976), who find that the cluster distribution is considerably flatter in M87 then in our galaxy. They suggest that the clusters in M87 formed relatively earlier during the collapse phase of the protogalaxy, before the gas distribution became as centrally concentrated as it did in our galaxy.

Fall and Rees (1978) has proposed that subclustering on all mass scales existed at the time of galaxy formation. In their theory, the mass scale of globular clusters (~10^5–$10^6 M_\odot$) was subsequently singled out for survival in the competition between tidal disruption (see Sec. V C.) and evaporation (see Sec. V E. and VII B.).

III. DYNAMICAL EVOLUTION OF LARGE N-BODY SYSTEMS: OVERVIEW OF THEORY AND NUMERICAL METHODS

A. Theory

1. Fundamental principles

The dynamical evolution of any bound, stellar system is determined by the nature of the mutual gravitational scatterings or "encounters" between stars in the system. For globular clusters and all other star systems with *large* N, the total number of stars, these encounters are characterized by several common dynamical features, including the following:

(1) The predominant interaction process between stars is two-body, small-angle scattering in a r^{-1} gravitational potential, resulting in small changes in star velocity.

(2) The dynamical time scale t_d is significantly shorter than the relaxation time scale t_r throughout the cluster interior.

(3) The rate of formation of tightly bound binary systems is negligibly small; see Sec. VI.B.

The theoretical basis for the above dynamical properties, which characterize all sufficiently large N-body systems, is summarized in the following three sections. For smaller systems with $N \lesssim 10^3$ these dynamical features no longer apply (see Sec. VI). Following a discussion of the main physical principles underlying classical N-body theory, we present a brief discussion of several numerical techniques recently employed to describe the evolution of large stellar systems.

2. Close versus distant encounters

The effect of occasional close encounters between stars, which produce large deflections and significant velocity changes, is generally much smaller than the effect of more distant ones in large N-body systems. If we denote by p_0 the impact parameter for a 90° deflection of two stars in hyperbolic orbit about each other, then

$$p_0 = G(m_1 + m_2)/v_{\rm rel}^2 , \tag{3.1}$$

where $m_1 + m_2$ is the total mass of the two stars and $v_{\rm rel}$ is the relative velocity at large separation. At a dis-

tance p_0 the kinetic and potential energies of the binary system are comparable. The timescale t_{ce} for a "close encounter" resulting in a deflection of 90° or more is then

$$t_{ce} = \frac{1}{\sigma_{ce} n v_{rel}} = \frac{v_{rel}^3}{\pi G^2 (m_1+m_2)^2 n}, \tag{3.2}$$

where n is the local star density in the cluster and $\sigma_{ce} = \pi p_0^2$ is the cross section for a 90° scattering. As is well known (Spitzer, 1962), use of the above timescale in a large N-body system gives a scattering mean free path too large by at least an order of magnitude. The reason is that r^{-1} potential fields decrease sufficiently slowly with distance so that the "collision" of two masses at large impact parameter $p \gg p_0$ results in a non-negligible scattering. Since the number of such distant encounters is so large, their cumulative effect is more important than that of the few close encounters.

For "distant encounters" with $p \gg p_0$, and $m_2 \gg m_1$, the velocity change suffered in one collision by m_1 is $|\Delta \mathbf{v}| = v_{rel}\theta$, where $\theta = 2p_0/p \ll 1$ is the deflection angle of m_1, and the differential cross section for this encounter is $\sigma(\theta) \simeq 4p_0^2/\theta^4$ (the Rutherford cross section in the limit $\theta \ll 1$). Thus the mean square deflection resulting from distant encounters per unit time is given by

$$\frac{d}{dt}\langle |\Delta v|^2\rangle = n v_{rel} \int |\Delta v|^2 \sigma(\theta) d\Omega = 8\pi p_0^2 n v_{rel}^3 \int_{p_0}^{p_{max}} \frac{dp}{p}, \tag{3.3}$$

where the integral has been cut off at some maximum value to avoid divergence. In a neutral plasma p_{max} is usually set equal to the Debye shielding distance since the potential vanishes exponentially for larger distances. No similar cutoff exists in the gravitational problem; hence the integral must be extended over the entire system. In a spherical star cluster one typically sets p_{max} equal to R_h, where R_h is the radius containing half of the mass (Spitzer and Hart, 1971a). The resulting log factor $\ln R_h/p_0$ can be evaluated further by employing the virial theorem for the cluster, which relates the cluster mean square velocity v_m^2 to the total gravitational potential energy in the cluster per unit mass Ω and to the total energy E. Assuming that most stars have the same mass we may write

$$v_m^2 = -\Omega = \frac{1}{2}\frac{GM}{\bar{R}}, \quad \frac{1}{\bar{R}} \equiv \left(\frac{\sum_{pairs} 1/r_{ij}}{(N^2/2)}\right) \tag{3.4}$$

(Chandrasekhar, 1942), where $r_{ij} = |\mathbf{r}_i - \mathbf{r}_j|$ is the separation between the ith and jth star in the cluster and M is the total mass of the cluster. Setting $\bar{R}$ equal to R_h gives a useful approximate form of the virial theorem:

$$v_m^2 \simeq \tfrac{1}{2}(GM/R_h), \tag{3.5a}$$

$$-E = \tfrac{1}{2}Mv_m^2 = \tfrac{1}{4}(GM^2/R_h). \tag{3.5b}$$

Then, using the relation for the mean relative velocity, we have

$$\overline{v_{rel}^2} = 2v_m^2, \quad R_h/p_0 \simeq \tfrac{1}{2}N. \tag{3.6}$$

The timescale for a net 90° deflection via repeated, small-angle scattering (i.e., when $\langle |\Delta v|^2\rangle^{1/2} \simeq v_{rel}$) is thus given by

$$t_r = \frac{v^2}{d\langle|\Delta v|^2\rangle/dt} = \frac{1}{8\pi p_0^2 n v_{rel} \ln(0.5N)} = \frac{v_{rel}^3}{8\pi G^2 m_2^2 n \ln(0.5N)}; \tag{3.7}$$

hence

$$t_r/t_{ce} \simeq (8\ln(0.5N))^{-1} \tag{3.8}$$

Since $N \sim 10^5$ for typical globular clusters, $t_r/t_{ce} \sim 10^{-2}$, and significant deflections are much more likely to be caused by many weak interactions than by a single, close collision.

3. Dynamical versus relaxation timescales

The timescale t_r computed in Eq. (3.7) for collisions to produce large changes in an initial velocity distribution is essentially a "relaxation time" for the system. When v_{rel} is set equal to $2v_m^2$, t_r measures the time required for a bound, gravitating, N-body system to reach quasi-Maxwellian equilibrium in its interior. In discussions of evolving N-body systems it is frequently convenient to employ the reference relaxation time defined by Spitzer and his collaborators (Spitzer and Hart, 1971a; Spitzer, 1975), which is the relaxation time at the mean density for the inner half of the cluster mass M, with stars assumed to have the rms velocity of the cluster as a whole. This timescale is given by

$$t_{rh} = \frac{v_m^3}{15.4G^2m^2n\ln(0.4N)} = \frac{0.060M^{1/2}R_h^{3/2}}{mG^{1/2}\log(0.4N)} \simeq 5\times10^8\,\mathrm{yr}\left(\frac{N}{5\times10^4}\right)^{1/2}\left(\frac{m}{M_\odot}\right)^{-1/2}\left(\frac{R_h}{5\,\mathrm{pc}}\right)^{3/2}, \tag{3.9}$$

where $m = M/N$ is the mean stellar mass. The factor of 0.4 appearing in the logarithm is somewhat uncertain, but provides a reasonable first approximation to most centrally condensed polytropic stellar systems [Spitzer, 1969; recently Hénon has argued that a careful analysis of the "nondominant" scattering terms of order $1/\ln N$ with respect to the dominant terms leads to a substantially lower value for the above coefficient, of order 0.15 for equal mass systems (Hénon, 1975)]. Defining the dynamical time for a stellar system as the time required for a star moving with the rms velocity to cross R_h, we have

$$t_d = \frac{R_h}{v_m} = \frac{1.58R_h^{3/2}}{(GM)^{1/2}} \sim 0.8\times10^6\,\mathrm{yr}\left(\frac{R_h}{5\,\mathrm{pc}}\right)^{3/2}\left(\frac{M}{10^5M_\odot}\right)^{-1/2}. \tag{3.10}$$

Comparing t_{rh} and t_d we find

$$t_d/t_{rh} = 26\log(0.4N)/N \tag{3.11}$$

(Spitzer and Hart, 1971a). The normalizations indicated in Eq. (3.10) are appropriate for typical globular clusters. It is clear then that for rich galactic clusters ($N \sim 10^3$), globular clusters ($N \sim 10^5$), and elliptical galaxies ($N \sim 10^{11}$), relaxation times significantly exceed dynamical times. Consequently, a typical star orbits the stellar system many times in reaction to the smooth, average potential field of the cluster before its energy E

and angular momentum J are changed appreciably. Therefore, in first approximation, large N-body systems satisfy Liouville's theorem, and the phase space density $f=f(E,J)$ in a cluster will be nearly constant around each orbit [see (5) below]. For typical globular and galactic clusters t_{rh} is shorter than the cluster age (see Sec. II), so that these clusters have certainly relaxed to Maxwellian equilibrium in their cores. For elliptical galaxies t_{rh} is significantly larger than the age of the universe, so that core relaxation cannot have been accomplished by two-body encounters. Instead, "violent relaxations" (Lynden-Bell, 1967) during the initial collapse of the protogalaxy must be responsible for the apparent equilibrium velocity profiles observed in galaxy cores (see Sec. IV).

Due to the strong central concentration of most relaxed stellar systems, the local relaxation time $t_r(r)$ can be considerably shorter than t_{rh} in the central core and considerably longer in the far halo. For isolated stellar systems, however, t_d approaches t_r only in the outermost halo or "fringe" of the cluster; for globular clusters orbiting the galaxy, the outer boundary is established by tidal effects and at the tidal radius r_t, t_d is still appreciably shorter than t_r.

4. Binary star formation

Binary star systems may form, in principle, from nondissipative three-body stellar encounters and from dissipative, two-body tidal interactions in the cluster. The number of tight binaries formed via three-body encounters is negligibly small ($\ll 1$) in large N systems ($N \gg 500$), as shown by Spitzer and Hart (1971a) and by Heggie (1975a). The number of binaries formed by two-body tidal encounters will be much larger (~50 in typical compact cluster cores), as pointed out by Fabian *et al.* (1975) and by Press and Teukolsky (1977), but never large enough to influence the dynamical evolution of a large N system. The formation and dynamical role of binary stars in clusters is discussed in greater detail in Sec. VI.B.

5. The Fokker-Planck equation and diffusion coefficients

The equation of motion of particle i may be written in the form (cf. Spitzer, 1975)

$$\frac{d\mathbf{v}_i}{dt} = -\nabla\phi(\mathbf{r}_i, t) + \mathbf{F}_i(t), \tag{3.12}$$

where ϕ is some smoothed-out average potential and $\mathbf{F}_i(t)$ is the force (per unit mass) on particle i resulting from discrete, irregular two-body encounters with other stars. The various approximation schemes for solution of Eq. (3.12) involve different frameworks for evaluating $\mathbf{F}_i$. Employing the Boltzmann equation (e.g., Huang, 1963) for the evolution of the distribution function of particles, $f(\mathbf{r}, \mathbf{v})$, one finds that the fluctuating field component $\mathbf{F}_i$ generates an effective "collision term" on the right-hand side of the equation:

$$\frac{df}{dt} = \frac{\partial f}{\partial t} + \mathbf{v}\cdot\frac{\partial f}{\partial \mathbf{r}} + \nabla\phi\cdot\frac{\partial f}{\partial \mathbf{v}} = \left(\frac{\partial f}{\partial t}\right)_{\text{collisions}}. \tag{3.13}$$

Since small-angle scatterings dominate the interactions between particles in large N systems, the collision term can be written in the usual way as an expansion in the small perturbations (e.g., in the velocity components) which arise from two-body encounters. Keeping the dominant first two terms in the expansion leads to the Fokker–Planck equation, first studied for homogeneous stellar systems by Chandrasekhar (1942), and later developed for more general and realistic systems by Rosenbluth *et al.* (1957).

Additional simplifications in the Fokker–Planck equation result from the fact that a large stellar system is very nearly collisionless (cf. discussion in Sec. III.A.3), so that Liouville's theorem is approximately satisfied and f is approximately a function of the energy and (in a spherical system) angular momentum, E and J. If $f(E,J,t)$ is the phase space density of stars with energy and angular momentum per unit mass in the range dE and dJ about E and J, respectively, then the Fokker–Planck equation for the time evolution of $f(E,J,t)$ is (cf. Spitzer and Shapiro, 1972; Lightman and Shapiro, 1977)

$$P(E)\frac{\partial f(E,J,t)}{\partial t} = -\frac{\partial}{\partial E}\left([f(E,J,t)\langle\Delta_p E\rangle] - \frac{1}{2}\frac{\partial}{\partial E}[f(E,J,t)\langle(\Delta_p E)^2\rangle]\right)$$
$$-\frac{1}{J}\frac{\partial}{\partial J}\left([f(E,J,t)J\langle\Delta_p J\rangle] - \frac{1}{2}\frac{\partial}{\partial J}[f(E,J,t)J\langle(\Delta_p J)^2\rangle]\right) + \frac{1}{J}\frac{\partial^2}{\partial E\,\partial J}[f(E,J,t)J\langle(\Delta_p E)(\Delta_p J)\rangle]. \tag{3.14}$$

Here a quantity $\langle\Delta_p K\rangle$ is the mean increment in K transferred in an orbital period $P(E)$ as a result of successive small-angle scatterings.

The quantities $\langle\Delta_p K\rangle$ are functions of E and J. They may be related to the standard (e.g., Chandrasekhar, 1942; Spitzer, 1962) radial and velocity-dependent "diffusion coefficients," by integrating the latter over an orbit of given E and J, e.g.,

$$\langle\Delta_p J\rangle = 2\int_{r_p}^{r_{ap}}\langle\Delta J\rangle\frac{dr}{v_r}, \tag{3.15}$$

where r_{ap}, r_p, v_r are, respectively, the apocenter, pericenter, and radial velocity. The energy and angular momentum diffusion coefficients $\langle\Delta E\rangle$, $\langle\Delta J\rangle$, $\langle(\Delta E)^2\rangle$, $\langle(\Delta J)^2\rangle$, and $\langle(\Delta E)(\Delta J)\rangle$ may in turn be related to the velocity diffusion coefficients $\langle\Delta v_\parallel\rangle$, $\langle(\Delta v_\parallel)^2\rangle$, and $\langle(\Delta v_\perp)^2\rangle$. Here $\langle\Delta v_\parallel\rangle$ is the velocity transfer along the direction of motion per unit time, $\langle(\Delta v_\perp)^2\rangle$ is the squared velocity transfer perpendicular to the direction of motion, per unit time, etc.

To obtain the velocity diffusion coefficients, one must average such expressions as Eq. (3.3) over a distribu-

tion of "field stars" with density $n(r)$. In many problems, the field star velocity distribution may be approximated as Maxwellian. For example, the "coefficient of dynamical friction" (drag), $\langle \Delta v_{\parallel} \rangle$, for a "test star" moving with velocity v, satisfies in such a case (Chandrasekhar, 1942; Spitzer, 1962; Spitzer and Hart, 1971a), assuming all stars have the same mass,

$$\langle \Delta v_{\parallel} \rangle = -2vA_D l_f^3 G(x)/x , \tag{3.16}$$

where

$$A_D \equiv 8\pi G^2 m^2 n \ln(0.4N) , \tag{3.17a}$$

$$l_f^2 \equiv 3/(2v_m^2) , \tag{3.17b}$$

$$x \equiv l_f v , \tag{3.17c}$$

and $G(x)/x$ is a slowly varying function tabulated in Spitzer (1962). In general $\langle \Delta v_{\parallel} \rangle / v$, $\langle (\Delta v_{\parallel})^2 \rangle / v^2$, and $\langle (\Delta v_{\perp})^2 \rangle / v^2$ are all of the same order and approximately equal to t_{rh}^{-1} [cf. Eqs. (3.9), (3.16), (3.17)]. The energy and angular momentum diffusion coefficients are, for example,

$$\langle \Delta E \rangle = v \langle \Delta v_{\parallel} \rangle + \tfrac{1}{2} \langle (\Delta v_{\perp})^2 \rangle + \tfrac{1}{2} \langle (\Delta v_{\parallel})^2 \rangle , \tag{3.18a}$$

$$\langle \Delta J \rangle = r [\langle \Delta v_{\parallel} \rangle v_t / v + \tfrac{1}{4} \langle (\Delta v_{\perp})^2 \rangle / v_t] , \tag{3.18b}$$

where v_t is the component of velocity transverse to the instantaneous radial direction. The reader is referred to the above quoted references and to an excellent review by Hénon (1973) for further details on both the Fokker–Planck approximation and the diffusion coefficients. Numerous applications are found below.

B. Numerical methods

Because direct N-body calculations which follow each star along its orbital trajectory are so expensive [see Aarseth *et al.* (1974)], with the cost $\propto N^3$ (Hénon, 1973), and because globular clusters ($N \sim 10^5$) spend most of their lifetime in a regime where statistical methods may be valid, various investigators have devised statistical methods for the numerical solution of globular cluster dynamical evolution. We will return briefly to the numerical N-body integrations for small $N (N \sim 10^3)$ systems in Sec. VI.C, which may apply to the very late stages of cluster evolution where the highly reduced size of the core requires such calculations. The statistical methods may be divided into Monte Carlo techniques, in which the discrete nature of the particles and their interactions is explicitly maintained in the modeling, and fluid-dynamical methods, in which the system is modeled as a smooth fluid with effective viscosity, etc., arising from two-body interactions. For a general review of numerical methods in stellar dynamics, we refer the reader to Aarseth and Lecar (1975).

1. Monte Carlo methods

The Monte Carlo numerical methods are stochastic realizations of the F–P equation. Two different Monte Carlo methods have been developed, both tailored for spherical stellar systems: the pioneering scheme of Hénon (1967, 1971, 1973) and the method of Spitzer and associates (initially described in Spitzer and Hart, 1971a, with later improvements; see Spitzer, 1975 for a general review). In Hénon's method, each star represents a much larger number of stars with identical velocities but arranged in a spherical shell. The E and J of each representative star, or "superstar," is tabulated and followed, but not the orbital phase. At regular time intervals shorter than t_r, a superstar is chosen at some random position on its orbit in accordance with the probability distribution given by its E, J, and the external potential ϕ [see Eq. (3.12)]. An adjacent superstar is then randomly chosen and the two experience a mutual two-body encounter. All of the parameters of the encounter are chosen at random, with the constraint that the initial conditions be satisfied and that the squared velocity deflection equal the mean squared velocity deflection which would have resulted from many two-body encounters at the same location. As a result of the encounter, new values of energy and angular momentum, E_1', J_1', E_2', J_2' are computed for the two colliding superstars.

In the calculations of Spitzer and associates, a large number (~1000) of superstars are followed in detail along their dynamical trajectories determined by the smooth potential $\phi(r)$ [see Eq. (3.12)]. The cluster is divided into 25 spherical regions each containing 40 superstars. At regular intervals the velocity components of a superstar are perturbed in accordance with the local diffusion coefficients [see Eqs. (3.16) and (3.17)], where the local values of the coefficients are obtained by averaging over all nearby stars in the same spherical region.

The principle difference between the above two methods is that Hénon's method explicitly maintains the details of the underlying two-body interactions while Spitzer's *averages* over these details; Spitzer's method follows dynamical orbits in detail, while Hénon's *averages* over the trajectories. Hénon's method has the advantage of being somewhat less expensive but does not have the capacity to consider effects in which the orbital details are important [like the escape of stars (see Sec. V.A.)].

2. Fluid-dynamical methods

Considerably faster, but more highly idealized, than either of the two methods discussed above is the fluid-dynamical approach of Larson (1970a, b). Larson takes velocity moments of the Boltzmann equation up to fourth order and solves the resulting system of equations. The system is comprised of six coupled differential equations in the variables ρ, $\langle v \rangle$, $\langle (v - \langle v \rangle)^2 \rangle$, $\langle w^2 \rangle$, $\langle (v - \langle v \rangle)^3 \rangle$, and $\langle (v - \langle v \rangle)^4 \rangle$, where v and w are the radial and tangential velocity components, respectively, and $\langle\ \rangle$ denotes local spatial averages. In order to incorporate the effects of relaxation, "collision terms" are included on the right-hand side of the Boltzmann equation [cf. Eq. (3.13)].

A principle assumption of Larson's method, which must be used to relate hybrid terms like $\langle w^2 (v - \langle v \rangle) \rangle$ to the basic independent variables given above and to evaluate the "collision terms," is that the system is never far from thermal and hydrostatic equilibrium. Such a restriction probably forbids an accurate treatment of the initial "violent relaxation" of a stellar system (cf. Sec. IV), in which the stellar system is far out of equilibrium, collectively oscillates, and loses all memory of initial conditions in a few relaxation timescales.

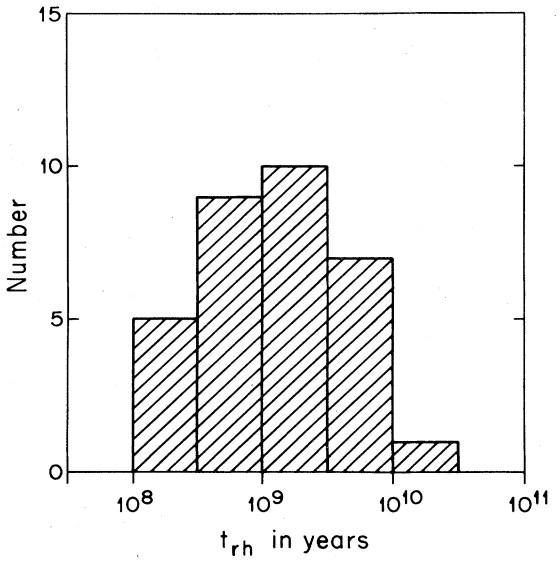

FIG. 5. Histogram showing the distribution of values of t_{rh} in 32 clusters. The quantity t_{rh} is the relaxation time for a star whose velocity equals the rms value for the cluster, and which is moving through a region of particle density equal to the mean value for the inner half of the cluster's mass. From Spitzer (1975).

IV. INITIAL STAGES OF CLUSTER EVOLUTION

A. Observational evidence for violent relaxation

Globular clusters have aged for many relaxation timescales (cf. Table I and Fig. 5) so there are no direct observations of the long-completed initial stages of cluster evolution. However, there exist other N-body systems which are much younger in relation to their relaxation timescales and they can give us a glimpse of these initial dynamical processes. For example, dwarf elliptical galaxies ($t_{rh} \sim 10^{11}$ yr) and rich clusters of galaxies like Coma ($t_{rh} \sim 10^{13}$ yr) are well fit by isothermal, density distributions (Zwicky, 1957; Oort, 1958; Peebles, 1969) as if they were fully relaxed, yet have relaxation timescales exceeding the age of the universe. Since it is unlikely that such systems formed with nearly thermal distributions, the only possible explanation (Ogorodnikov, 1958; King, 1962) is that some collective relaxation process has occurred which is much more rapid than relaxation due to successive two-body encounters. For purposes of comparison, the latter process, which occurs on the timescale t_{rh}, will be called "two-body relaxation."

B. Theory of violent relaxation

If the gravitational potential in which a star moved were strictly time independent, the star would conserve its energy and thermalization could not occur. For a cluster of stars in macroscopic equilibrium the large-scale gravitational potential is indeed nearly time independent. It is only the small fluctuating components of the potential field produced as another star passes nearby [cf. Eq. (3.12)] which allow energy exchange between pairs of stars and are the mechanism of two-body relaxation.

If the cluster is not initially in macroscopic equilibrium, however, then it will undergo macroscopic oscillations on a (rapid) dynamical time scale t_d [see Eq. (3.10)]. As shown in Eq. (3.11), t_d is much smaller than t_{rh} for large N-body systems, i.e., $t_d/t_{rh} \sim \ln N/N$. In such a situation a star experiences an external gravitational field which changes by order unity in a time t_d, thus permitting the cluster as a whole to evolve on a dynamical timescale. The importance of collective effects in stellar dynamical relaxation can be seen even in the expression for the two-body relaxation timescale t_{rh} [cf. Eq. (3.9)]. If coherence is mimicked by reducing the number of independent gravitating objects N while keeping the total mass $M = mN$ fixed, then t_{rh} decreases in proportion to N. The rapid evolution of nonequilibrium clusters due to strong collective effects has been called "dynamical phase mixing" ("phase de mélange dynamique") by Hénon (1964) and "violent relaxation" by Lynden-Bell (1967).

Because of the inequality $t_d \ll t_{rh}$, the stellar system can be considered collisionless during violent relaxation. Consequently the stellar distribution function $f(\mathbf{r}, \mathbf{v})$ is a solution of the collisionless Boltzmann (Vlasov) equation, Eq. (3.13) with $(\partial f/\partial t)_{\text{collisions}} = 0$,

$$\frac{\partial f}{\partial t} + \mathbf{v} \cdot \frac{\partial f}{\partial \mathbf{r}} + \nabla\phi \cdot \frac{\partial f}{\partial \mathbf{v}} = 0 . \tag{4.1}$$

Two important results emerge promptly from Eq. (4.1): phase space density is conserved along a stellar trajectory (Liouville's theorem) and the steady-state distribution function cannot depend upon stellar mass, which occurs nowhere in the equation. The latter result means that no mass segregation can occur (heavy stars should not sink to the center), a conclusion which follows physically from the equivalence principle (in an external potential ϕ all particles feel the same acceleration).

A cluster will be displaced from quasisteady macroscopic equilibrium when a sizeable fraction of its mass does not satisfy virial equilibrium. Examples, in terms of macroscopic variables, are zero angular momentum clusters with initially very nonspherical shapes, or clusters with virial coefficient $\alpha \equiv |2T/W|$ not initially near unity, where T and W are the total kinetic and gravitational potential energies, respectively. In such situations a cluster of total energy E and total mass M will oscillate about an equilibrium radius

$$R_0 \sim \tfrac{1}{2}(GM^2|E|^{-1}), \tag{4.2}$$

with period

$$P \sim t_d \sim 2\pi G M^{5/2} |E|^{-3/2} . \tag{4.3}$$

Unless the density is perfectly uniform and the stellar velocities perfectly radial, however, oscillations will not remain coherent (different shells will oscillate at different periods); subsequently, Landau damping will set in and the oscillations will damp out in a few periods.

There are many steady-state distributions compatible with the conserved quantities and in macroscopic equilibrium. We might expect, however, that as a result of

violent fluctuations the system has undergone sufficient phase mixing to have relaxed towards some unique, statistically probable state. Such a quasiequilibrium, "violently relaxed" distribution function f would be applicable until individual stellar encounters become important, after which f would slowly drift towards a true Maxwell–Boltzmann form (leading to mass segregation).

The statistics of the quasiequilibrium distribution resulting from violent relaxation were first considered by Lynden-Bell (1967) (see also Saslaw, 1969, 1973 for review and discussion). Because of Liouville's theorem no two elements of occupied phase space can cross as the system evolves, leading to an exclusion principle for the distribution of phase elements in phase space cells. Because there is no mass segregation, the distribution function will incorporate equipartition of energy per unit mass, $\tilde{E} \equiv \frac{1}{2}v^2 + \phi$. From the above, one straightforwardly finds that the most probable coarse-grained distribution function (for a zero angular momentum system) satisfies Fermi–Dirac statistics (Lynden-Bell, 1967):

$$\bar{f} = \eta \frac{1}{\exp[\beta(\tilde{E} - \mu)] + 1} . \tag{4.4}$$

Here $\bar{f} d^6\tau$ is the total mass in the phase space element $d^3r d^3v \equiv d^6\tau$ and β, μ, and η are constants which must be chosen to yield the correct total mass and energy of the system. When the system has net rotation, $\tilde{E} \to \tilde{E} - (\boldsymbol{\Omega} \times \mathbf{r}) \cdot \mathbf{v}$ in Eq. (4.4), where Ω is independent of r, i.e., uniform rotation.

The constant η is the typical total mass in stars per unit phase volume in an occupied microcell (unit) of phase space. The value of η is determined at the time of star formation, since it is a conserved quantity, in addition to M and E, during violent relaxation. Clearly the coarse-grained distribution function $\bar{f} \leq \eta$. The system is degenerate when $\bar{f} \sim \eta$. For a stellar system occupying a volume V, the distribution is degenerate whenever

$$v_m \sim \left(\frac{E}{M}\right)^{1/2} \lesssim v_F \equiv \left(\frac{M}{V\eta}\right)^{1/3} , \tag{4.5}$$

that is, when the mean dispersion velocity is less than the "Fermi velocity" v_F. Lynden-Bell (1967) has suggested that realistic stellar systems are always nondegenerate after violent relaxation. In the numerical experiments (see Sec. IV.C below) the degree of degeneracy of the system is well determined by the initial configuration. In the nondegenerate limit Eq. (4.4) yields the Maxwell–Boltzmann expression (with no dependence on particle mass)

$$\bar{f} \propto \exp(-\beta\tilde{E}) . \tag{4.6}$$

The distribution function for a spherically symmetric, zero angular momentum cluster is isotropic at all radii [cf. Eq. (4.6)]. However, during violent relaxation stars at large radius and angular momentum never pass through the middle and central regions where the potential is changing rapidly. These stars experience roughly constant mass interior to their orbits and are little affected by violent relaxation. Thus, if phase space is not initially occupied by such stars, it will not be after violent relaxation. although a halo composed of stars in nearly radial orbits can be produced during the violent relaxation phase, as discussed in Sec. IV.C below. A refinement to the distribution function given by Eq. (4.6) which approximately includes these effects is (cf. Lynden-Bell, 1967)

$$\bar{f} \propto \exp[-\beta(\tilde{E} + h^2 R_0^{-2})] , \tag{4.7}$$

where $h \equiv |\mathbf{r} \times \mathbf{v}|$ is the angular momentum per unit mass. The above distribution function indicates that stars move isotropically at small radii $r \ll R_0$ and predominantly radially at large radii $r \gg R_0$.

The above considerations of the most probable quasiequilibrium distribution function assume that sufficient phase mixing has occurred to make all phase states accessible. Kadomtsev and Pogutse (1970) have provided a semiquantitative analytic treatment of the time-dependent approach of a violently relaxing collisionless system towards equilibrium. Their results indicate that the final state will be of the form of Eq. (4.4) if and only if the initial deviation from the final state is large.

C. Numerical calculations of violent relaxation

Numerical calculations by various investigators of the initial evolution of a collisionless system of self-gravitating point particles tend to confirm some features of the above theoretical expectations. We should emphasize here that to obtain an absolutely clear distinction between effects occurring on the dynamical timescale and on the two-body relaxation timescale a large ($N \gtrsim 10^3$) N-body calculation is required. Typical dynamical behavior is illustrated in Fig. 6, showing the damped dynamical oscillations of the total kinetic energy of a spherically symmetric system of 1000 equal mass concentric shells with an initial virial coefficient $\alpha = 0.5$ (Bouvier and Janin, 1970). The calculations also indicate that after a few violent oscillations, in which regions at larger radii have larger amplitudes and longer periods, the system settles into a quasiequilibrium configuration. As expected, no mass segregation occurs as a result of violent relaxation (Hohl and Campbell, 1968). After steady state has been achieved the system has a marked core–halo structure with a nearly isothermal density profile in the inner regions, $r \lesssim R_0$, and a density falling more rapidly than isothermal in the outer region, $r > R_0$ [cf. Fig. 7, from Gott (1973), showing the density profile for both rotating and nonrotating systems]. The structure of this initially formed halo is, in fact, similar to that formed over longer periods of time by two-body relaxation (cf. Sec. V.A).

Halo stars at large mean radii are found to have nearly radial orbits as predicted(e.g., Spitzer and Thuan, 1972). Such high-energy orbits are produced from those stars with initial orbital parameters which require that they lag slightly behind the bulk of the stars in the early collapse and reexpansion, and thus fall inward through a huge potential well but rebound outward through a much more shallow well. This transfer of energy to stars via "potential scattering" has its analog in the two-body relaxation buildup of the halo through multiple scatterings with core stars (see Sec. V.A.2).

Another common feature of the calculations is a drop-

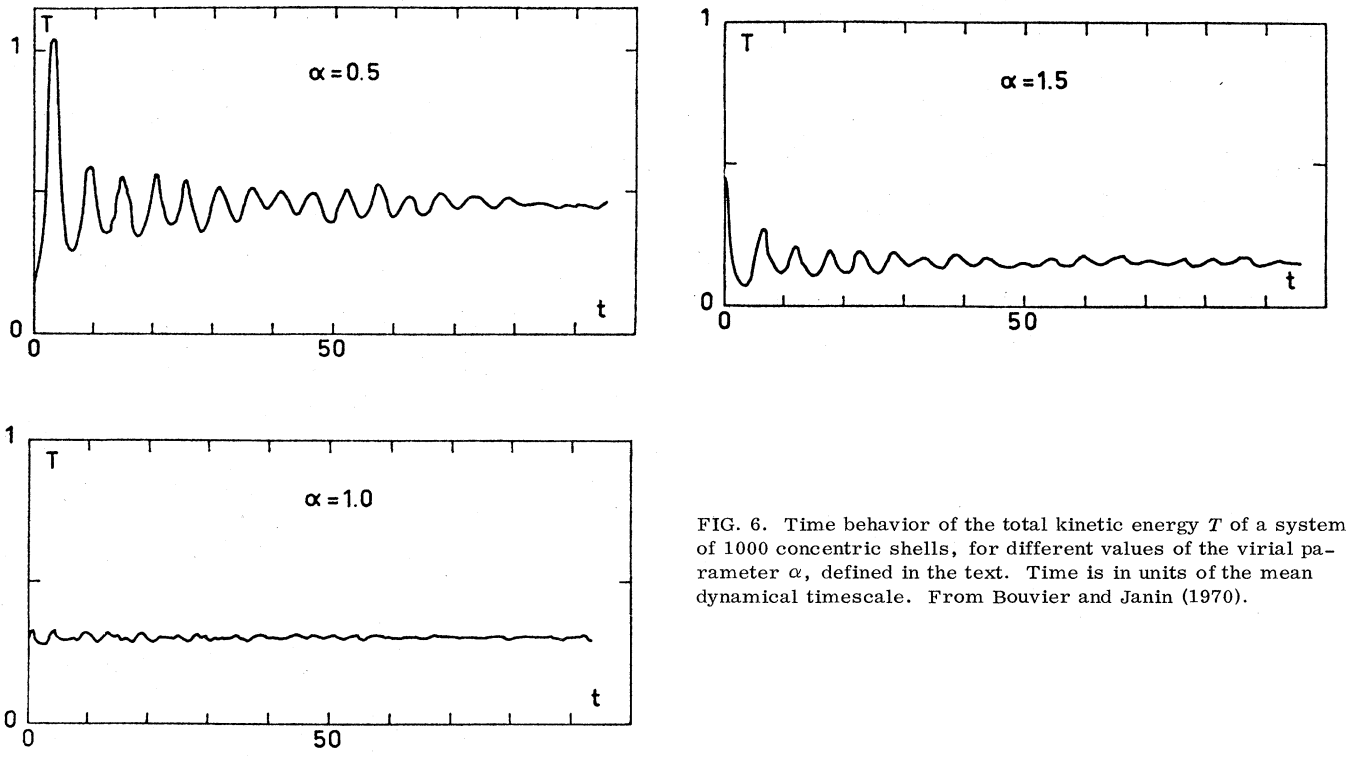

FIG. 6. Time behavior of the total kinetic energy T of a system of 1000 concentric shells, for different values of the virial parameter α, defined in the text. Time is in units of the mean dynamical timescale. From Bouvier and Janin (1970).

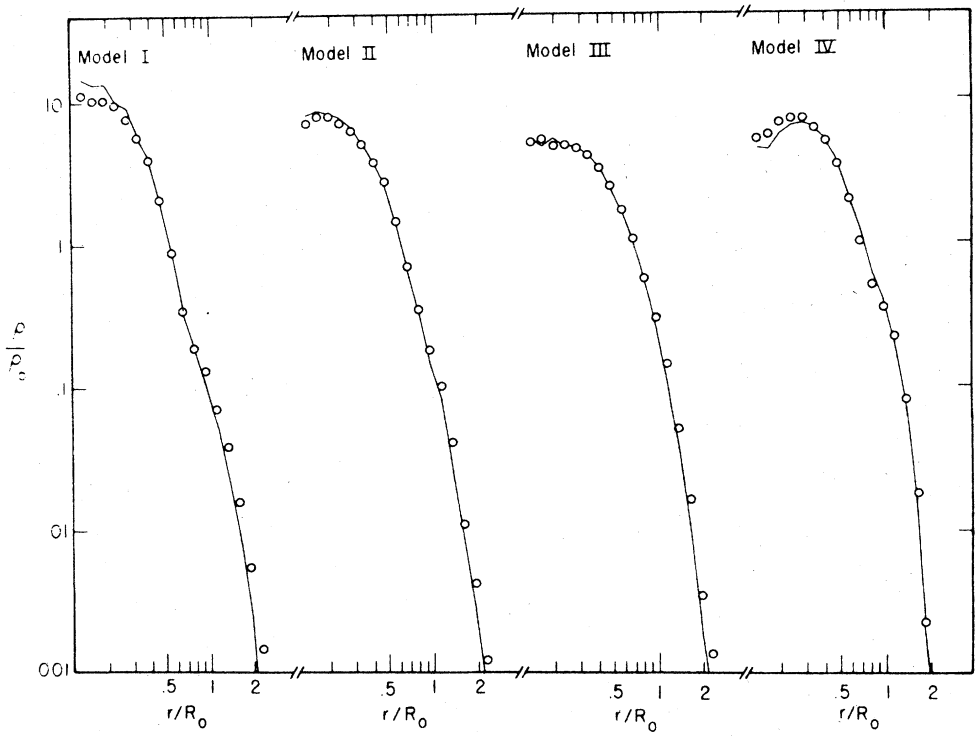

FIG. 7. Stellar density in the galactic plane as a function of radius for the equilibrium models. The open circles represent the actual runs of density with radius while the solid line represents that expected from satisfaction of the stationary collisionless Boltzmann equation. The density $\rho_0 = 3M_{\rm gal}/4\pi R_0^3$ is a standard precollapse density which is the same for all four models. Model I is nonrotating and the remaining models have varying degrees of net angular momentum. From Gott (1973).

off of the velocity dispersion in the outer regions $r > R_0$. This is a consequence of the escape of high-velocity stars and of the depopulation of tangentially moving stars in this region.

The numerical calculations also explore the role of initial conditions. If a zero angular momentum system begins with virial coefficient $\alpha = 1$, and is initially spherical with uniform density and velocity dispersion, then there are no large-scale oscillations (Hénon, 1964; Bouvier and Janin, 1970) but there can be rearrangement of positions and velocities. The calculations of Bouvier and Janin indicate that systems which do not undergo large-scale oscillation do not attain a Lynden-Bell type distribution. On the other hand, systems with an initially spherical shape, $\alpha = 1$, and substantial angular momentum violently oscillate along the rotation axis (Gott, 1973) and may come much nearer to the predicted final distribution. In general, systems with nonequilibrium initial geometry but with α near unity form less pronounced halos, although their inner regions may still be well described by Eq. (4.6). An extreme example of the role of nonequilibrium initial geometry is given by one of Peebles' (1970) three-dimensional, N-body models in which the system was initially distributed uniformly inside a cone of half-angle = 30°. The final density distribution is very nearly isothermal in the region $r \lesssim \frac{1}{2}R_0$, but is systematically high in the outer regions.

Another feature of the initial conditions explored by the numerical experiments relates to the question of degeneracy of nondegeneracy. In the one-dimensional calculations of Cuperman *et al.* (1969) and Lecar and Cohen (1971), each initial configuration consists of uniformly occupied patches of phase space with a specified value of η for the occupied regions. When the initial configuration is more or less a single patch covering the origin of phase space, then $f \sim \eta$, the system is degenerate in the sense of Eq. (4.5) and (Cuperman *et al.*, 1969) relaxes to a quasi-Fermi–Dirac distribution (with a high-energy tail). When the initial configuration consists of several isolated patches in phase space, distributed around the origin, the system begins nondegenerate and relaxes to a configuration resembling the Maxwell–Boltzmann distribution (Lecar and Cohen, 1971).

V. QUASISTEADY EVOLUTIONARY PHASE

A. Characteristic regions of the cluster

After a few oscillation periods [where the cluster period P is comparable to t_d; cf. Eq. (3.10)] following the initial collapse, the cluster settles into a quasistatic equilibrium structure which changes slowly, on relaxation timescales. The equilibrium structure of an isolated cluster during this phase may be divided into three distinct regions, in a first approximation: *Region I*, an isothermal core; *Region II*, the cluster halo; and *Region III*, the escaping stars. For most clusters orbiting the galaxy, Region III is distorted by the tidal gravitational force of the galaxy and is not observed. We discuss each region below; for simplicity we first discuss one-component cluster models and then discuss the effects of a distribution of stellar masses. All numerical estimates refer to a stellar mass $m = M_\odot$.

1. Region I: The isothermal core

The innermost region of a globular cluster is essentially in local thermodynamic equilibrium. This equilibrium is established by violent relaxation following dissipationless collapse and is maintained by distinct, two-body encounters in the core. Since relaxation times in the core are shorter than t_{rh}, local thermodynamic equilibrium would be quickly established (in comparison to the age of the universe $t_H = 1/H \sim 2 \times 10^{10}$ yr $\times [H/55 \text{ km s}^{-1} \text{ Mpc}^{-1}]^{-1}$, where H is Hubble's constant) even in the absence of violent relaxation. Moreover, violent relaxation only equilibrates energy *per unit mass* in the cluster (cf. Sec. IV), and energy equilibration, leading to mass segregation, requires a duration $\sim t_{rh}$.

The density profile in an isothermal sphere in local equilibrium is well known (see, for example, Chandrasekhar, 1942). Assuming a Maxwellian distribution function $f(E) \propto \exp(-3E/v_m^2)$, where $E = v^2/2 + \phi(r)$ is the total energy per unit mass of a star in the cluster, v is the velocity, and $\phi(r)$ is the potential, we may write for the density $n(r)$

$$n(r) \propto \int_{\mathbf{p}} f(E) d^3\mathbf{p} \propto \exp[-3\phi(r)/v_m^2], \tag{5.1}$$

where the integral is over all momentum states, p. According to Eq. (5.1) we can write

$$n(r) = n_0 \exp[-3\phi(r)/v_m^2], \tag{5.2}$$

where n_0 is the central density and $\phi(0)$ has been set equal to zero. (In multi-component systems, $V_m^2 \propto m^{-1}$, indicating mass segregation.) Poisson's equation requires

$$\frac{1}{r^2}\frac{d}{dr}\left[r^2 \frac{d\phi(r)}{dr}\right] = 4\pi G\rho = 4\pi G m n_0 \exp[-3\phi(r)/v_m^2], \tag{5.3}$$

where m is the mass of an individual star and $\rho(r) = mn(r)$ is the mass density. Equation (5.3) can be cast into dimensionless form by introducing the nondimensional variables

$$\psi = 3\phi/v_m^2, \quad \xi = (v_m^2/12\pi n_0 m G)^{-1/2} r. \tag{5.4}$$

Substituting Eq. (5.4) into Eq. (5.3) yields

$$\frac{1}{\xi^2}\frac{d}{d\xi}\left(\xi^2 \frac{d\psi}{d\xi}\right) = e^{-\psi}, \tag{5.5}$$

which can be solved when supplemented by the two boundary conditions at the cluster center: $\psi = d\psi/d\xi = 0$ at $\xi = 0$. The above boundary conditions ensure that the potential function and potential gradient (i.e., gravitational force) both vanish at the center. Note that the nondimensional isothermal equation (5.5) need only be integrated once for all cluster input parameters. Specification of $\rho_0 \equiv n_0 m$ and v_m^2 merely scales the dimensionless solution.

The density profile $n = n_0 e^{-\psi}$ obtained from numerical integration of Eq. (5.5) is plotted in Fig. 8 as a function of the dimensionless radius ξ. Also plotted in the figure is the surface density profile $\nu(x)$, where $\nu(x)$ repre-

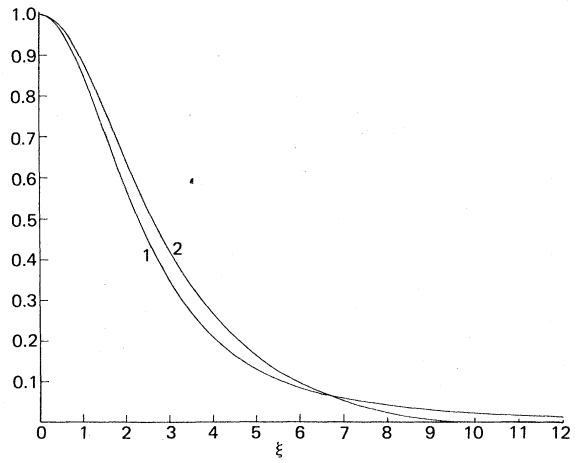

FIG. 8. The isothermal density profiles. Curve 1 illustrates the radial profile $e^{-\psi}$ and curve 2 the projected profile $\nu(\xi)$. See text. From Chandrasekhar (1942).

sents the total number of stars per unit area in the line of sight at a distance x from the center, projected on the plane of the sky. The surface density is given by

$$\nu(x)=\int_{-\infty}^{\infty} n(s)ds=\left(\frac{n_0}{3\pi G m v_m^2}\right)^{1/2}\int_x^{\infty}(\xi^2-x^2)^{1/2}e^{-\psi}\frac{d\psi}{d\xi}d\xi \tag{5.6}$$

(Chandrasekhar, 1942), where s is measured along the line of sight a distance x from the cluster center, and both s and x are measured in the same dimensionless units as r. The surface density $\nu(x)$ is clearly most useful in allowing direct comparisons of theoretical models with star counts taken from photographic plates.

Since the isothermal equation (5.5) yields the asymptotic solution $e^{-\psi}\sim 2/\xi^2$ as $\xi\to\infty$, we have $M(r)=\frac{4}{3}\pi n r^3 \propto e^{-\psi}\xi^3\to\infty$. Since the total mass M of a cluster must be finite, the isothermal approximation apparently must break down at some finite radius R_c, defining the inner (isothermal) "core" of the cluster. The physical reason for the breakdown is clear: if the entire cluster were confined in a box with perfectly reflecting walls the system would achieve thermal equilibrium everywhere with no net flow of stars or energy out of the system. (See, however, the "gravothermal catastrophe" of Sec. VI.A.) However, since the system is not confined by rigid walls, the high-velocity stars occupying the tail of the Maxwellian velocity distribution invariably escape. Stellar escape proceeds on dynamical timescales t_d, while the distribution function cannot be replenished on timescales shorter than the relaxation time t_{rh}; consequently, significant departures from thermal equilibrium must exist for the most energetic stars.

The escape rate of stars out of the isothermal core and into the halo (and out of the cluster) can be estimated from the following simple argument (Ambartsumian, 1938; Spitzer, 1940): From the virial theorem, Eq. (3.4),

$$v_m^2=\frac{GM}{2R_h}=-\frac{1}{2}\phi\,, \tag{5.7a}$$

where ϕ is the mean gravitational potential and the factor of $\frac{1}{2}$ avoids a double counting of particles. Then the mean escape velocity $\bar{v}_\infty$ is defined by

$$E_\infty=\tfrac{1}{2}\overline{v_\infty^2}+\phi=0\,, \tag{5.7b}$$

or

$$\overline{v_\infty^2}=4v_m^2\,. \tag{5.7c}$$

Suppose we assume that all stars in the tail of the Maxwellian distribution with velocity v exceeding $(\overline{v_\infty^2})^{1/2}=2v_m$ escape from the cluster, and that the tail is replenished in a relaxation time t_{rh}. The escape rate of stars F is then given by

$$F=\dot{N}\simeq-\nu\frac{N}{t_{rh}}\,, \tag{5.8}$$

where ν is the fraction of stars with $v>2v_m$:

$$\nu=\left(\frac{54}{\pi}\right)^{1/2}\int_{2v_m}^{\infty}\exp\left(-\frac{3v^2}{(2v_m^2)}\right)\frac{v^2}{v_m^2}\frac{dv}{v_m}=0.00739\,. \tag{5.9}$$

The dot above the N in Eq. (5.8) refers to differentiation with respect to time t. Numerically, the escape rate during the quasisteady contraction phase thus equals

$$F\simeq 1\times 10^{-6}\ \mathrm{yr}^{-1}(M/10^5M_\odot)^{1/2}(R_h/5\,\mathrm{pc})^{-3/2}\,. \tag{5.10}$$

The escape rate given by the naive theory above is essentially confirmed by detailed numerical calculations by Spitzer and his colleagues (see, Spitzer, 1975 for a comprehensive summary and review of this work), although the numerical factor ν is somewhat uncertain, especially as it determines the rate of core evolution (see Sec. V.E).

To accommodate the drop in the number of high-velocity stars below a Maxwellian distribution due to escape, a "lowered Maxwellian" distribution function has been proposed for star clusters by Michie (1963) and King (1965). The function f takes the form

$$f(E)=C[\exp(-3E/v_m^2)-C']\,, \tag{5.11}$$

where C is a normalization constant and C' is a constant ≥ 1. In contrast to the fully isothermal distribution discussed previously, a distribution function of the form of Eq. (5.11) causes the density to fall to zero at a finite "tidal radius" r_t representing some tidal cutoff imposed on the cluster by the galaxy [see Eq. (5.21)]. Thus a dimensionless "concentration parameter" $r_t(v_m^2/G\rho_0)^{-1/2}\equiv r_t/R_c$ must be specified for each King model, after which one integrates an equation similar to (5.5), but with $n(r)$ given by the f of Eq. (5.11) instead of by Eq. (5.1). The dimensionless solution may then be scaled, as in the isothermal model, by choice of v_m and ρ_0. (See King, 1966.)

The above distribution function has the problem that it depends only on E, while in the halo regions the realistic orbits are predominantly radial, and f presumably depends on J as well. Nevertheless, f given above does not require that stars have zero energy to escape the cluster; the constant C' reduces the escape energy below zero. Moreover, the "lowered Maxwellian" distribution function given above represents a significant improvement over the (pathological) isothermal sphere and is in reasonable agreement with the equilibrium dis-

tributions obtained by the Monte Carlo calculations of Hénon (1973) and Spitzer (1975), and the fluid calculations of Larson (1970b) for the quasisteady phases of cluster evolution.

The outer boundary of the isothermal core R_c is essentially the radius at which the magnitudes of the first and second terms in brackets in Eq. (5.11) are comparable. The condition $\exp[-3E(R_c)/v_m^2] \sim C'$ gives $R_c \sim R_h \sim GM/v_m^2$, since $E(r) \sim -GM/r$. All the way to the outer fringes of the halo, R_h provides the only length scale in the cluster. At radii $r > R_h$, the density falls rapidly and the local relaxation time increases dramatically, preventing the system from reaching thermal equilibrium. Typical core dispersion velocities are $v_m^2 \sim GM/R_h \sim 10$ km s^{-1}.

2. Region II: The halo

The halo of a globular cluster can be generated initially by violent relaxation (cf. Sec. IV) during the initial dynamical collapse of the protocluster. Over longer periods of time, after stellar escape becomes important, the halo is maintained by stars which gain energy by two-body encounters with stars in the dense, isothermal core and accumulate in highly eccentric orbits extending far from the system at apocenter but passing through the central regions at pericenter. As halo stars increase their energy with time, their binding energies per unit mass ($-E$) approach zero and the fraction of time they spend far from the system center increases to arbitrarily large values, as their periods $P(E)$ increase according to Kepler's law $P(E) = 2\pi GM/(-2E)^{3/2}$.

The density profile in the halo can be obtained directly from the distribution function, Eq. (4.7) modified to account for tidal cutoff as in Eq. (5.11), in the limit of nearly zero E satisfying $-3E/v_m^2 \ll 1$ (Spitzer, 1975). It is, perhaps, more instructive to obtain the density profile from the scaling argument (Shapiro and Lightman, 1976) reproduced immediately below, which explicitly incorporates the physical fact that the halo is characterized by an outward flux of energy and stars, which eventually escape from the cluster entirely.

The quasi-steady-state behavior of the halo is characterized by *dynamical*, rather than thermal, equilibrium, whereby a constant net flux of stars and energy flows out of the region. As the energy of a particular group of stars occupying the radial zone between r and $2r$ in the halo is continually exchanged with core stars, the halo stars will be scattered *out* of this zone in a time t_r, an effective relaxation time. However, the timescale associated with the *net* diffusion of stars (or energy) across a sphere at r may be considerably longer, since stars (and energy) from neighboring radial zones are scattered *into* the zone between r and $2r$ in roughly the same timescale. Clearly, no physical quantity can be transported from one zone to the next on a *net* rate exceeding $\sim t_r^{-1}$. In general, the net energy and net particle diffusion timescales will not be equal, and only the *minimum* of the two will be equal to t_r. The boundary zone between the halo and escape regions in the cluster specifies the magnitude of the *net* flux of stars and energy out of the halo.

Specifically, let the star and energy diffusion timescales at radius r in the cluster be denoted by $t_{\mathcal{F}}(r)$ and $t_{\mathcal{E}}(r)$, respectively. Steady state requires that both the net star flux $\mathcal{F}$ and net energy flux $\mathcal{E}$ be constant, independent of radius. If $n(r)$ is the stellar density and $E(r)$ the mean energy (per unit mass) at r, then the number of stars between r and $2r$ is roughly nr^3 and in steady state we have

$$\mathcal{F} \sim \frac{n(r)r^3}{t_{\mathcal{F}}(r)} = \text{const}, \tag{5.12a}$$

$$\mathcal{E} \sim \frac{n(r)r^3E(r)}{t_{\mathcal{E}}(r)} = \text{const}. \tag{5.12b}$$

In thermal equilibrium the constants appearing on the right-hand sides of Eqs. (5.12) are zero. In dynamic equilibrium they are generally nonzero and Eqs. (5.12) give

$$t_{\mathcal{E}}(r) \propto t_{\mathcal{F}}(r)E(r), \tag{5.13}$$

demonstrating the inequality of the *net* star and energy diffusion timescales. We can determine the constant of proportionality in Eq. (5.13) by considering ϵ_2, the rms change of energy of a halo star during one orbit from apocenter, through the dense core, and back again to apocenter. Halo stars interact mainly with the core rather than with other halo stars. The short time they spend in the core is more than compensated by the higher density there. Since all halo stars move with nearly the same velocity $v \sim (GM_c/R_c)^{1/2}$ during their periastron passage through the core, they all experience roughly the same energy change ϵ_2 each period, independent of their energy E. Consequently, ϵ_2 is given by the (random walk) relation

$$\epsilon_2 \sim \left[\frac{P(E)}{t_r}\right]^{1/2} |E| \sim \text{const}. \tag{5.14a}$$

Note that ϵ_2 may also be written in terms of the energy diffusion coefficient (cf. Sec. III.A.5),

$$\epsilon_2 = \langle(\Delta_p E)^2\rangle^{1/2}. \tag{5.14b}$$

Since $E \sim -GM_c/r$, Eq. (5.14a) implies that halo stars relax *faster* with increasing r:

$$t_r(r) \sim t_{rh}(r/R_c)^{-1/2}. \tag{5.15}$$

This result follows because ϵ_2 becomes an increasingly large fraction of E, as the latter decreases with increasing mean radius r. Evidently, the limiting factor in the escape rate of stars is their initial evaporation from the core to the inner halo, since Eq. (5.15) implies that *stars can diffuse through Region II in a time as short as a few* t_{rh}. We point out that the above discussion and equations apply only to Region II, where stars still interpenetrate and interact with the core.

In steady state, the constant outward flux of stars in the halo provides a constant escape rate of positive energy stars ejected from the outermost halo or "fringe" beyond $r \gtrsim r_{\epsilon_2}$. At this radius $r_{\epsilon_2} \sim GM/\epsilon_2$ stars can acquire positive energy in just one additional passage through the core and can escape. Since at r_{ϵ_2} there are no ingoing stars, the net diffusion time for stars to move from $\sim\frac{1}{2}r_{\epsilon_2}$ to r_{ϵ_2} equals the timescale for their binding energy ($-E$) to decrease by a factor of 2. Thus $t_{\mathcal{E}}(r_{\epsilon_2}) \sim t_{\mathcal{F}}(r_{\epsilon_2})$ and Eq. (5.13) gives

$$t_{\mathcal{E}}(r) \sim (r_{\epsilon_2}/r) t_{\mathcal{F}}(r) . \tag{5.16}$$

For $R_h < r < r_{\epsilon_2}$, $t_r(r) = \min[t_{\mathcal{E}}(r), t_{\mathcal{F}}(r)] = t_{\mathcal{F}}(r)$. The disparity in diffusion timescales merely reflects the fact that the energy is nearly conserved in a cluster experiencing stellar evaporation so the net energy-loss time is considerably longer than the net stellar-loss time. Substituting $t_{\mathcal{F}}(r) \sim t_r \propto r^{-1/2}$ into Eq. (5.12a) yields the required halo density distribution law,

$$n(r) \propto r^{-7/2} . \tag{5.17}$$

The halo density profile given by Eq. (5.17) provides a reasonably good fit to the Monte Carlo data for the halo obtained by Spitzer *et al.* (e.g., Spitzer, 1975); Eq. (5.17) can also be obtained analytically by straightforward integration of the one-dimensional Fokker–Planck equation in E space, with suitable approximations (Spitzer and Shapiro, 1972). A numerical estimate for the outer boundary of the halo r_{ϵ_2} is given in the next section. Note that the power law of Eq. (5.17) implies that the halo mass is concentrated at the *inner* boundary of the halo. Because the isothermal distribution of the core concentrates most of the core mass at the *outer* boundary of the core, we conclude that most of the cluster mass lies at the boundary between the core and halo. Figure 9, from Spitzer and Thuan (1972), illustrates numerical confirmation of the predicted density run in the core and halo.

3. Region III: The escape region and tidal limit

For isolated clusters in space, as r exceeds r_{ϵ_2} the star distribution receives a contribution from unbound, noninteracting stars with energy $E \sim \epsilon_2$ moving radially outward to infinity with constant velocity $v_\infty \sim \epsilon_2^{1/2}$. Since steady state requires $F = \mathcal{F} \sim m v_\infty r^2 = \text{const}$, we have for

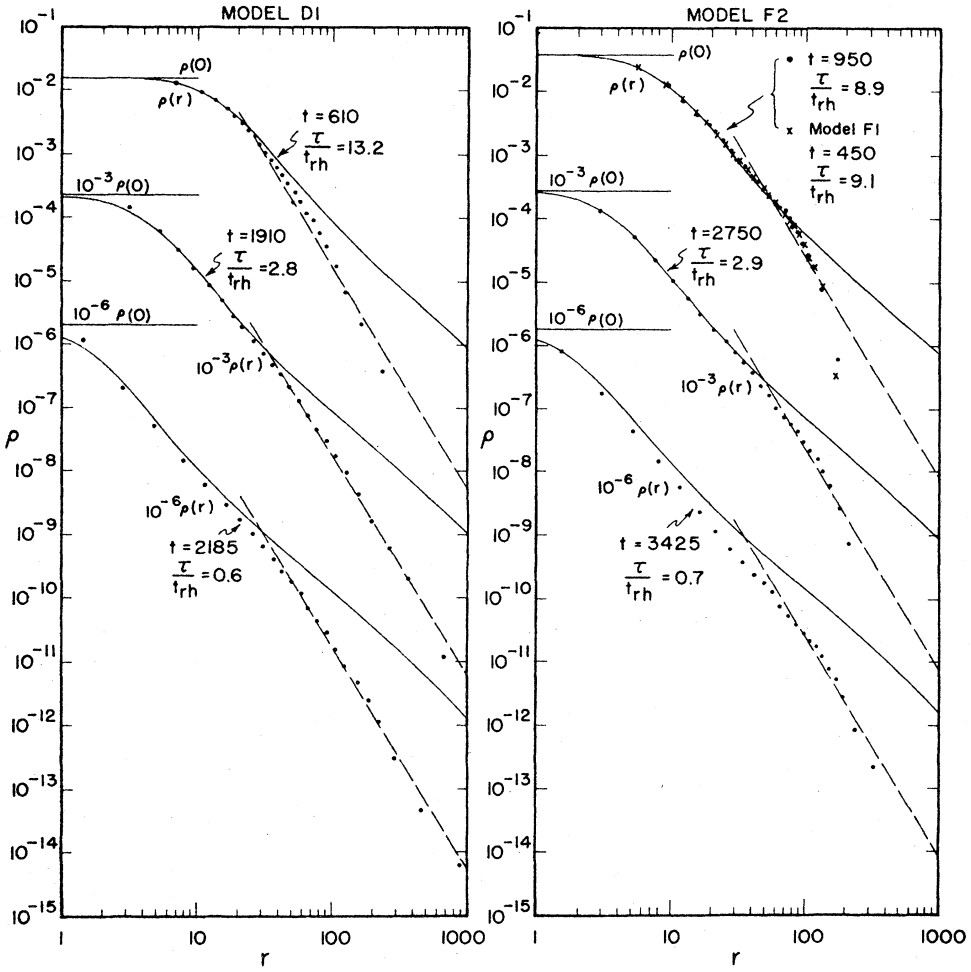

FIG. 9. Density ρ as a function of radius r. The points show the average density within regions containing 40 adjacent shells, plotted against the median radius of each group of shells. For each of the two models shown, values are plotted at three successive times, with $\rho(r)$ multiplied by 10^{-3} and 10^{-6}, respectively, at the two later times. The solid lines show $\rho(r)$ in an isothermal sphere, fitted to the central regions, together with the central density $\rho(0)$; the dashed lines show ρ varying as $r^{-3.5}$, with the same constant of proportionality at all three times. Model D starts off with an initial collapse, since the kinetic energy T is only one-fourth the negative gravitational energy $-W$ at the start, while model F is initially a homogeneous sphere in equilibrium, with all stars in circular orbits. In this figure t_{rh} is the initial value of the mean relaxation timescale, denoted by t_{rh0} in the text, and $\tau \equiv t_{cc} - t$ is the time to collapse; see text and Eq. (5.38). From Spitzer and Thuan (1972).

this region (out to some large radius)

$$n(r) \propto r^{-2} . \tag{5.18}$$

Clearly Eq. (5.18) is not a true steady solution for arbitrarily large r, as it gives an infinite mass as $r \to \infty$. Nevertheless, the density profile given by Eq. (5.18) applies to the outer regions (just outside r_{ϵ_2}) of idealized, isolated clusters with large N and has been confirmed by more detailed numerical calculations by Spitzer and Shapiro (1972). They have shown that, as r increases from $\sim r_{\epsilon_2}$ to $\sim 10 r_{\epsilon_2}$, the ratio of densities of bound to unbound stars decreases from ~10 to ~1 and that the mean energy of the escaping stars equals $0.58\epsilon_2$. In order of magnitude, the rms energy ϵ_2 can be obtained from Eq. (5.14), where the right-hand side can be evaluated at the inner edge of the halo at $r \sim R_h$. Then using Eq. (3.11) and setting $P(E) \sim t_d$ and $|E| \sim v_m^2/2$, we obtain

$$\epsilon_2 \sim 3(\log 0.4N/N)^{1/2} v_m^2 \sim 10^{-2} v_m^2 , \tag{5.19}$$

where the last equality assumes $N \sim 10^5$. The outer boundary of an isolated cluster can now be estimated from Eqs. (5.19) and (3.5) to be

$$r_{\epsilon_2} \sim \frac{GM}{\epsilon_2} \sim \left(\frac{N}{\log 0.4N}\right)^{1/2} R_h \sim 500\,\mathrm{pc} \left(\frac{R_h}{5\,\mathrm{pc}}\right) . \tag{5.20}$$

In reality the gravitational tidal field of the galaxy determines the effective outer boundary of most globular clusters. The tidal cutoff radius r_t of a cluster orbiting the galaxy is given, approximately, by

$$r_t \sim R_G \left(\frac{M}{M_G}\right)^{1/3} \sim 100\,\mathrm{pc} \left(\frac{R_G}{10\ \mathrm{kpc}}\right) \left(\frac{M}{10^5 M_\odot}\right)^{1/3} , \tag{5.21}$$

where R_G is the orbital distance from the galactic center at pericenter and $M_G = 1.4 \times 10^{11} M_\odot$ (Allen, 1974) is the total mass of the galaxy. Observations of globular clusters in our galaxy do indeed indicate that they are tidally limited, with stellar density profiles falling rapidly to zero as cluster radii approach $r_t < r_{\epsilon_2}$ (see, for example, Peterson and King, 1975, and references contained therein). The principal effect of the tidal field, in addition to modifying the stellar density distribution in the far halo, is to reduce the required escape energy of a halo star below $-\epsilon_2$, thereby increasing the escape rate. Monte Carlo computer calculations by Spitzer and Chevalier (1973) of spherically symmetric, tidally limited clusters indicate that the escape rate increases by at most a factor of 2 for $r_t/R_h \sim 9.3$ [i.e., $\nu = 0.015$ in Eq. (5.8)] and by roughly an order of magnitude for $r_t/R_h \simeq 3.1$ ($\nu = 0.05$). Thus, according to Eq. (5.21), only the few globular clusters orbiting close to the galactic center will experience an appreciably enhanced escape rate due to tidal effects. However, any conclusions concerning tidal forces drawn from spherically symmetric model calculations must be regarded as tentative.

B. Mass segregation

1. Equipartition and equilibrium profiles

The tendency for the dense, inner regions of the cluster to reach thermal equilibrium leads to energy equipartition among the different stellar mass groups:

$$\tfrac{1}{2} m_1 v_{m_1}^2 = \tfrac{1}{2} m_2 v_{m_2}^2 = \text{etc.} = \text{const} , \tag{5.22}$$

where m_1 and m_2 are the masses of individual stars in two such groups, each with nearly Maxwellian velocity distributions, with rms velocities v_{m_1} and v_{m_2}, respectively. The resulting disparity of rms velocities between the distinct mass groups invariably leads to mass segregation, with the heaviest stars most strongly concentrated toward the cluster center. The dynamical Monte Carlo calculations by Spitzer *et al.* indicate that equipartition and mass stratification is accomplished in roughly one relaxation time [see Fig. 10, from Spitzer (1975)]. More precisely, if the lighter stars (m_1) predominate in a stellar cluster [the Salpeter mass distribution function, derived for the solar neighborhood, gives $N(m)dm \propto m^{-2.3} dm$ (Salpeter, 1955)] then the "equipartition time" t_{eq} for the heavier stars (m_2) is related to t_{rh} by (Spitzer, 1969; 1975)

$$\frac{t_{eq}}{t_{rh}} \sim 0.44 \frac{m_1}{m_2} \left(1 + \frac{v_{m_2}^2}{v_{m_1}^2}\right)^{3/2} \lesssim 1 . \tag{5.23}$$

The dynamical calculations also indicate that the total rate of escape from the core into the halo and beyond is still approximately given by Eqs. (5.8) and (5.9) in multiple-mass component systems, but that the rate is higher for the lighter stars than for the heavier ones. The latter result is clear, of course, since the larger rms velocities for the lighter group imply that a larger fraction of these stars have velocities exceeding the escape velocity at the cluster center. However, the larger rms velocities of lighter stars also imply longer relaxation timescales. The result is that differences in escape rates of light and heavy stars are never very great, as shown in the Monte Carlo calculation of Spitzer (1975) and the small-N, numerical computations of Wielen (1968) and Aarseth and Woolf (1972).

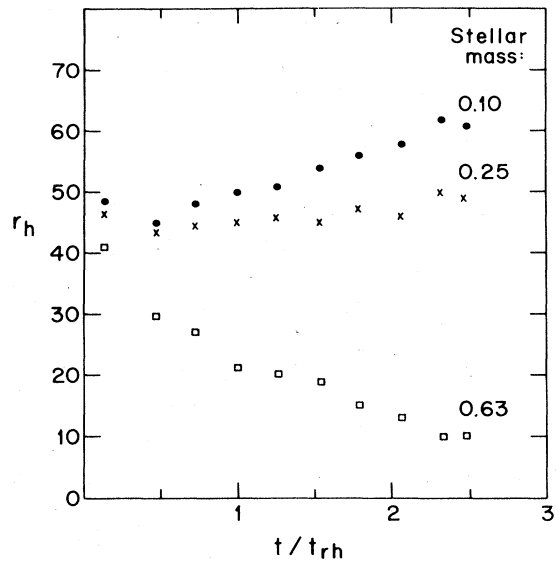

FIG. 10. Radius containing half the mass for each of three mass groups. Time is in units of the initial mean relaxation time. From Spitzer (1975).

Recently, Da Costa and Freeman (1976) have constructed multimass component, equilibrium models of globular clusters. Following King (1966), they modify the "lowered Maxwellian" velocity distribution function given by Eq. (5.11) to include a finite tidal limit *and* a distribution of stellar masses. The resulting multimass, lowered Maxwellian distribution function, which assumes energy equipartition, is substituted into Poisson's equation for the potential, and a self-consistent dynamical model is determined. They find that the most massive stars are strongly concentrated toward the cluster center, while the low-mass stars are almost evenly distributed throughout the cluster. All mass classes exhibit a rapid decrease in their stellar densities as the tidal radius r_t is approached, as the radius r_t is independent of stellar mass [see Eq. (5.21)]. For the globular cluster M3, the observed radial distribution of surface brightness and star counts over five decades in surface brightness can be fit extremely well by the tidally limited, multimass (i.e., 10 mass groups from 0.83 to $0.12 M_\odot$) component model of Da Costa and Freeman. The model for M3 gives a total number of stars $N \simeq 10^6$ with an average stellar mass $m \sim 0.33 M_\odot$; more than half the stars have masses below $0.5 M_\odot$; 8.8% are white dwarfs and 0.05% are HB stars. The total "mass to light" ratio in solar units is $M/L_v \simeq 1.6 (M_\odot/L_\odot)$, where L_v is the luminosity (erg s^{-1}) in the visual band (cf. Sec. II.A). Da Costa and Freeman find no evidence for a deficiency of low-mass stars.

In general, the fitting of multicomponent equilibrium models to observations can yield significant information, but the credibility of the results necessarily diminishes with increasing number of fitting parameters, such as the mass spectrum and total mass in each mass group. Nevertheless, the excellent fit obtained by Da Costa and Freeman, together with the similarity of their resulting mass function to the Salpeter (1955) mass function constitutes strong evidence that mass segregation occurs in globular clusters in approximately the manner predicted by the theory.

2. The mass-segregation instability

As first theoretically predicted by Spitzer (1969), if a sufficient fraction of the total cluster mass is in the heavier stars, equipartition between heavy and light stars cannot be achieved. For a two-component system of stars of mass m_1, and $m_2 > m_1$ with a finite polytropic mass distribution (pressure proportional to some power of density, $p \sim \rho v^2 \propto \rho^\gamma$ and $\gamma > 6/5$), Spitzer (1969) finds that equipartition can be achieved only if

$$M_2/M_1 < \beta (m_1/m_2)^{3/2} . \tag{5.24}$$

Here M_2 and M_1 are the total masses in heavy and light stars, respectively, and β is a slowly varying function of m_2/m_1, which has a value of approximately 0.16 for $m_2/m_1 \gg 1$. Qualitatively similar results have been obtained for an artificially confined isothermal distribution of stars (Saito and Yoshizawa, 1976; Lightman, 1977). Recent work by Vishniac (1978) indicates that the generalization of Eq. (5.24) for a continuous distribution of particle masses is the requirement that δ satisfy $\delta \gtrsim 3.5$, where $N(m)dm \propto m^{-\delta} dm$ is the number of particles of mass between m and $m+dm$. This result suggests that systems with a Salpeter (1955) mass function, $\delta \sim 2.3$, may not be able to achieve equipartition.

A rough explanation of the inability to achieve equipartition is given as follows: As equipartition is approached the heavy stars sink to the core of the cluster. If the total mass in heavy stars is small enough, the core potential will be dominated by the light stars. The heavy stars can then form a subsystem whose radius will adjust to enclose a mass of light stars whose attraction just balances the isothermal "pressure" in compliance with the virial theorem. If, however, there is sufficient mass in the heavy stars that the subsystem of heavy stars in the core becomes self-gravitating, then the subsystem decouples from the light stars. The equilibrium dispersion velocity of the core subsystem can be driven above the equipartition value [cf. Eq. (5.22)], after which energy is transferred from heavy stars to light stars. Because the subsystem of heavy stars is self-gravitating and has negative specific heat, it contracts and heats up with the energy loss, thus increasing the temperature gradient between heavy and light stars and accelerating the collapse process [cf. Fig. 14, from Lightman and Fall (1978)].

The timescale τ_{ms} for the collapse of the core of predominantly heavy stars due to conduction losses to the halo of light stars can be obtained from the expression for the time rate of change of E_2, the total energy of the heavy stars per unit mass (Spitzer and Hart, 1971a)

$$\frac{dE_2}{dt} = -\frac{1}{2}\frac{v_{m_2}^2}{t_{eq}}\left(1 - \frac{m_1 v_{m_1}^2}{m_2 v_{m_2}^2}\right) . \tag{5.25}$$

Here v_{m_1} and v_{m_2} are the mean square values for the velocities of the light and heavy stars, respectively, and t_{eq} is the equipartition timescale defined in Eq. (5.23). If R_{h2} is the radius containing half the mass of heavy stars, then the initial evolution of the heavy particles may be given as (Spitzer and Hart, 1971b)

$$\tau_{ms} = -\frac{R_{h2}}{dR_{h2}/dt} = \chi t_{eq}\left(1 - \frac{m_1 v_{m_1}^2}{m_2 v_{m_2}^2}\right)^{-1} , \tag{5.26}$$

where χ is a numerical factor which varies between 1 and 4 and depends on the details of the mass distribution in the core. Recent semianalytic calculations of two-component systems by Lightman and Fall (1978) indicate that when M_2/M_1 exceeds the limit of Eq. (5.24), the core of heavy stars contracts by conductive losses for a total time $t_e \sim 5 t_{rh} (m_2/m_1 - 1)^{-1}$, after which self-interaction dominates and quickly drives M_2 to a singularity (cf. Sec. V.E.2 and Fig. 14). Monte Carlo calculations for large N systems by Spitzer and Hart (1971b) and by Spitzer and Shull (1975) confirm the general features of the above discussion. When a population of heavy stars is not able to come into equipartition with the remaining cluster, the resulting dense subsystem of heavy stars, in self-virial equilibrium, may succeed in collapsing to a stage where stellar collisions and/or binary formation become important in the subsystem. We consider such processes in more detail in Sec. VI.

It is interesting to contrast these results with direct

N-body numerical calculations of small N systems (cf. Sec. VI.C), which generally have fluctuations too large to ever relax to quasi-isothermal distributions. In systems with $N=50$ and $N=100$ Aarseth (1966) found no tendency towards equipartition of energy. Other numerical experiments of larger $N \leq 500$, e.g., Aarseth and Saslaw (1972), find significant mass segregation but no tendency to establish local equipartition of kinetic energy. For the conductive losses of the mass-segregation instability to occur as described above, it is probably necessary to have both the spatial mass segregation and the maintenance of a local temperature characterizing the large N systems.

C. Gravothermal shock heating

It has been recently pointed out by Ostriker, Spitzer, and Chevalier (1972) that the evolution of a globular cluster will be influenced by gravitational shock heating, which occurs whenever the cluster passes through the galactic disk. The variation with height z above the galactic plane of the gravitational acceleration $g(z)$ produces a differential acceleration across the cluster which causes an initial compression of the cluster in the z direction and can effectively heat the cluster stars. Since stars outside the core, where the effect is most significant, have orbital periods longer than the passage time through the disk, the entire effect can be computed in the impulse approximation.

Ostriker *et al.* (1972) estimate the relative acceleration with respect to the cluster center dv_z/dt of stars situated a distance $Z = z - z_c$ from the center z_c by

$$\frac{dv_z}{dt} = g(z) - g(z_c) \simeq Z \frac{dg}{dz}(z_c) . \tag{5.27}$$

Multiplying both sides of the above expression by dt, setting dz_c/dt equal to V_{z_c}, the velocity of the cluster center through the disk, one obtains upon integration

$$\Delta v_z = \frac{2Z g_m(z_m)}{V_{z_c}} , \tag{5.28}$$

where z_m is the value of z above which $g(z)$ is essentially constant. Symmetry above and below the galactic plane has been assumed. The corresponding energy change per unit mass ΔE is $\frac{1}{2}(\Delta v_z)^2$, so the heating rate becomes

$$\frac{dE}{dt} = \frac{\frac{1}{2}(\Delta v_z)^2}{\frac{1}{2}P_c} = \frac{4 g_m^2 Z^2}{P_c V_{z_c}^2} , \tag{5.29}$$

where P_c is the orbital period of the cluster, which passes through the plane twice each period. Defining a shock disruption time t_{sh} by $t_{sh} \equiv -E_h/dE/dt$, where $E \simeq -0.2GM/R_h$ is the mean energy (per unit mass) of the cluster of mass M, and dE/dt is evaluated at $r = R_h$ [cf. Eqs. (3.4) and (3.5)], Ostriker *et al.* find

$$t_{sh} = \frac{3GMP_c V_{z_c}^2}{20 R_h^3 g_m^2} . \tag{5.30}$$

To estimate t_{sh} they take $z_m = 250$ pc and $g_m = 4.7\times10^{-9}$ cm s^{-2} from Oort (1965), $1\times10^8 \lesssim P_c \lesssim 4\times10^9$ yr, and $75 \lesssim V_{z_c} \lesssim 400$ km s^{-1}, which gives

$$t_{sh} \simeq 9\times10^{12}\ \text{yr} \left(\frac{M}{10^5 M_\odot}\right)\left(\frac{R_h}{5\ \text{pc}}\right)^{-3} \times \left(\frac{P_c}{4\times10^8\ \text{yr}}\right)\left(\frac{V_{z_c}}{300\ \text{km s}^{-1}}\right)^2 . \tag{5.31}$$

It is clear from Eq. (5.31) above and Eq. (3.9) that $t_{rh} \ll t_{sh}$ for most globular clusters at the present epoch; hence shock heating is unlikely to have influenced the structure of the inner, isothermal core of globulars significantly. However, since the heating rate varies as Z^2 [see Eq. (5.29)], the influence of gravitational shocks may be significant in the outer regions of clusters. Numerical calculations by Spitzer and Chevalier (1972) indicate that shock heating can increase the escape rate and the initial rate of core contraction. They find that the escape rate may be written in the form

$$-\frac{1}{N}\frac{dN}{dt} = \frac{\nu}{t_{rh}} + \frac{\beta}{t_{sh}} , \tag{5.32}$$

where ν was discussed previously for tidally limited clusters, and $\beta \simeq 2$. Ostriker *et al.* (1972) argue that mass segregation combined with gravitational shock heating in the outer regions of clusters may cause the escape of most of the low-mass stars from clusters, thereby accounting for their low mass-to-light ratio. Da Costa and Freeman (1975) have been able to fit the observed light distribution of M3 with a multicomponent, tidally limited model which *assumed* no deficiency in low-mass stars. It is not clear, however, whether an equally good fit could have been obtained with light stars absent. Further observations are needed to resolve this important issue.

An additional consequence of gravothermal shock heating, as pointed out by Tremaine *et al.*(1975), is that globular clusters in the central regions of the galaxy may be sufficiently decelerated to ultimately plunge into the galactic nucleus.

D. Rotating clusters

The above discussion dealing with quasistatic, equilibrium cluster configurations assumed that clusters are spherically symmetric and that they do not possess any net angular momentum. Yet in one of the earliest observational studies of globular clusters, Shapley (1930) found that many clusters are characterized by a small but nonzero apparent ellipticity $\epsilon \equiv 1 - (c/a)$, where a and c are the semimajor and semiminor axes, respectively. King (1961) has shown that the observed ellipticities can be attributed to rotation and that rotating clusters are flattened in much the same way as rotating rigid bodies. He also pointed out that the ellipticities could *not* be due to galactic tidal forces, since the ellipticity measurements referred to the inner regions of the clusters where the equipotential surfaces were nearly spherical and essentially undisturbed by the tidal field.

The existence of nonzero cluster ellipticities is not surprising—it is apparently a consequence of intrinsic spin—but the small values of the observed ellipticities is somewhat curious. Compared to galaxies, globular clusters are anomalously spherical in shape. The flattest elliptical galaxies observed are of type E7 (where: the notation En designates an elliptical (E) galaxy with

$n \equiv 10\epsilon$), corresponding to an axial ratio 33:1, while SO and spiral galaxies have axial ratios as large as 20:1. In striking contrast, the flattest globular cluster measured by Shapley (1930), NGC 6273 (M19), has an apparent ellipticity $\epsilon \lesssim 0.4$. Most clusters in his survey exhibit ellipticities less than 0.2.

The difference in shape between globular clusters and typical galaxies is most unusual in light of recent theoretical results of Thuan and Gott (1975) on the formation of rotating, equilibrium, spheroidal systems. These authors show, using Maclaurin spheroid models (i.e., uniform density, uniformly rotating equilibrium configurations with isotropic internal pressure), that dissipationless collapse, conserving angular momentum, of an initially spherical protogalaxy can result in an equilibrium configuration with ϵ as high as 0.709. They also demonstrate that if the initial state is nonspherical, or if energy is dissipated, the final configuration can be even more oblate. Thus, unless the angular momenta of protoclusters is unusually low in comparison to protogalaxies, the initial ellipticities of some clusters should approach ~0.7.

A possible explanation of the above paradox was recently provided by Shapiro and Marchant (1976), who pointed out that escaping stars ejected from N-body systems during their quasistatic dynamical evolution can carry away excess angular momentum in addition to mass. They showed that, depending on their initial ellipticities, clusters may become more or less spherical as they evolve. Adopting a Maclaurin spheroid model for a rotating cluster, Shapiro and Marchant demonstrated that rotating systems with $\epsilon < 0.739$ become more spherical as they evolve, a result first suggested by Agekian (1958). Since the relaxation times of most galaxies greatly exceed the Hubble time, $T \sim 10^{10}$ yr, quasisteady evolution will not have proceeded for a sufficiently long time to substantially alter the initial dynamical structure and shape of galaxies. However, the relaxation times of globular clusters are much shorter ($t_{rh} \sim 10^8$–10^9 yr) so that $t_{rh}/T \ll 1$; consequently, significant evolutionary changes will have occurred in these clusters since their formation. Hence, even if some clusters were formed with ellipticities comparable to those of the flattest ellipticals (as suggested by the dissipationless collapse model), they would *now* be more spherical, in agreement with observations.

The effect described by Agekian (1958) and Shapiro and Marchant (1976) can be summarized by the following qualitative discussion. Assume that an equilibrium, N-body system can be approximated by a Maclaurin spheroid in virial equilibrium, with uniform rotation and isotropic pressure. This assumption is roughly consistent with the work of Lynden-Bell (1967), who has shown that the statistically most probable distribution function for the relaxed core of a rotating N-body system is that of solid-body rotation with nearly isothermal, Maxwellian residual velocities [see Eq. (4.4) and following discussion]. The energy of a Maclaurin spheroid of mass $M = Nm$ is given by

$$E = \frac{W}{2} = -\frac{3}{10}\frac{G(Nm)^2}{a}\frac{\sin^{-1}e}{e}, \tag{5.33}$$

where W is the gravitational potential energy and the eccentricity $e = [1-(c/a)^2]^{1/2}$. The eccentricity is directly determined by the ratio of the rotational kinetic energy to the potential energy, $t_e \equiv |T_{\rm rot}/W|$, where $T_{\rm rot} = 5J^2/(4Nma^2)$ and where (cf. Chandrasekhar, 1969)

$$t_e = \frac{1}{2}\frac{[(3-2e^2)\sin^{-1}e - 3e(1-e^2)^{1/2}]}{e^2\sin^{-1}e}. \tag{5.34}$$

When $t_e = 0$ (no rotation), $e = 0$, and when $t_e = \frac{1}{2}$ (no random motion), $e = 1$. Consider the escape of stars from the cluster. Since escaping stars carry no energy (see Sec. V.E.), E and W remain constant with time; hence $a \propto N^2$ and $t_e \propto J^2/N^5$. Accordingly, t_e increases with time if a typical escaping star carries off angular momentum, $J_{\rm esc} < 5\langle J\rangle/2$, where $\langle J\rangle \equiv J/N$ is the mean angular momentum per star. Otherwise $t_{\rm eq}$ decreases with time. Now consider escape from a characteristic region in the cluster where stars have a mean rotation velocity u and a rms (Maxwellian) dispersion w about the mean. From Eq. (5.7c) we have that the rms total velocity v satisfies $v \equiv (u^2+w^2)^{1/2} = v_\infty/2$. Since all escaping stars populate the tail of the Maxwellian, they all have velocities $v \sim v_\infty$ in the direction of u; escape in other directions is suppressed by the Maxwellian exponential in all cases. Thus the mean value of $J_{\rm esc}$ carried off by an escaping star is

$$J_{\rm esc} \simeq \langle J\rangle 2v/u. \tag{5.35}$$

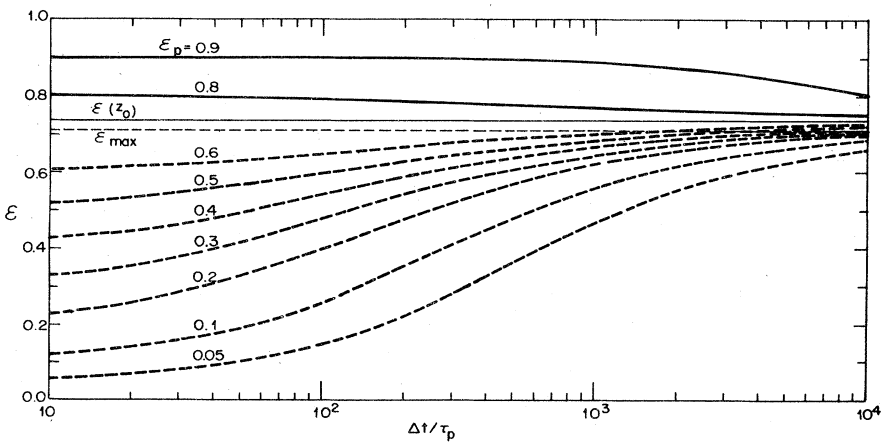

FIG. 11. The ellipticity ϵ, as a function of time Δt, into the past for clusters with various present ellipticities ϵ_p and relaxation times τ_p. All evolutionary curves asymptotically approach the value $\epsilon(z_0)$ for sufficiently large Δt. The dashed line $\epsilon_{\rm max}$ denotes the maximum ellipticity that can be achieved via dissipationless collapse.

When t_e is very small (slow rotation), we have $u \ll v$; so $J_{esc} \gg \langle J \rangle$; hence nearly spherical systems (with low t_e) have $\dot{t}_e < 0$ and become more spherical with time. However, in cold, nearly flat systems, we have $v \sim u$ and $J_{esc}/\langle J \rangle \sim 2 < 5/2$. Accordingly, flat systems become flatter with time. Agekian (1958) and Shapiro and Marchant (1976) find that the transition occurs at $t_e = 0.30$, corresponding to an ellipticity $\epsilon = 0.739$.

The evolution of cluster ellipticities with times as determined by Shapiro and Marchant (1976) is shown in Fig. 11, where $\epsilon(t)$ is plotted as a function of $\Delta t/\tau_r$ for various values of ϵ_p. Here $\Delta t = t_p - t$ is the time elapsed from an earlier time t to the present time t_p, τ_r is the present relaxation time, and ϵ_p is the present ellipticity of a cluster. (Thus the ellipticity is shown for earlier epochs in the cluster's history.) From the figure, it is evident that a cluster with an ellipticity presently in the range $0.1 \lesssim \epsilon_p \lesssim 0.3$ had an ellipticity nearly twice as large at an early epoch $\sim 100\tau_r$ years ago ($\sim 10^{10}$ yr). Figure 11 demonstrates that, according to the naive theory described above, the primordial distributions of cluster and elliptical galaxy ellipticities could have been quite comparable and have slowly grown dissimilar through cluster relaxation and spin-down.

E. Secular core contraction

The quasistatic, equilibrium stage in the dynamical history of a globular cluster is characterized by a slow, secular contraction of the isothermal core and outward growth of the halo region. This intermediate phase of cluster evolution is terminated by the complete collapse and end-point evolution of the core (Sec. VI). Due to the differences in timescales and processes, it is useful to consider separately one- and multicomponent star systems.

1. Single-component systems

The long, secular phase of core contraction, for one-component systems, can be examined analytically by a simple homological model which assumes that the core evolves independently of the halo and moves through a sequence of increasingly compact configurations in virial equilibrium containing successively fewer and fewer stars (see, for example, von Hoerner, 1958; Miller and Parker, 1964; Spitzer and Saslaw, 1966; Lynden-Bell, 1975).

Adopting Eq. (5.8) for the escape rate of stars from the inner core, where we might expect $\nu \sim 10^{-2}$ for single-component systems [cf. Eq. (5.9)], and Eq. (3.5) for the mean square velocity v_m^2 of the core, we may write

$$\dot{N}_c \simeq -\nu N_c/t_{rh} \tag{5.36}$$

and

$$-E_c = \frac{1}{2} N_c m v_m^2 = \frac{1}{4} \frac{G(N_c m)^2}{R_c} = \text{const}, \tag{5.37}$$

where $t_{rh} \propto N_c^{1/2} R_c^{3/2}/\ln(0.4N)$ is given by Eq. (3.9). In Eq. (5.36), N_c refers to the total number of core stars, each assumed to have mass m, and in Eq. (5.37), E_c represents the total core energy, evaluated according to the virial theorem. In the limit of large N_c ($\sim 10^4$–10^5 for cluster cores) the escaping stars will have nearly zero energy [i.e., $\epsilon_2/v_m^2 \sim [\log(0.4N_c)/N_c]^{1/2} \ll 1$, according to Eq. (5.19)] so E_c *remains constant during core contraction*. This result, together with Eq. (5.37), implies that during contraction $R_c \propto N_c^2$; hence $t_{rh} \propto N_c^{7/2}$, if we neglect the additional weak logarithmic dependence of t_{rh} on N_c. Assuming this variation, Eq. (5.36) may be integrated immediately, yielding

$$\frac{N_c}{N_{c0}} = \left(1 - \frac{t}{t_{cc}}\right)^{2/7}, \tag{5.38}$$

where $N_c = N_{c0}$ and $t_{rh} = t_{rh0}$ at $t = 0$ and

$$t_{cc} = (2/7\nu) t_{rh0} \tag{5.39}$$

is the "core collapse" timescale. Employing Eq. (5.38) together with the proportionality relationships between parameters indicated above, we obtain

$$\frac{R_c}{R_{c0}} = \left(1 - \frac{t}{t_{cc}}\right)^{4/7}, \tag{5.40}$$

$$\frac{v_m^2}{v_{m0}^2} = \left(1 - \frac{t}{t_{cc}}\right)^{-2/7}, \tag{5.41}$$

$$\frac{n_c}{n_{c0}} = \left(1 - \frac{t}{t_{cc}}\right)^{-10/7}, \tag{5.42}$$

where the mean core number density n_c is defined by $n_c = 3N_c/(4\pi R_c^3)$. According to Eqs. (5.38)–(5.42), the core of a globular cluster will undergo collapse to a singular state of zero radius and infinite density in a finite time t_{cc}. Note from the self-similar homology equations that at any time t, the time to collapse is the same multiple $2/(7\nu)$ of the instantaneous value of $t_{rh}(t)$ since $t_{rh}(t)$ decreases linearly with time to zero (aside from the slowly varying $\log N$ factor). Note also that the number of stars in the core $N_c(t)$ goes to zero as the singular state is approached. In Sec. VI we will see that the finite sizes of stars prevent the system from evolving all the way to a singular state, but Eqs. (5.38)–(5.42) apply for a very large fraction of the collapse time.

The numerical coefficient ν is difficult to calculate theoretically, since it is quite sensitive to the effective escape velocity from the core [cf. Eq. (5.9)], and is only reliably computed by numerical experiment. Spitzer and Harm (1958), who consider the exact equation for stellar diffusion in velocity space in a square well potential, obtain a theoretical value $\nu \sim 0.0113$, instead of 0.00739 obtained in Eq. (5.9). Their result would indicate a collapse time $t_{cc} \sim 25 t_{rh0}$. King (1958, 1965, 1966) has considered the effects of the strong central concentration in a cluster and has provided somewhat improved versions of Eq. (5.36).

Significantly, the detailed Monte Carlo simulations of Spitzer and colleagues (see Spitzer, 1975, for a review) and Hénon (1971) and the fluid-dynamical calculations of Larson (1970b) confirm the secular rate of contraction of the core given by the homological (evaporation) model. For one-component models, the effective value of t_{cc} is found to be in the range ~ 12–$19\ t_{rh0}$, leading to an "effective" value ν of ~ 0.02.

Figures 12 and 13, from Spitzer and Thuan (1972) and Larson (1970b), respectively, illustrate the numerical

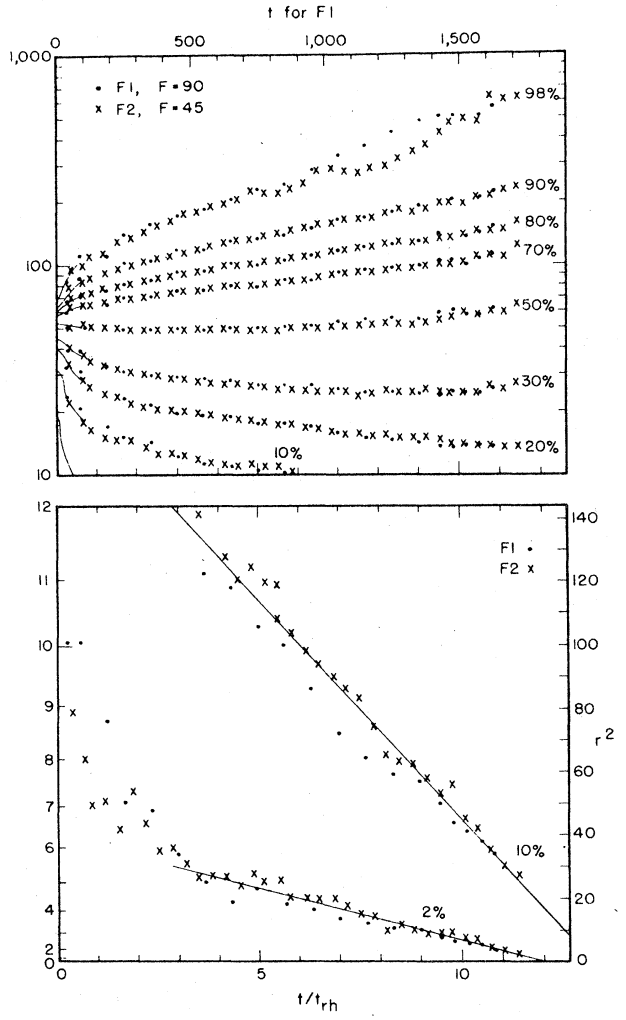

FIG. 12. Time behavior of radii containing fixed amounts of mass, denoted by R_M in the text, for a one-component system. Here radii are labeled with their percentages of the initial cluster mass and t_{rh} is the initial value of the mean relaxation timescale, denoted by t_{rh0} in the text. From the Monte Carlo computations of Spitzer and Thuan (1975).

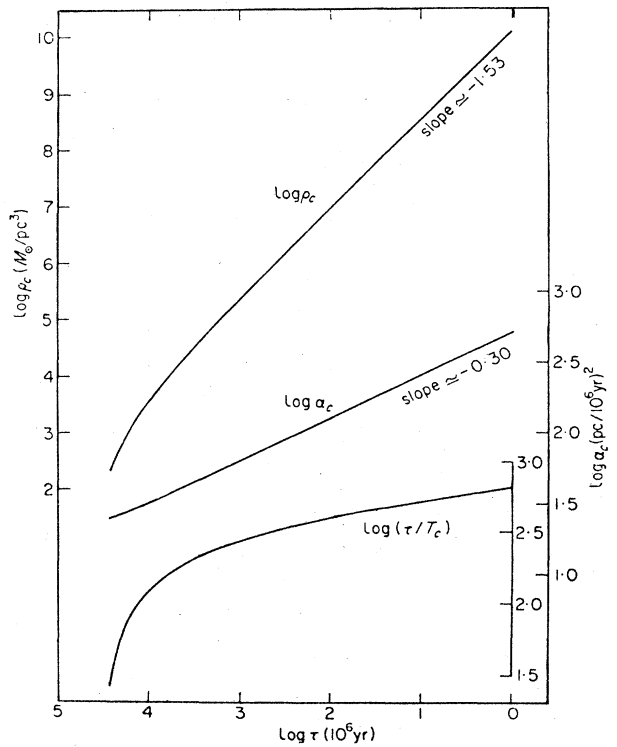

FIG. 13. Time behavior of the central density and squared velocity dispersion, ρ_c and α_c, respectively, for the collapse of a one-component system. Here τ has the same meaning as in Fig. 9. From the fluid dynamical calculations of Larson (1970b), with the permission of the Council of the Royal Astronomical Society.

results for the evaporative evolution of one-component models. Spitzer and Thuan (1972) are able to follow the collapse for ~95% of the collapse time. Graphed in Fig. 12 are the radii R_M of spheres containing a fixed amount of mass, labeled by their fraction of the initial mass of the system M_0. The outer fixed-mass radii expand, representing the outward expansion of the halo. The inner radii, after an initial period of several t_{rh} in which the system settles down to homologous evolution, begin decreasing approximately as the square root of the time to collapse, $R_M \propto (1 - t/t_{cc})^{0.5}$. This numerical result is quite consistent with that predicted by the theory of evaporative evolution, Eqs. (5.38)–(5.42) as emphasized by Press (1976). While R_M lies well within R_c (remember that R_c is the core radius, containing an ever decreasing amount of mass), the density inside R_M is the core density ρ_c. Thus if R_{M_i} is the radius containing a mass M_i, $M_i = \frac{4}{3}\pi\rho_c R_{M_i}^3$, or using Eq. (5.42) with $\rho_c = mn_c$, we find

$$R_{M_i} = R_{c0}\left(\frac{M_i}{M_{c0}}\right)^{1/3}(1 - t/t_{cc})^{10/21}, \tag{5.43}$$

agreeing quite well with the numerical results. Once $M_c < M_i$, the core radius R_c passes within R_M, Eq. (5.43) ceases to be valid, and the curve for R_M turns around and begins increasing. For each M_i this occurs at a time t_i satisfying

$$(1 - t_i/t_{cc}) \gtrsim (M_i/M_{c0})^{21/6}. \tag{5.44}$$

Such a turnaround has not yet occurred in the curves of Fig. 12 for $M_i = 2\%-10\% M_0$ ($M_0 \sim 2-4M_{c0}$), because the evolution is followed only for $(1 - t/t_{cc}) \gtrsim 0.05$. Spitzer and Thuan's (1972) numerical values for the behavior of the density and mean dispersion velocity in the inner regions,

$$\rho_c \propto (1 - t/t_{cc})^{-1.5}, \quad v_m^2 \propto (1 - t/t_{cc})^{-0.21},$$

also agree well with those predicted by the evaporation theory [cf. Eqs. (5.41) and (5.42)].

Graphed in Fig. 13 are the time evolution of the central density and dispersion velocity ($\alpha_c \propto v_m^2$) obtained by Larson (1970b), who was able to follow the evolution for > 99.99% of the collapse time. In the model shown, Larson (1970b) finds the numerical results,

$$n_c \propto (1 - t/t_{cc})^{-1.53}, \quad v_m^2 \propto (1 - t/t_{cc})^{-0.30},$$

over many decades of density increase, after the homologous evolution sets in. Again, the numerical results are quite consistent with those predicted by the evaporation theory for the middle phase of cluster evolution.

We must point out that the detailed numerical calculations described above indicate that a true description of core collapse can be quite complex. Modeling core collapse by naive evaporation theory discussed above represents a drastic oversimplification.

The main justification for adopting this crude analytic model is twofold: (1) it provides timescales for core collapse in reasonable agreement with more detailed numerical calculations and (2) the predicted variations of the core parameters with time (and with each other) agree roughly with the numerical results. More generally, the evaporation model satisfies the physically reasonable requirement that fewer and fewer stars in the core plunge toward greater and greater binding energy as time increases (cf. Sec. VI.A).

2. Multicomponent systems

In realistic systems with a mass spectrum, energy conduction between different mass groups, as briefly described in Sec. V.B, complicates the description of the evolution. Detailed Monte Carlo calculations by Spitzer and Hart (1971b) and by Spitzer and Shull (1975) indicate that the heaviest particles in the system can collapse towards a singularity in just a few mean relaxation timescales, i.e., substantially faster than the time for core collapse in one-component systems.

Lightman and Fall (1978) have recently proposed an approximate theory for the core collapse of two-component stellar systems which makes the assumption that a synthesis of the simple conduction theory of Sec. V.B with the simple evaporation theory above can be used to model the main features of the realistic systems. Although the crude conduction–evaporation theory is clearly oversimplistic, it leads to results in reasonable agreement with detailed numerical calculations and affords a semiquantitative framework for analyzing the end-point evolution of the cluster. Employment of the virial theorems for the two (homogeneous) mass groups and Eqs. (5.23) and (5.25) for energy transfer lead to an equation for the evolution of the virial (core) radius of the heavy particles:

$$\frac{\dot{R}_2}{R_2} = -\frac{1}{1+4\theta}\left[(1+\theta)\left(1-\frac{m_1 v_1^2}{m_2 v_2^2}\right) t_{\rm eq}^{-1} - 2\frac{\dot{M}_2}{M_2}(1-\theta) + 2\theta\frac{\dot{M}_1}{M_1} - 6\theta\frac{\dot{R}_1}{R_1}\right] , \quad (5.45)$$

where $\theta \equiv \rho_2/\rho_1 = (M_2/M_1)(R_1/R_2)^3$. A similar equation holds for the time evolution of the virial (core) radius of the light particles R_1. Here $M_2(t)$ and $M_1(t)$ are assumed to decrease according to evaporation theory, each obeying an equation of the form of Eq. (5.36) with the appropriate self-relaxation timescales t_{r2} and t_{r1}, respectively. (The evaporation formula for M_2 is only appropriate after it becomes self-gravitating, $\theta \gtrsim 1$.) The mean velocities of heavy and light particles are denoted by v_2 and v_1, respectively.

It is convenient to divide into two regimes the evolution and collapse of the heavy particles: the conductive and evaporative regimes. Initially, the first term on the right-hand side of Eq. (5.45) dominates, corresponding to domination of the evolution by energy transfer from the hotter heavy particles to the cooler light particles. [After violent relaxation, $v_1 = v_2$; hence $T_1 = (m_1/m_2)T_2$.] Eventually, the second term dominates the first, corresponding to domination of the evolution by self-interactions, modeled here by self-evaporation. The relative contributions of evaporation and conduction can be measured approximately by a "collapse parameter" ξ [cf. Eqs. (5.45) and (5.36)]:

$$\xi \equiv 2(t_{\rm eq}/\gamma t_{r2}) . \quad (5.46)$$

Here γ is the "effective" value of $1/\nu$ in Eq. (5.36), i.e., $\gamma \approx 50$ (cf. above discussion). The collapse parameter exceeds unity for virial radii R_2 less than the "evaporation radius" R_{2e},

$$R_{2e} \sim 0.1 R_1 (\gamma/50)^{-2/3} (M_2/M_1)^{-1/3} . \quad (5.47)$$

Because the initial decrease of R_2 is approximately exponential, the time τ_e required for R_2 to decrease to R_{2e} does not depend much upon its initial value R_{20}:

$$\tau_e \sim 4 t_{r0} (m_2/m_1 - 1)^{-1} \ln(R_{20}/R_e) . \quad (5.48)$$

Here t_{r0} is the initial mean relaxation timescale of the system as a whole.

Figure 14 from Lightman and Fall (1978) portrays the time evolution of one of their models. Here the evolution begins immediately after violent relaxation (cf. Sec. IV), whereby $v_2 = v_1$ and $R_2 = R_1$ initially. Because of their hotter temperature, the heavy particles begin losing energy to the light particles, thereby cooling and contracting. The ratio $(v_2/v_1)^2$ decreases until the heavy particles become self-gravitating, $R_2/R_1 \sim (M_2/M_1)^{1/3}$. If the latter condition occurs before equipartition is reached, $(v_2/v_1)^2_{\rm eq} = m_1/m_2$ (as it does in this model), subsequent heat transfer from the heavy particles (now with negative specific heat) to the light particles causes $(v_2/v_1)^2$ to increase (cf. Fig. 14). Note that when the collapse parameter ξ reaches about unity, the evolution of all quantities accelerates: heavy particles begin to evaporate rapidly out of the inner core and the core radius R_2 goes quickly to zero.

Once the evaporation regime begins, the heavy particles effectively become a one-component system, evolving according to the equations [(5.38)–(5.43)] above. As long as M_2/M_1 is initially small, < 0.5, the light particles undergo relatively little evolution during the entire collapse of the heavy particles; they act mainly as an energy sink of large heat capacity, allowing the heavy particles to lose enough energy to contract to a self-gravitating and rapidly evolving independent subsystem. It is significant that a small amount of mass can collapse to a singularity without visibly affecting the bulk of the system.

Both the functional behavior of the quantities in Fig. 14 and the overall timescale of inner core collapse agree reasonably well with detailed calculations of Spitzer and Hart (1971b) and Spitzer and Shull (1975). In the following section, the crude conduction–evaporation model above will be extrapolated to provide a

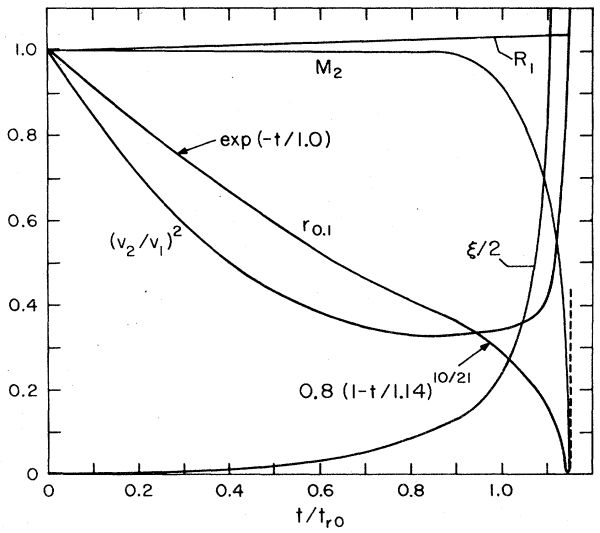

FIG. 14. Time evolution of a two-component stellar system in which a simple conduction–evaporation model is used to approximate the detailed gravitational interactions. The ratio of particle masses, m_2/m_1, is 5 and the initial ratio of total mass in heavy to light particles is 0.1. At $t=0$ the heavy and light components of the system have equal mean velocities, $v_2=v_1$, and equal core radii $R_2=R_1$, corresponding to the period immediately following violent relaxation. M_2 is the total mass of heavy particles within the heavy particle core radius R_2 (not shown), and $r_{0.1}$ is the radius containing 10% of the initial mass of heavy particles. Analytic approximations to $r_{0.1}$ are indicated by arrows. R_1, M_2, and $r_{0.1}$ are in units of their initial values and t is in units of the initial mean relaxation timescale of the combined system. When more than 90% of the heavy particles have evaporated out of the inner core $M_2 \lesssim 0.1$, $r_{0.1}$ abruptly increases, as shown by the dashed line. The relative importance of evaporative self-interactions to conductive interactions with light particles in the evolution and collapse of the heavy particle core is measured by the "collapse parameter" ξ [see text and Eqs. (5.45) and (5.46)]. From Lightman and Fall (1978).

framework for analyzing the end-point evolution of the core.

VI. LATE STAGES OF CLUSTER EVOLUTION

As the collapse of the cluster core proceeds, new processes eventually become important in determining the subsequent evolution of the cluster. This end-point evolution is dominated by the effects of binaries and by dissipative effects associated with the finite size of stars. These various end-point processes are discussed below. Since all of these effects become significant only after the heavy particle subsystem falls to $\lesssim$ 100–1000 stars, direct N-body calculations with finite-size stars are probably required to accurately determine the final evolutionary behavior.

A. Core collapse prior to end-point evolution: The gravothermal catastrophe and the evaporation model

A decade and more ago Antonov (1962) and later Lynden-Bell and Wood (1968) demonstrated that a self-gravitating gas of energy E and mass M confined within a rigid, nonconducting sphere of radius r_s could not achieve (isothermal) equilibrium if $\alpha \equiv -Er_s/(GM^2) \gtrsim 0.355$. The speculated resulting evolution of the gas, in which an increasingly large temperature gradient between the contracting core and outer regions *conducts* energy from the former to the latter, has been called the "gravothermal catastrophe" by Lynden-Bell and Wood (1968).

The idealized gravothermal catastrophe reflects the basic tendency of a self-gravitating system to increase its entropy by forming a dense core and an extended halo, a configuration which becomes increasingly prominent in the late stages of core collapse in the numerical experiments. It also reflects the necessity for the density profile in real stellar systems to fall below the isothermal value well outside the core to satisfy the requirements of finite total mass (see Sec. V.A.1). For completeness we shall give a brief review of this idealized phenomenon.

Consider the isothermal equilibrium configurations available to a self-gravitating confined gas, obtained as truncated solutions of the isothermal Emden (1907) equation. The artificial confining sphere is required because a completely isothermal gas does not have a finite radius and has infinite total mass (Emden, 1907). Figure 15 from Lynden-Bell and Wood (1968) gives a graph of the value of the externally fixed parameter α for each equilibrium configuration, the latter forming a one-parameter sequence parametrized by the ratio of central to surface density ρ_0/ρ_s. As can be seen in the figure, for values of $\alpha > \alpha_{\max} \simeq 0.355$, where $\alpha_{\max}$ corresponds to a critical density contrast $(\rho_0/\rho_s)_{\rm crit} \simeq 709$, no equilibrium solutions exist (Antonov, 1962; Lynden-Bell and Wood, 1968). The explanation for this lack of an equilibrium solution and subsequent thermal runaway, confirmed by the dynamical calculations of Larson (1970a) for the idealized confined gas, is very similar to that for the mass segregation instability, Sec. V.B. In the present case the steep density contrast within the isothermal gas creates a core–halo structure which replaces the role of the heavy star–light star structure in the previous situation.

As one might expect, apportioning the total mass in a multiple-mass component system has a destabilizing effect on confined isothermal gas spheres which represents an enhancement of the gravothermal catastrophe (Saito and Yoshizawa, 1976; Lightman, 1977). In general, $\alpha_{\max}$ is a function of the ratio of particle masses and total mass fractions present, but is less than 0.355 for all but one-component systems. Because of mass segregation, for a given α the two-phase core-halo structure and the disparity between core and halo specific heats are more pronounced than in the single-component case.

To what extent does the idealized gravothermal catastrophe provide an understanding of core collapse in realistic systems? Such systems are not confined by rigid walls and, accordingly, are characterized by stellar evaporation. Realistic stellar systems thus evolve with time and never achieve the true equilibrium conditions assumed in the models illustrating the idealized gravothermal catastrophe. Is late core collapse driven by

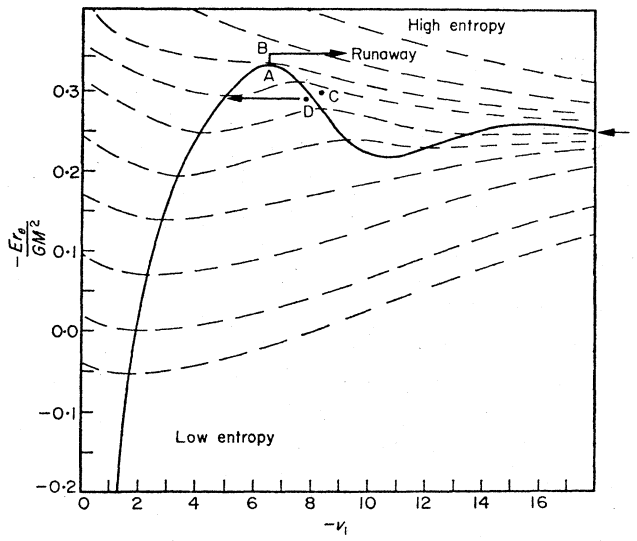

FIG. 15. Energy-radius density contract relationship for a self-gravitating gas of total energy and mass, E and M, respectively, confined within an isolated rigid sphere of radius r_e. The isothermal equilibrium solutions (solid line) from a one-parameter sequence parametrized here by $-v_1 \equiv \ln(\rho_0/\rho_s)$, the natural logarithm of the central to surface mass density. Dashed lines are schematic and indicate curves of constant entropy at fixed energy E, with each succeeding curve representing an entropy higher than that of the curve below it. No equilibrium configurations are available for systems with the externally fixed dimensionless energy exceeding ~0.355. Equilibrium configurations to the right of the maximum A represent local minima in the entropy and are thus unstable. From Lynden-Bell and Wood (1968), with the permission of the Council of the Royal Astronomical Society.

evaporation or conduction? It is clear that a *fixed* amount of mass cannot collapse to a singularity: in the absence of a confining wall to prevent escape of positive-energy stars, the resulting infinite binding energy cannot be absorbed from the collapsing core. Accordingly, realistic core collapse must be characterized by evaporating mass from the core. Moreover, the numerical calculations of core collapse indicate that the collapse proceeds homologously in the case of one-component systems and that the behavior can be approximated by the naive evaporation model described above (Sec. V.E.1). In the more realistic case of multicomponent systems, a simple conduction–evaporation model (Sec. V.E.2) adequately describes the evolution of the inner core of heavy stars after they evolve to an independent (≈ one-component) stellar subsystem. Accordingly, we adopt this approximate description of core collapse in the following sections to consider the influence of new processes in the core at the onset of endpoint evolution.

B. Effects of binaries

As we shall show, binary stars can be ignored in the early and intermediate stages of cluster evolution, unless present initially in large numbers, in a narrow range of binding energy. In the late stages of core collapse, when the total number of stars in the heavy particle subsystem is down to $\lesssim$ 100–1000, stochastic processes involving binaries may become important. If the core succeeds in collapsing down to a few stars, a single binary can dominate the evolution of the remaining stars. For a discussion of numerical N-body calculations of binary processes, see Aarseth (1974) and Aarseth and Heggie (1976) and references therein. Most of the recent detailed analytical studies of binaries have been done by Heggie (e.g., Heggie, 1975a, b) and by Hills (1975a, b), with some recent approximate calculations by Lightman and Fall (1978).

A binary is defined to be "hard" or "soft" depending on whether its binding energy E_B is greater than or less than the local stellar thermal energy ϵ,

$$\epsilon \equiv \tfrac{1}{2} m \langle v^2 \rangle , \tag{6.1}$$

$$x \equiv E_B/\epsilon < 1: \text{ soft}, \tag{6.2a}$$

$$x > 1: \text{ hard}. \tag{6.2b}$$

Because soft binaries do not absorb or release much energy upon being disrupted or created, respectively, we shall neglect them in our present discussion of the effects of binaries, although soft binaries may harden and become important in the presence of tidal dissipation (Milgrom and Shapiro, 1978).

1. Formation of binaries by three-body processes

A simple argument of Spitzer and Hart (1971a) demonstrates that binary star formation via three-body gravitational encounters is unimportant in large N-body systems. The argument begins by observing that three stars must simultaneously experience a close encounter to form a hard binary, with one of the stars taking up the necessary energy to bind the other two. In one relaxation timescale, the number of close two-body encounters in a system of N stars is proportional to $N/\log(0.4N)$[cf. Eq. (3.8)]. The probability that a third star is within the same close encounter distance during any of these events is $\sim (p_0 n^{1/3})^3 \propto N^{-2}$, where p_0 and n are the close encounter distance and number density, respectively, and $n^{-1/3}$ is the mean separation between stars [see Eq. (3.6)]. The *total* number of binaries formed per unit time by three-body processes, $\dot{N}_{B3}$, may thus be written as

$$\dot{N}_{B3} \sim \frac{3\times 10^{-4}}{\log(0.4N)} \left(\frac{N}{10^5}\right)^{-1} t_{rh}^{-1} , \tag{6.3a}$$

where the overall numerical coefficient has been taken from the more exact calculations of Heggie (1975a). If the total number N of stars remaining in the core is used instead of time as an independent variable, and the evaporation laws, Eqs. (5.36) and (5.37), are used with $\gamma \equiv \nu^{-1}$, then the number fraction of "three-body binaries" f_{B3} satisfies the approximate relation (Lightman and Fall, 1978)

$$f_{B3}(N) \equiv N_{B3}/N \sim \frac{1500}{\log(0.4N)} \left(\frac{\gamma}{50}\right) N^{-2} . \tag{6.3b}$$

2. Formation of binaries by two-body processes

As first suggested and estimated by Fabian *et al.* (1976), sufficiently close tidal interactions between two

stars can dissipate enough orbital kinetic energy to bind the two stars in a binary system. Because the tidal force varies rapidly (i.e., as the inverse cube) with the distance of closest approach, the critical impact parameter d which results in a binary is a few stellar radii and is only a weak function of the initial relative velocity of the two stars. In a detailed calculation of the nonradial oscillations of polytropic stars, in which the orbit is assumed to be initially parabolic, Press and Teukolsky (1977) have obtained the approximate expression

$$d \sim 3r_* \left(\frac{v_{\rm rel}^2}{Gm/r_*}\right)^{-0.1}, \tag{6.4}$$

where r_* denotes the stellar radius. With Eq. (6.4), the cross section for two-body tidal capture can be computed [see Sec. VI.D and Eqs. (6.28) below] taking gravitational focusing into account. Using Eq. (59) of Press and Teukolsky and Eq. (3.9) for t_{rh}, the *total* number of binaries formed per unit time by two-body processes, $\dot{N}_{B2}$, may be written

$$\dot{N}_{B2} = \frac{25}{\log(0.4N)} \left(\frac{r_*}{R_\odot}\right)^{0.9} \left(\frac{m}{M_\odot}\right)^{-0.9} \times \left(\frac{v_m}{10\,\mathrm{km\,s^{-1}}}\right)^{1.8} \left(\frac{N}{10^5}\right) t_{rh}^{-1}. \tag{6.5a}$$

Aside from the weak dependence of d on $v_{\rm rel}^2 (m/r_*)^{-1}$ and its resulting contribution to Eq. (6.5a), $\dot{N}_{B2}$ is functionally identical to the rate for stellar collisions [cf. Eq. (6.34)], and numerically larger by the simple factor $d/(2r_*) \sim 2$. Comparing Eqs. (6.3) and (6.5a) and using the definition of the binding parameter δ, cf. Eq. (6.30), we may write

$$\frac{\dot{N}_{B2}}{\dot{N}_{B3}} \sim 1.0\times10^{-2}\delta^{0.9}N^2 = 8\times10^4 \left(\frac{v_m}{10}\right)^{1.8} \left(\frac{m}{M_\odot}\right)^{-0.9} \times \left(\frac{r_*}{R_\odot}\right)^{0.9} \left(\frac{N}{10^5}\right)^2. \tag{6.5b}$$

Even though $\dot{N}_{B2} \gg \dot{N}_{B3}$, the number of hard binaries formed by two-body processes will constitute a negligible fraction of the total number of stars until the late stages of collapse.

Eventually the end-point evolution of the collapsing subsystem of heavy particles in a realistic stellar system will be affected by tidal dissipation and formation of "two-body binaries." To estimate when these binaries constitute a sizeable fraction of stars in the subsystem core, Eq. (6.5a) can be integrated. Again, one can use N (now the total number of stars in the subsystem of heavy stars) as an independent variable and Eqs. (5.36) and (5.37) for N and R when the core of heavy stars enters its evaporation regime with initial values $N = N_0$ and $R = R_e$ (cf. Sec. VI.E.2). The number fraction of two-body binaries, f_{B2}, then has the solution (Lightman and Fall, 1978)

$$f_{B2}(N) \equiv \frac{N_{B2}}{N} \sim \frac{60}{N} \left(\frac{\gamma}{50}\right)\left(\frac{r_*}{R_\odot}\right) \left(\frac{R_e}{0.5\ \mathrm{pc}}\right)^{-0.9} \times \left(\frac{N_0}{5\times10^3}\right)^{1.9} \ln\left[\frac{\ln(0.4N_0)}{\ln(0.4N)}\right]. \tag{6.6}$$

The normalized value of R_e here comes from Eq. (5.47) and a cluster core size of ~3 pc; the normalized value of N_0 corresponds to a cluster core of mass $5\times10^4 M_\odot$ in which heavy stars of $\sim 1M_\odot$ comprise 10% of the total mass. The explicit dependence of $f_{B2}(N)$ on the actual size of R_e comes from the fact that the stellar radius introduces a scale length, unlike the case of "three-body binaries." From Eq. (6.6), *evidently the collapsing subsystem of heavy stars evaporates down to* $N \lesssim 100$ *stars before most stars become "two-body binaries"* ($f_{B2} \gtrsim \frac{1}{2}$) and begin to dominate the end-point evolution. At a somewhat larger value of N (perhaps a few hundred) two-body dissipation will accelerate the collapse above the rate given by stellar evaporation alone (cf. Sec. VI.B.5). It also seems clear that two-body binary formation and dissipation will become important somewhat before collisions and coalescence become important because of the slightly larger cross section (~2) of the former (see Sec. VI.D below).

After initial capture, further energy dissipation during successive periastron passages will circularize the orbit on a timescale $\Delta t_c \sim 30$ yr, comparable to that given by Eq. (6.33) below. Thus a final binding energy of $E_B \sim Gm^2/d$ is achieved where, approximately, an amount ϵ of this energy was removed from the initial orbital kinetic energy of the interacting stars. Since $E_B \gg \epsilon$ [cf. Eqs. (6.4) and (6.30)], binaries formed in such a manner are quite hard. In fact, since so much energy must be dissipated by internal motions in the stars ($d \sim 3r_*$) and the timescale Δt_c is much shorter than a stellar thermal ("Kelvin–Helmholtz") timescale (e.g., Clayton, 1968)

$$t_{th} \sim 10^7\ \mathrm{yr}(m/M_\odot)^{-2.7}, \quad m \leq 10M_\odot$$
$$\sim 10^5\ \mathrm{yr}\,(m/M_\odot)^{-0.7}, \quad m > 10M_\odot, \tag{6.7}$$

it is possible that the two stars will swell tremendously during the dissipation process. The typical outcome could be that a single coalesced object is eventually produced by the tidal capture of two stars.

3. Hardening of hard binaries

One of the main results of both the theory (e.g., Heggie, 1975a, b) and numerical results (e.g., Aarseth, 1974, 1975; Wielen, 1975) is that hard binaries become harder while most soft binaries become softer as a result of their interactions with other stars. This can be understood as the attempt of locally interacting particles to achieve equipartition of their kinetic energies. Here we neglect the role of (tidally induced) dissipative encounters between single stars and binaries.

Consider the interaction of a binary of energy E_B with a single star. Unless the distance of closest approach is of the order of the binary separation d, the binary will act as a single star, producing an elastic scattering. When the pericenter approaches ~d, the energy exchange will be comparable to $E_B \sim Gm^2/d$. The cross section for such an inelastic interaction is $\sigma \sim \pi d(2p_0)$, taking into account the usual gravitational focusing effect [cf. Eq. (6.28)]. Then using the expression for p_0, Eq. (3.1), and Eq. (3.9), the rate of binary hardening E_B is (Heggie, 1975a; Hills, 1975a)

$$\dot{E}_B \sim \frac{0.7\epsilon}{\log(0.4N)t_{rh}}\left[\frac{n}{\langle n\rangle}\left(\frac{v_m^2}{\langle v^2\rangle}\right)^{3/2}\right], \tag{6.8}$$

where the numerical factor and expression in brackets (n is local density and $\langle n\rangle$ is mean density) result from the more accurate calculations. Note that the rate of binary hardening is independent of binary energy because of reduction in cross section with increasing energy transfer [cancellation of d in Eq. (6.8)].

As the core contracts in the intermediate and late stages of evolution and if ϵ increases at a faster rate than E_B, hard binaries will become soft and will be disrupted. The mean cluster kinetic energy increases on a timescale proportional to t_{rh} [cf. Eq. (5.41)]. From Eq. (6.8), it is clear that binaries satisfying $x\sim 1$ harden at this same rate, aside from the slowly varying logarithmic and numerical factors. One may easily show, using Eqs. (3.5a), (5.36), (5.37), (6.1), (6.2a), and (6.8), that the "hardness" of a binary, x, created at $x\sim 1$ at N_c stars in the core, has a hardness at some smaller N (and later time) given by (Lightman and Fall, 1978; Heggie, 1975a)

$$x(N,N_c)\simeq \frac{0.7\gamma}{\log(0.4N)}\left(1-\frac{N}{N_c}\right)+\frac{N}{N_c}. \tag{6.9}$$

Although the numerical factors in Eq. (6.9) are not known with certainty, it seems clear that as the core evaporates down to small N, x approaches a maximum value ~10 (taking $\gamma\sim 50$). This maximum must be compared with the maximum value of x allowed for "efficient" binaries, x_E (cf. Sec. VI.B.4) below.

4. Core heating by binaries and effects of an initial population of binaries

To determine the dynamical effects of binaries, we must estimate the rate at which hard binaries heat the core. Such heating manifests itself in the recoil energy of a hard binary and its single-star collision companion, following a superelastic scattering between the two. Evidently such heating is not significant enough to prevent the first core collapse in the small N-body numerical experiments ($N\leq 500$) (cf. Sec. VI.C), but could possibly be important in a large N system with a large initial fraction of binaries, as pointed out by Heggie (1975a) and by Hills (1975b).

A crucial limiting factor in the ability of binaries to heat the core is the fact that only binaries in a very narrow range of hardness are effective. Consider the energy transferred from the internal binding energy of a binary to the recoil energy of each collision, ΔE_B. A certain fraction y of this energy goes into the recoil of the single star and the remaining fraction $(1-y)$ goes into the binary recoil. As long as neither binary nor single star gain sufficient recoil energy to escape the system, all of the energy transfer ΔE_B is given to the core, $\Delta E_c=\Delta E_B$. But once the binary or the colliding single star have sufficient recoil to escape (which occurs for sufficiently high values of $\Delta E_B/\epsilon$), some of the energy transfer is lost in the escaping star and $\Delta E_c<\Delta E_B$. If the binary has mass m_b and the single star mass m_s and the average stellar mass is m, then an analysis quite similar to that leading to Eq. (5.7) shows that the single star will escape when

$$\Delta E_B/\epsilon \geq \frac{1}{y}\left(\frac{4m_s}{m}-1\right), \tag{6.10}$$

and the binary will escape when

$$\Delta E_B/\epsilon \geq \frac{1}{1-y}\left(\frac{4m_b}{m}-1\right). \tag{6.11}$$

Calculations of y require knowledge of the cross section for the superelastic scattering process. For the case of $m_b=2m_s$, Heggie's (1975a) numerical results indicate $y\sim\frac{2}{3}$. For $m_b\gg m_s$, clearly $y\sim 1$. These two special cases are shown in Fig. 16, illustrating the relation between ΔE_B and ΔE_c.

If one defines a binary heating efficiency

$$\mathcal{E}\equiv\Delta E_c/\Delta E_B, \tag{6.12}$$

then $\mathcal{E}$ clearly drops below unity as $\Delta E_B/\epsilon$ increases above a few. Since $\Delta E_B\lesssim E_B$, only binaries with $x\lesssim x_E\lesssim 3$–10 are efficient in heating the core. The importance of this limiting factor can be easily seen in the effect of

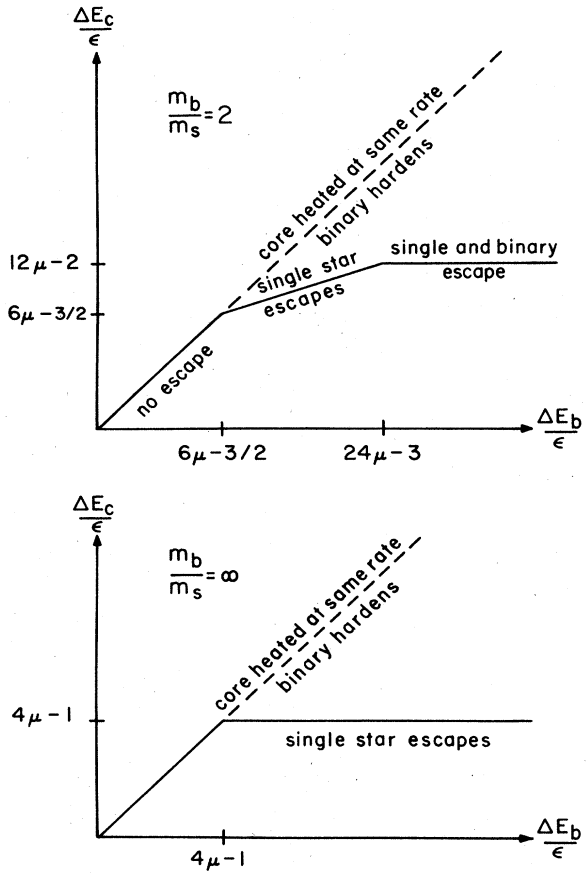

FIG. 16. Efficiency of core heating by binary-single star interactions. Here m_b and m_s are the mass of the binary and single star, respectively, and μ is the ratio of the mass of the single star to the average stellar mass in the system. The mean thermal energy of a star is ϵ, and ΔE_b and ΔE_c are the increase in binary binding energy and recoil energy transferred to the cluster, respectively, as a result of the binary-single star encounter. When encounters are sufficiently energetic to eject participating stars, the heating efficiency decreases.

binary heating on the dynamical evolution of the core. If f_B is the fraction of all stars which are binaries and $\bar{\mathcal{E}}$ is the average efficiency factor, then the rate at which binaries heat the core is [cf. Eq. (6.8)]

$$\dot{E}_c \sim f_B N_c \bar{\mathcal{E}} \dot{E}_B \sim \frac{2 f_B \bar{\mathcal{E}} E_c}{\ln(0.4N) t_{rh}} . \tag{6.13}$$

Combining Eq. (6.13) with Eqs. (6.19) and (5.8) then shows that the core radius obeys the approximate equation

$$\frac{\dot{R}_c}{R_c} = \frac{2}{t_{rh}}\left[\frac{f_B \bar{\mathcal{E}}}{\ln(0.4N_c)} - \frac{1}{\gamma}\right]. \tag{6.14}$$

Here γ is the effective value of ν^{-1} in Eqs. (5.36) and (5.39), i.e., $\gamma \sim 50$ for essentially one-component systems. Note that for sufficiently large values of $f_B \bar{\mathcal{E}}$, the cluster can actually begin by expanding. Taking f_B as constant and no cutoff value x_E for efficient binaries ($\bar{\mathcal{E}} = 1$) Hills (1975b) has investigated the contraction and reexpansion of clusters with a large initial population of binaries. From Eq. (6.14), it is clear that the cluster will reexpand when $N = N_{\rm bounce}$, where

$$N_{\rm bounce} \sim 3 \exp(f_B \bar{\mathcal{E}} \gamma). \tag{6.14'}$$

It is very difficult to measure binary populations in globular cluster cores, but Eq. (6.14') indicates that unless $f_B \bar{\mathcal{E}} \gtrsim 0.1$, which seems unlikely (Flannery, 1977), an *initial* population of binaries probably has little dynamical effect on cluster evolution until possibly the final stages of core collapse. Binaries *formed* by two-body processes will also have little effect, since the heating efficiency of these very close binaries ($x \gg x_E$) is low until the late stages of core collapse. For the case of an insignificant number of initial binaries in the hardness range $1 \lesssim x \lesssim x_E$, Eqs. (6.9), (6.14), and (6.3b) can be used to show that binary heating by "three-body binaries" is not important until the core has evaporated down to an $N \lesssim 100$, i.e., below the value of N where the mean field, small-angle scattering approximation probably breaks down.

5. Accelerated collapse due to two-body tidal dissipation

Two-body tidal interactions in the core lead to the dissipation of cluster (kinetic) energy. The total dissipation rate arises from three processes: (1) bound–bound interactions in which a soft binary pair tightens somewhat via tidal interaction but is eventually disrupted, (2) free–free interactions in which an unbound pair dissipates some, but not all, of the energy required to become bound, and (3) free–bound interactions in which an interacting unbound pair becomes hard (or coalesces; see Sec. VI.D). For these processes we have approximately $\dot{E}_c \sim \dot{N}_{B_2} \epsilon$; more exactly

$$\frac{\dot{E}_c}{E_c} = \frac{8.7\times10^{-4}}{\log(0.4N)}\left(\frac{r_*}{R_\odot}\right)^{0.9}\left(\frac{m}{M_\odot}\right)^{-0.9}\left(\frac{V_m}{10\ \text{km s}^{-1}}\right)^{1.8} t_{rh}^{-1} \tag{6.15a}$$

(Milgrom and Shapiro, 1978). Inserting the above rate into Eq. (6.19) for homological collapse with dissipation, we find that such dissipation *accelerates* the rate of core collapse above the rate given by evaporation above. Dissipation dominates whenever the rms core velocity exceeds a critical velocity

$$V_{m,\rm crit} \simeq 48[\log(0.4N)]^{5/9}\left(\frac{r_*}{R_\odot}\right)^{-1/2}\left(\frac{m}{M_\odot}\right)^{1/2} \text{km s}^{-1} . \tag{6.15b}$$

Dissipation-dominated core collapse can drive the core to a high-density "singular" state *before* all of the stars have evaporated. For typically observed cluster parameters for one-component systems ($N \sim 10^5$ solar-type stars and $V_m \sim 10$ km s^{-1}) the above equations give $V_{m,\rm crit} \sim 80$ km s^{-1}, $N(V_m = V_{m,\rm crit}) \sim 2000$ and $N_f \sim 700$, where N_f is the number of stars remaining in the core when R_c approaches zero. Apparently, $M_f = mN_f \sim 10^2$–$10^3\ M_\odot$ represents an upper limit to the mass available for the formation of supermassive objects (e.g., supermassive stars and/or black holes; see Sec. VI.D) during the final stages of core collapse. In any case, the effects of tidal dissipation must be included in any detailed model which describes the final stages of core contraction.

C. Small N-body systems

When the cluster as a whole, or a small subsystem in self-virial equilibrium, has evolved due to the evaporation of stars and core contraction to the point where $N \lesssim 10^3$ stars, large fluctuations around the mean statistical behavior become important. The statistical treatment of large N-body systems may then not be applicable, and direct N-body numerical simulations become necessary. These latter computations have been performed for $N \lesssim 10^3$ by Aarseth, Wielen, and others, utilizing sophisticated regularization techniques for close encounters (e.g., Kustaanheimo and Stiefel, 1965).

In the direct N-body calculations (and also in the Monte Carlo calculations for $N \gg 10^3$), stars are treated as mass points. This procedure thereby ignores two-body binary formation, tidal dissipation, and star collisions and coalescence, processes which may dominate the final phase of core collapse (see Secs. VI.B and VI.D). Nevertheless, some of the features of systems of $N \lesssim 10^3$ point masses may still be applicable to realistic core collapse, and it is instructive to compare the results of the numerical calculations with the theory for such systems. The next generation of N-body calculations will presumably include dissipative effects.

The principal results of the direct N-body calculations are the following (see, for example, Wielen, 1975; Aarseth, 1975, 1974): (i) Radii containing fixed amounts of mass evolve in time at approximately the rate given by the Monte Carlo calculations of large N-body systems [cf. Fig. 17, from Aarseth *et al.* (1974)]. (ii) During the initial and intermediate stages of cluster evolution, stars escape at about the same rate found for the large N systems. The escaping stars have an energy which is of the order of the mean thermal energy of a star. The escape mechanism involves discrete close encounters. (iii) If one defines a density-weighted core radius (cf. Aarseth, 1974) by

$$R_{c\rho} \equiv \sum r_i \rho_i / \sum \rho_i , \tag{6.16a}$$

$$\rho_i \equiv m_i r_{i3}^{-3} , \tag{6.16b}$$

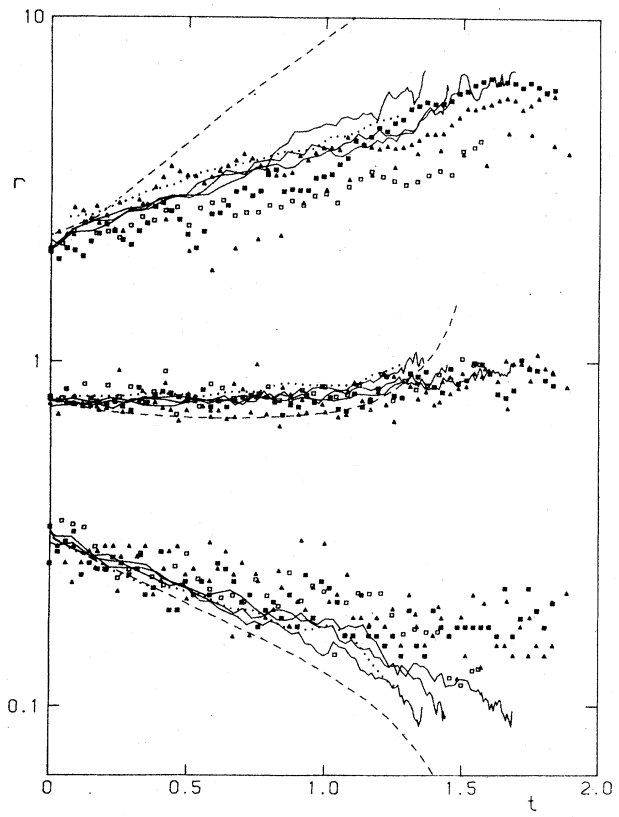

FIG. 17. Radii containing 10%, 50%, 90% of the mass, plotted versus time for a cluster with stars of equal masses. Open triangles and squares: N-body integrations with $N=100$, $N=250$ (Wielen). Filled triangles and squares: N-body integrations with $N=250$ (Aarseth). Full lines: Monte Carlo models (Hénon). Dotted lines: Monte Carlo model (Shull and Spitzer). Dashed lines: fluid-dynamical model (Larson). The unit of time is approximately 10 initial mean relaxation timescales. From Aarseth, Hénon, and Wielen (1974).

where r_{i3} is the distance from particle i to the third nearest neighbor, the core contracts and loses mass until it is reduced to a few stars which contain a hard binary. In a multispecies system the central hard binary is composed of heavy stars. This "first core collapse" occurs on about the same timescale t_{cc} as that required for the large N systems to obtain infinite density, $t_{cc}\sim 15t_{rh_0}$ for single-component systems and 3–5 times smaller for multispecies systems. The collapse thus appears to be a scaled-down, small-N analog of large N core collapse [cf. Wielen (1975)]. See Figures 18 and 19, from Aarseth (1974). (iv) By the time core collapse produces a hard central binary, only a few percent of the initial mass has escaped from the system. (v) Subsequent to the first core collapse, both the mass and radius of the core increase from their minimum values. The remaining evolution is dominated by the hard central binary, which continually hardens by absorbing a large fraction of the total system binding energy (Aarseth, 1975). This hardening may cause the remaining stars to evolve through a series of contractions and reexpansions as it heats the stellar system. The final reexpansion phase has been modeled with Monte

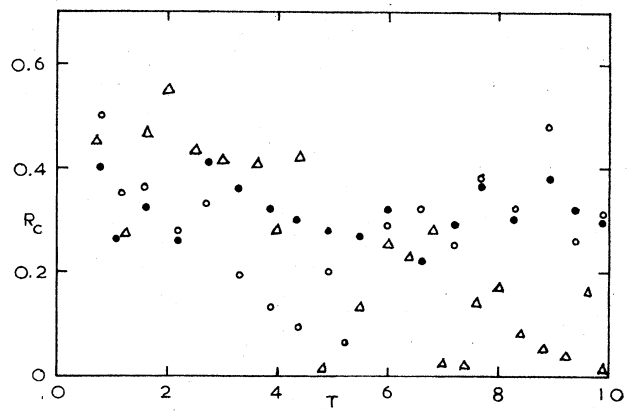

FIG. 18. Core radius, defined in Eq. (6.16), as a function of time, where the latter is measured in units of the initial dynamical (crossing) timescale. Filled circles refer to a model with equal masses and 250 particles. Open circles refer to a model with a mass spectrum and 250 particles. Triangles refer to a model with a mass spectrum and 500 particles. From the direct N-body computations of Aarseth (1974).

Carlo methods by Hénon (1975); cf. Sec. VI.F.

Since the first core collapse proceeds until only a few stars remain in a manner analogous to the large N systems, it appears that core heating by binaries in $N\leq 500$ systems does not constitute a significant dynamical effect during the initial period (cf. Sec. VI.B). We are tempted to extrapolate these results to the large N systems up to the emergence of the dominating central binary (ignoring collisions for the moment). We must remind ourselves, however, that for small N in the range $<10^3$ the relaxation timescale is not much longer than the dynamical time [cf. Eq. (3.11)], $t_{rh}\gtrsim 3t_d$, and that the results may thus differ qualitatively.

It is clear from the theory that escaping stars should carry away more and more energy as N decreases, as pointed out, for example, by Spitzer (1975). As was

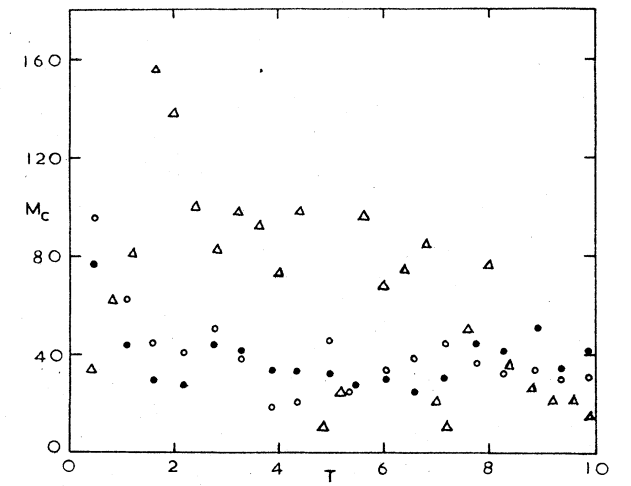

FIG. 19. Core masses as functions of time. The quantity M_c is the mass within the radius R_c for the same models as shown in Fig. 18. From Aarseth (1974).

mentioned in Sec. V.A, a star escapes with an average energy $\epsilon_{es} \sim 1/2\epsilon_2$. Rewriting our expression for ϵ_2 [cf. Eq. (5.19)], we then have

$$\frac{\epsilon_{es}}{\epsilon} \sim 0.2\left(\frac{N}{250}\right)^{-1/2}\left(\frac{\log(0.4N)}{2}\right)^{1/2}. \tag{6.17}$$

Accordingly, even on the basis of the large N-body (energy diffusion) theory, we can understand qualitatively result (ii).

Results (i) and (iii) suggest that the homological laws for the large N regime may be extrapolated into the small N domain. A modified quasihomological law for core collapse when the energy carried away by escaping stars may no longer be negligible can be simply derived as follows:

$$\dot{E}_c = \dot{N}_c\epsilon_{es} \sim -3\left(\frac{\dot{N}_c}{N_c}\right)E_c\left[\frac{\log(0.4N)}{N_c}\right]^{1/2}, \tag{6.18}$$

where we have used $E_c = -\epsilon N_c \propto N_c^2/R_c$ [cf. Eq. (3.5b)]. Now, using the relation

$$\frac{\dot{E}_c}{E_c} = \frac{2\dot{N}_c}{N_c} - \frac{\dot{R}_c}{R_c}, \tag{6.19}$$

obtained by differentiating the virial expression for E_c, Eq. (6.18) can be solved for $R_c(N_c)$, yielding

$$\frac{R_c}{R_{c0}} = \left(\frac{N_c}{N_{c0}}\right)^2 e^{-A}, \tag{6.20}$$

where

$$A \equiv -6[\log(0.4N_c)]^{1/2}\left(\frac{1}{N_c^{1/2}} - \frac{1}{N_{c0}^{1/2}}\right). \tag{6.21}$$

For $N_c \gg 1$, we recover the usual "constant energy core" relation $R_c \propto N_c^2$ (cf. Sec. V.E). Equation (6.20) clearly indicates that the core contracts more rapidly than N_c^2 with decreasing N_c because of energy loss to escaping stars. However, the effect is small until $N_c \lesssim 100$ ($A \gtrsim 1$).

A second small N effect is a departure from the usual halo distribution and maintenance discussed previously. As N decreases, the rms angular momentum transfer by the cluster to a halo star in one orbit, j_2, becomes comparable to the latter's mean angular momentum j_H. When this occurs the halo stars will get scattered out of the "escape cone" intersecting the core *before* they can make sufficient orbital passages through the core to get boosted out of the cluster. For N smaller than this critical "freezing" limit N_f, halo stars become "frozen" into the cluster, "fossilizing" via their pericenters the radius of the core at the time they were produced. To calculate N_f, we simply equate j_2 to j_H. If $\langle j\rangle$ is the mean angular momentum of a cluster star, then the expression for the dispersion j_2 is similar to the random walk expression for ϵ_2 [cf. Eq. (5.14a)],

$$j_2 \equiv \langle(\Delta_p J)^2\rangle^{1/2} \sim \langle j\rangle\left(\frac{t_d}{t_{rh}}\right)^{1/2}. \tag{6.22}$$

Since most halo stars occupy the region immediately outside the isothermal core, where $j \propto r^{1/2}$ and $n(r) \propto r^{-7/2}$, $\langle j\rangle \sim 2$–$3\, j_H$. Then setting $j_2 \sim j_H$ and using Eq. (6.22) and Eq. (3.11) yield

$$N_f \sim 500\text{–}1000. \tag{6.23}$$

For $N \lesssim N_f$ the halo stars begin to accumulate without evaporating, and the cluster maintains, approximately, constant total mass as the core mass decreases to zero. This is in qualitative agreement with the numerical N-body result (iv).

From the above simple picture, together with mass and energy conservation, one may also calculate a modified density distribution for the halo when $N < N_f$ (Press and Lightman, 1978). If a typical star (mass dM) ejected by the collapsing core gets "frozen" into the cluster at a times the instantaneous core radius, then the energy of the core has decreased by $dE = -GMdM/(aR)$, where M and R are the mass and radius of the core. This relation, together with the relation $E = -GM^2/R$ (which defines an effective core radius R), gives a differential relation for the distribution of halo stars as the remaining core shrinks to successively smaller radii:

$$\left(2 - \frac{1}{a}\right)\frac{dM}{dR} = \frac{M}{R}, \tag{6.24}$$

leading to a halo density law

$$\rho \propto r^{-(5a-3)/(2a-1)}. \tag{6.25}$$

The entire distribution is parametrized by the single unknown a, plausible values of which might be $a \sim 2$–3. Note that the power index ranges only from -2 to -2.5 for the entire allowed range of a, $1 \leq a < \infty$ and that the distribution of this "small-N halo" is always less steep than that for the "large-N halo," $\rho \propto r^{-7/2}$ [cf. Eq. (5.17)].

D. Stellar collisions and coalescence

1. An approximate theory

As core contraction proceeds as discussed above, eventually the stellar density grows sufficiently large that contact collisions between stars become important. Very energetic collisions can disrupt stars completely. Less energetic collisions may eject only a small amount of stellar material, yet still dissipate sufficient energy to bind the parent stars into a single coalesced object. Such coalesced stars will then eventually undergo gravitational collapse (and, possibly, supernovae explosions) releasing mass and energy. These dissipative processes, together with binary formation (cf. Sec. VI.B), will determine the ultimate state of the globular cluster core.

Stellar collisions and coalescence clearly involve complicated physics and have been treated only approximately and in very special cases (e.g., Ulam and Walden, 1964; Gold *et al.*, 1965; Spitzer and Saslaw, 1966; Colgate, 1967; Sanders, 1970; Seidl and Cameron, 1972; see Spitzer, 1971 and Saslaw, 1973 for reviews). Most calculations apply to galactic nuclei, where stellar velocities are of the order ~1000 km s^{-1}. Because stars are so weakly bound in globulars (v is initially ~10 km s^{-1} and only $\lesssim 100$ km s^{-1} when collisions become important as discussed below) stellar collisions in globular clusters will differ qualitatively from those in galactic nuclei. Recently, Fall and Lightman (1977) have considered the effects of collisions and coalescence in the late stages of core collapse of globular clusters.

The timescale for a star to experience physical contact with another star, the collision timescale t_c, is given by

$$t_c = (n\sigma_c v_{\rm rel})^{-1}, \tag{6.26}$$

where n is the number density of stars, σ_c is the collision cross section, and $v_{\rm rel}$ is a typical relative velocity. Because of gravitational focusing, the collision cross section can be significantly larger than the geometrical cross section. From conservation of energy and angular momentum, one easily derives σ_c for two stars of masses m_1 and m_2 and radii r_{*1} and r_{*2}

$$\sigma_c = \pi(r_{*1}+r_{*2})^2\left(1+\frac{v_0^2}{v_{\rm rel}^2}\right), \tag{6.27a}$$

where

$$v_0^2 = 2G(m_1+m_2)/(r_{*1}+r_{*2}). \tag{6.27b}$$

A simple "rule of thumb" for calculating the cross section for a collision requiring a pericenter separation l involves the close encounter distance p_0 [cf. Eq. (3.1)]:

$$\sigma \sim \begin{cases} \pi l^2 & l \gg 2p_0 \\ \pi l(2p_0) & l \ll 2p_0 \end{cases} \tag{6.28}$$

If Eqs. (6.26) and (6.27) are averaged over a thermal stellar velocity distribution, one obtains for the collision time for star 1 [cf. Hills and Day (1976)]

$$t_c = 2\times10^{11}\ {\rm yr}\left(\frac{r_{*1}+r_{*2}}{R_\odot}\right)^{-1}\left(\frac{n}{10^5\ {\rm pc}^{-3}}\right)^{-1} \times\left(\frac{\langle v^2\rangle^{1/2}}{10\ {\rm km\ s}^{-1}}\right)\left(\frac{m_1+m_2}{M_\odot}\right)^{-1} \times\left(\frac{2m_1}{m_1+m_2}\right)^{-1/2}\left[1+\frac{4}{3}\left(\frac{m_1+m_2}{2M_\odot}\right)\frac{\langle v^2\rangle}{v_0^2}\right]. \tag{6.29}$$

In subsequent discussion we will typically employ the virial theorem [Eq. (3.5)] to write t_c in terms of the core radius R_c and core star number N_c, in place of the variables n and $\langle v^2\rangle$.

Assuming that no core evolution occurs, the above collision timescale can be used to estimate the number of collisions which have occurred in a cluster core of age $\sim10^{10}$ yr. Using data from Peterson and King (1975) for n and $\langle v^2\rangle$ for 70 globular clusters, Hills and Day (1976) have calculated that an average of 3.3% of all the core stars in globulars have suffered collisions, with a maximum of 41% in the case of M80. As core evolution proceeds, however, t_c drops considerably and collisions become frequent as discussed below.

The outcome of stellar collisions depends significantly on the "relative binding parameter" δ,

$$\delta \equiv \frac{\langle v^2\rangle}{2Gm/r_*} = 4\times10^{-4}\left(\frac{v}{10\ {\rm km\ s}^{-1}}\right)^2\left(\frac{m}{M_\odot}\right)^{-1}\left(\frac{r_*}{R_\odot}\right), \tag{6.30}$$

which measures the binding energy per mass of the star to the cluster relative to the star's self-gravitating binding energy per unit mass. (For simplicity, we consider here only the average star of mass m and radius r_*; in Secs. VI.D.3 and VI.D.4 the distinction between large and small stars is discussed.) For large δ, corresponding to large kinetic energy upon impact, stellar collisions tend to be disruptive, while for small δ, stellar collisions tend to result in coalescence with less mass loss, as pointed out by Colgate (1967).

The most detailed treatment of collisions is the two-dimensional hydrodynamical calculation by Seidl and Cameron (1972), who considered head-on (zero impact parameter) collisions between two solar-type stars to form a single coalesced star. Their results indicate that for $\delta = 8$, 60% of the total mass is ejected to infinity, while for $\delta = 0$, only 5% of the total mass is lost. It seems unlikely that "grazing" collisions, dominant in globular clusters, can eject as much mass as direct collisions [cf. Sanders (1970)]. One uncertainty in calculating the mass loss is the effect of increased nuclear burning and possible detonation in the initially disturbed coalesced star. Approximate considerations by Spitzer and Saslaw (1966) indicate that the nuclear energy released during the collision is a small fraction of the thermal energy released for small values of δ. In the absence of more refined calculations, we shall assume that mass loss in collisions in globular clusters, where $\delta \ll 1$, throughout most of the "collision regime," is negligible.

An approximate method for the treatment of off-axis collisions, originally devised by Spitzer and Saslaw (1966) and modified for "soft collisions" ($\delta \ll 1$) by Sanders (1970), involves dividing each star into rectangular tubes whose axes lie along the direction of relative motion. It is then assumed that each separate pair of colliding mass tubes conserves linear momentum and suffers a completely inelastic collision. For grazing collisions of similar stars, these approximations may be justified because the outer surface layers will always be colliding supersonically, and thus will be decoupled from the rest of the stellar material. Furthermore, the strong shocks generated in the outer stellar layers should dissipate energy efficiently (Colgate, 1967).

If the total energy dissipated according to the above scheme, ΔE_T, exceeds the initial orbital kinetic energy in the center of mass $T_{\rm 0c.m.}$, then the stars will become bound to each other, will return for further collisions, and will eventually coalesce (Colgate, 1967). Consider a grazing collision between two stars of mass m and radius r_* in which a fraction f of the total mass lies in the overlapping collision region. A simple analysis in the center of mass frame indicates [cf. Colgate (1967) and Sanders (1970)]

$$\Delta E_T \sim f m(U_{\rm rel}/2)^2, \tag{6.31a}$$

and

$$T_{\rm 0c.m.} = m(v_{\rm rel}/2)^2, \tag{6.31b}$$

where $U_{\rm rel}$ is the relative *impact* velocity. If $\delta \ll 1$, so that the initial kinetic energy is small, then $U_{\rm rel}^2 \sim 2Gm/r_*$. If we also use the fact that $\langle v_{\rm rel}\rangle^2 = 2\langle v^2\rangle$ and use Eq. (6.30), we obtain an approximate criterion for a collision to produce a coalescence, $\Delta E_T \geq T_{\rm 0c.m.}$:

$$f \gtrsim 2\delta. \tag{6.32}$$

Because of the smallness of δ for globular clusters, the first collision a star undergoes will typically bind it to its collision companion. Only grazing collisions, which have the largest cross section, need be considered.

We can estimate an upper limit to the time interval between the first collision and final coalescence, Δt_c.

The orbital period P of two stars of mass m and orbital binding energy E is given by Eq. (4.3), with $M \to m$. Since the dissipated energy probably increases for each successive collision, the total time Δt_c is less than twice the first orbital period, as collisions occur more and more frequently due to increasing $|E|$. Since $|E|/m \sim \Delta E_T/m \sim \langle v^2 \rangle$ for the first period,

$$\Delta t_c \lesssim 2\pi t_{\rm hydro}\, \delta^{-3/2} \sim 30\ {\rm yr} \left(\frac{\langle v \rangle}{10{\rm km\ s^{-1}}}\right)^{-3/2} \left(\frac{m}{M_\odot}\right), \quad (6.33)$$

where $t_{\rm hydro} \equiv (Gm/r_*^3)^{-1/2}$ is the oscillation time of a star. Note that Δt_c does not depend upon stellar radius r_*. The number of collisions before final coalescence is $< (Gm^2/r_*)/\Delta E_T \sim \delta^{-1}$.

We next analyze what happens as coalescence occurs. If Eqs. (3.7). (6.26), (6.27), and (6.30) are combined, the ratio of the relaxation timescale to the collision timescale for equal mass stars is found to be

$$\frac{t_{rh}}{t_c} \sim \frac{2\delta(1+\delta)}{\log(0.4N)} . \quad (6.34)$$

While $\delta \ll 1$, we may assume that the dynamical behavior of coalesced stars is always in thermal equilibrium with the remaining stars.

If the main sequence lifetime $t_{\rm ms}$ of a star is less than the time to its next collision, t_c, the star will evolve off the main sequence. Because of violent hydrogen mixing, the coalescence of two stars probably produces a new massive star whose age on the main sequence starts at zero [cf. Sanders (1970)]. The ratio of t_c to $t_{\rm ms}$ for $m < 10 M_\odot$ may be expressed as [cf. Eqs. (2.3) and (6.29)]

$$\frac{t_c}{t_{\rm ms}} = 400 \left(\frac{N_c}{10^5}\right)^{-1/2} \left(\frac{R_c}{5{\rm pc}}\right)^{5/2} \left(\frac{m}{M_\odot}\right)^{5/2} \left(\frac{r_*}{R_\odot}\right)^{-1} . \quad (6.35)$$

As we shall see in Sec. VI.D.2, collisions do not become important until N_c and R_c become small, leading to the result that $t_c \ll t_{\rm ms}$ in the collision regime. For $m > 10 M_\odot$, the inequality is even stronger. Thus, unlike many situations in galactic nuclei (cf. Sanders, 1970), stars in globular clusters lack sufficient time to evolve off the main sequence once collisions become important [until "saturation" occurs; cf. Eq. (6.45)].

The nature of the massive stars built up from collisions and coalescence in globular clusters is difficult to calculate. It is easily shown [cf. Eq. (6.29)], that the timescale for stars to come into internal thermal equilibrium t_{th} [cf. Eq. (6.7)] is substantially longer than t_c in the collision regime for globular clusters. Thus stars are far out of thermal equilibrium and any sensible mass radius relation for the built-up stars, e.g.,

$$\frac{r_*}{R_\odot} = \left(\frac{m}{M_\odot}\right)^{\mu} , \quad (6.36)$$

poses a formidable task for detailed calculation. In contrast, many interesting cases in galactic nuclei, where $t_{th} \ll t_c$, allow one to assume the main sequence relation $\mu \sim 0.7$ [cf. Sanders (1970)], a relation completely unjustified in globular clusters. As we shall see, the most massive objects which can be formed are quite sensitive to Eq. (6.36).

2. Evolution of cluster cores: The collision regime versus the evaporation regime

The evolution of globular cluster cores evolving under the influence of evaporation and collisions may be modeled approximately by averaging variables, e.g., n, $\langle v^2 \rangle$, over the entire core and using characteristic values for these variables. Then, approximate differential equations for the evolution of the number of core stars, $N_c(t)$, average stellar mass $m(t)$, and core energy $E_c(t)$ are (in the remainder of this section we follow the work of Fall and Lightman, 1977)

$$\dot{N}_c = -\frac{N_c}{\gamma t_{rh}} - \frac{N_c}{t_c} , \quad (6.37a)$$

$$\dot{m} = \frac{m}{t_c} , \quad (6.37b)$$

$$\dot{E}_c = \frac{-N_c \epsilon}{t_c} = \frac{E_c}{t_c} . \quad (6.37c)$$

The first term in Eq. (6.37a) expresses the familiar stellar evaporation (cf. Sec. V.E), where γ is ~50 for an essentially single-component system. The second term in Eq. (6.37a) expresses the reduction in N_c for each stellar collision. Equation (6.37b) expresses the build-up of the average stellar mass due to collisions and coalescence. Note that in the absence of evaporation, Nm = const, as it should. Equation (6.37c) expresses the fact that each collision between a pair of unbound stars removes an energy $\sim\epsilon$ from the orbital kinetic energy of the cluster (see Sec. VI.B.5). Additional energy dissipated on successive collisions of stars after the initial binding collision comes out of the internal energy of the binary rather than out of the cluster orbital energy; dissipation due to tidal encounters between unbound stars would accelerate core collapse and is ignored here.

From Eqs. (6.19), but with an additional term $2\dot{m}/m$, and Eqs. (6.37b) and (6.37c), one easily deduces a relation between m, R_c, and N_c:

$$R_c \propto m N_c^2 . \quad (6.38)$$

Until collisions become important and m begins increasing, $R \propto N^2$, as in the collision-free evaporation regime.

From Eq. (6.37a) it is clear that collisions dominate when $t_c \ll \gamma t_{rh}$. Using Eq. (6.34) we can then divide the evolution into two regimes, depending on the size of the "collision parameter,"

$$\beta = \frac{\log(0.4N_c)}{2\gamma\delta} . \quad (6.39)$$

For $\beta \gg 1$, a stellar system is in its "evaporation regime" and for $\beta \ll 1$ it is in its "collision regime." Galactic nuclei are clearly in the collision regime ($\beta \sim 10^{-2}$) while observed globular clusters ($\beta \sim 100$–500) have not yet evolved into their collision regime. (However, as shown in Sec. VII. B, many globular clusters could well have already collapsed and dissolved, passing through the collision regime.) While clusters are in the evaporation regime, Eqs. (5.38)–(5.42) hold and show that β decreases monotonically with decreasing

N_c, $\beta \propto N_c \log(0.4N_c)$. Once $\beta \lesssim 1$, Eqs. (6.37a), (6.37b), and (6.38) give

$$m \propto N_c^{-1}, \tag{6.40a}$$

$$R_c \propto N_c, \tag{6.40b}$$

so that β continues to decrease.

An important question is: How many stars are left in the cluster when collisions first become important? To obtain this critical number $N_{\rm crit}$ one "evolves" the cluster through the evaporation regime, where m, $r_* \sim$ const, $R_c \propto N_c^2$, until $\beta \sim 1$, obtaining

$$N_{\rm crit} \log(0.4N_{\rm crit}) \sim 1 \times 10^3 \left(\frac{\gamma}{50}\right)\left(\frac{r_*}{R_\odot}\right) \times \left(\frac{N_{c0}}{10^5}\right)^2 \frac{R_{c0}}{5\,\mathrm{pc}}^{-1}, \tag{6.41}$$

where N_{c0} and R_{c0} are the initial values of the number of stars and core radius, respectively. The actual size in parsecs of R_{c0} enters Eq. (6.41) because the stellar radius introduces a length scale. Eqation (6.41) indicates that $N_{\rm crit}$ might be in the range ~100–1000 for typical globular clusters. A similar conclusion has been obtained by Lecar (1976). Evidently, buildup of massive stars through collisions and coalescence is not now occurring in the observable portion of globular cluster cores, where $N_c \gtrsim 10^4$.

We point out that the above normalizations and values apply only to one-component cluster cores. As is discussed in Sec. V.E.2, it is quite possible that a small, self-gravitating subsystem of heavy stars in multicomponent clusters could evolve into its own collision regime, well ahead of the rest of the cluster. Equation (6.41) can then be applied to the subsystem, if the rhs is evaluated when the subsystem begins its self-evaporative evolution (cf Sec. V.E.2). The results may be expressed in a form very similar to Eqs. (6.6) and (6.15b) in Sec. VI.B; $N_{\rm crit}$ for physical collisions is somewhat *smaller* than the value of a few hundreds for tidal dissipation to become important. *This represents an upper limit to the size of a massive object which could be formed.* The dynamical influence of the resulting singularity must then be considered (cf. Sec. VI.F), but may be unimportant until the rest of the cluster has also evolved substantially (cf. Sec. VII.B).

3. Heavy-mass runaway and limits to mass growth

It is easy to show that a strong instability exists in which the most massive stars increase their size at a greater rate than average stars increase their size, because the former have greater gravitational focusing and larger physical size. This result was first illustrated in one of the Monte Carlo runs of Sanders (1970). Consider a larger than average star of mass $M \gg m$ and radius $R_* \gg r_*$. Then Eq. (6.29) indicates that the time for M to collide with an average star satisfies $T_c \sim (r_*/R_*)(m/M)t_c$. Thus

$$\dot{M} = \frac{m}{T_c} \sim \left(\frac{R_*}{r_*}\right)\left(\frac{M}{m}\right)\frac{m}{t_c}. \tag{6.42}$$

Combining Eqs. (6.36), (6.37b), and (6.42), we obtain

$$\frac{dM}{dm} \propto \left(\frac{M}{m}\right)^{1+\mu}, \quad M \gg m. \tag{6.43}$$

Thus, as long as the effective radius of a star increases with increasing mass, $\mu \gtrsim 0$, M will achieve an infinite value for finite m.

What are the limits to growth of the largest mass in the system? The obvious maximum limit is $mN_{\rm crit}$. However, a lower limit is probably realized. As first pointed out by Colgate (1967), as M increases, its mass per unit area decreases. Eventually, a collision between it and an average star of mass m will not dissipate enough energy to bind the two together in a bound system. We can obtain an approximate relation for this "saturation mass" $M_{\rm sat}$ by equating the product of the mass swept out of the massive star M by m and the impact velocity squared of m at M to the orbital kinetic energy in the center of mass system (neglecting central mass concentration in M):

$$\left(\frac{M}{R_*^2 r_*^2}\right)\left(\frac{GM}{R_*}\right) \sim \epsilon. \tag{6.44}$$

Using Eqs. (6.30) and (6.36), we obtain for Eq. (6.44)

$$\frac{1}{2}\left(\frac{M_{\rm sat}}{m}\right)^{3\mu-2} \delta \sim 1, \tag{6.45}$$

where the factor of $\frac{1}{2}$ is probably not reliable, but chosen to agree with approximate numerical results of Sanders (1970). Equation (6.45) indicates the important fact that *the largest mass which can be built up as a result of collisions and coalescences depends crucially on the mass-radius relation (value of μ)*. For collisions between stars of equal mass ($m = M$), Eq. (6.45) is still approximately valid, if interpreted as the onset of the regime where collisions are disrupting instead of coalescing ($\delta > 1$). Typically δ and M/m both increase in time until Eq. (6.45) is satisfied, at which point the growth of M dramatically slows down and M/m begins decreasing.

4. Results of model calculations

Simple model calculations by Fall and Lightman (1977) for clusters in which all stars remain in equipartition assume that negligible mass loss from stars occurs in the collision–coalescence processes and that binding energy per unit mass in coalesced stars is conserved, $r_* \propto m(\mu = 1)$, as was assumed by Colgate (1967). It is found that Eq. (6.41) is a good approximation for the number of average mass stars at the onset of the cluster collision regime. A few large stars always experience a runaway. In a typical model with $N_{c0} = 2 \times 10^5, R_{c0} = 3.5\,\mathrm{pc}, m_0 = 0.5M_\odot, \gamma = 50$, the most massive star saturates at $M \sim 35M_\odot$, at which point there are ~600 stars of average mass $m \sim 3M_\odot$, and $\delta \sim 0.2$. Subsequent evolution of the system is very uncertain because of the small numbers of stars, and effects of binary formation, but the system may evolve into 25–50 stars, each of mass 20–40 $M_\odot$. Similar calculations for stellar collisions in a small subsystem of heavy stars yield a smaller saturation mass for the

most massive star, plus a much smaller total number of stars.

E. Dynamical influence of a massive black hole in a globular cluster

Since massive black holes may form as the end product of core collapse in spherical stellar systems, we consider in this section the dynamical behavior of a large N-body system containing a massive collapsed object at its center. The results may be applicable to fully evolved galactic nuclei as well as to globular clusters, if black holes form in these systems. Massive black holes may also form primordially during the early gas-dynamic collapse and fragmentation stages of globular clusters and other bound systems in the early universe. Although black hole masses will be normalized to $10^3\,M_\odot$ in this section we point out that the dynamical calculations of core collapse, Secs. VI.B and VI.D suggest ~100 $M_\odot$ as a more reasonable upper limit to the size of a central black hole which can be formed in a globular cluster.

1. Distribution of stars around a central black hole

Peebles (1972a, b) in his pioneering analysis of this problem, pointed out that stars in the core of a stellar system will be drawn toward the center by the potential field of the black hole. The resulting "cusp" in stellar systems containing massive black holes may provide a relatively clean *dynamical* probe for massive collapsed objects in N-body systems. Peebles suggested that the stellar density varied as a power law in the cusp region $r_t<r<r_a$. Here r_a is given by

$$r_a\sim\frac{GM}{v_m^2}\sim 4.3\times10^{-2}\,\mathrm{pc}\;M_3(v_m/10\,\mathrm{km\ s^{-1}})^{-2} \tag{6.46}$$

and is the "capture" radius within which core stars with velocity dispersion v_m^2 are bound to the black hole of mass $M(\equiv M_3\times10^3\,M_\odot)$, and $r_t\ll r_a$ is the radius at which stars are tidally disrupted by the black hole. Beyond r_a the gravitational field of the hole has little influence on the core density, which maintains a nearly constant value of n_c. All stars are assumed to have the same mass m, with $m\ll M\ll M_c$, where M_c is the total core mass. If these stars have a characteristic radius r_* then we have, approximately,

$$r_t\sim r_*\left(\frac{M}{m}\right)^{1/3}\sim 2\times10^{-7}\,\mathrm{pc}\;(r_*/R_\odot)(m/M_\odot)^{-1/3}M_3^{1/3}. \tag{6.47}$$

The distribution of stars in the cusp region is established by a steady, *inward* drift of stars from the isothermal core at $r\gtrsim r_a$ into $r<r_a$ to maintain a constant, central star distribution in the face of continual tidal disruption at $r\sim r_t$. The inward, net diffusion rate of stars $\mathcal{F}$ toward the black hole is maintained by the local, two body, small-angle scattering of stars in their mutual gravitational potential fields. As energy and angular momentum are exchanged in these collisions, some stars lose energy and drift closer to the black hole while other stars gain energy and move out into the core. On net, the destruction of bound stars (with respect to the ambient core) at $r\sim r_t$ with negative energy results in an *outward* flux of energy $\mathcal{E}$ from the cusp into the core. The presence of a star "sink" at the center of the cluster results in significant departures from thermal equilibrium there.

The inward flux of stars $\mathcal{F}$ and outward flux of energy $\mathcal{E}$ leads to a state of dynamical equilibrium in the cusp, not thermal equilibrium. Consequently the distribution function is more appropriately described by a power-law function of the form

$$f(E)=\kappa|E|^p, \tag{6.48}$$

with κ and p nearly constant in the self-similar region $r_t\ll r\ll r_a$, far from the boundary zones (Peebles, 1972b). Equation (6.48) yields a density profile of the form

$$n(r)\propto r^{-(p+3/2)}. \tag{6.49}$$

Recently, calculations first performed by Bahcall and Wolf (1976) and later by Shapiro and Lightman (1976) and Lightman and Shapiro (1977) have shown that the appropriate density law in the self-similar cusp zone $r_t\ll r\ll r_a$ is

$$n(r)\simeq n_c(r/r_a)^{-7/4}, \tag{6.50}$$

which corresponds to the power-law phase space density distribution with $p\simeq\frac{1}{4}$.

A simple scaling argument (Shapiro and Lightman, 1976), which employs Eqs. (5.12a), (5.12b), (5.13) in Sec. V.A, together with the discussion immediately preceding these equations, can be used to obtain Eq. (6.50). This scaling argument assumes for simplicity that the distribution of stars in the cusp is nearly isotropic [i.e., $f=f(E)$] and neglects the consumption of low-J, highly eccentric stars which pass within r_t at pericenter. The analysis distinguishes between the net diffusion timescales associated with star and energy transport in the cusp (cf. Sec.V.A.2). Since the energy (per unit mass) of a typical bound star orbiting the black hole at radius r is $E\simeq -GM/r$, the two timescales are related by

$$t_{\mathcal{E}}\propto t_{\mathcal{F}}r^{-1} \tag{6.51}$$

from Eq. (5.13). The proportionality constant in the above expression can be obtained by noting that the absence of outgoing stars at r_t implies that the net diffusion time for stars to move from $2r_t$ to r_t equals the timescale for their (negative) energy to decrease by a factor of 2. Thus $t_{\mathcal{E}}(r_t)=t_{\mathcal{F}}(r_t)$ and from Eq. (6.51)

$$t_{\mathcal{E}}(r)\sim(r_t/r)t_{\mathcal{F}}(r). \tag{6.52}$$

For $r>r_t$, we have $t_{\mathcal{E}}(r)<t_{\mathcal{F}}(r)$, and according to our discussion in Sec. V.A, we may equate $t_{\mathcal{E}}(r)$ to the local relaxation timescale at r:

$$t_{\mathcal{E}}(r)\sim t_r(r)\sim\frac{\langle v^2\rangle^{3/2}}{G^2m^2n}. \tag{6.53}$$

In Eq. (6.53) n is the local density at r, and the (slowly varying) dimensionless logarithmic factor in the denominator of t_r is ignored. For bound stars near the black hole $\langle v^2\rangle\sim GM/r$ so Eqs. (5.12b) in Sec. V.A, (6.52) and (6.53) yield $n(r)\propto r^{-7/4}$ in agreement with Eq. (6.50).

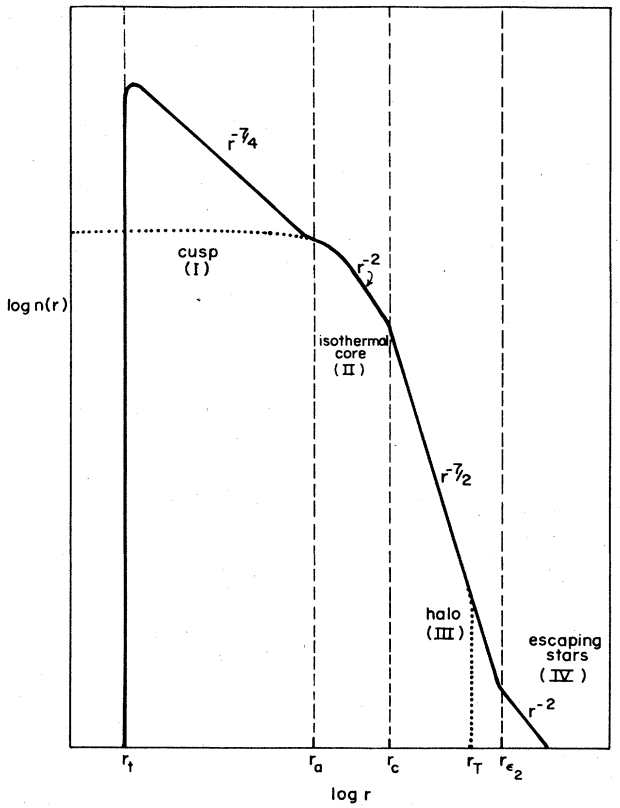

FIG. 20. The stellar density $n(r)$ as a function of radius r in an isolated spherical cluster containing a massive, central black hole. In the absence of a black hole, the isothermal core extends from $r=0$ to the core radius at $r=r_c$ and there is no cusp (dotted line in I). In the presence of the galactic tidal field, the density falls sharply at the galactic tidal radius r_T (dotted line in III). See text for discussion of the various regions. From Shapiro and Lightman (1976).

The entire run of the stellar density profile in an isolated, spherical cluster containing a central black hole is illustrated schematically in Fig. 20. The behavior of $n(r)$ in the isothermal zone $r_a \lesssim r \lesssim R_c$ and in the halo $r \gtrsim R_c$ was previously described in Sec. V.A. There it was noted that the density in a typical cluster in our galaxy falls rapidly to zero at some finite radius $r_T < r_{\epsilon_2}$ due to the galactic tidal field. To detect a massive black hole in a cluster it is necessary to resolve the central cusp region $r \lesssim r_a$ in the cluster core. If the cluster is located a distance d from the earth, with the cusp subtending an angle θ_a, we have from Eq. (6.46)

$$\theta_a \sim 1''(d/10\,\mathrm{kpc})^{-1}(v_m^2/100\,\mathrm{km^2\ s^{-2}})^{-1}M_3\,, \tag{6.54}$$

which must be compared with the "seeing" disk (i.e., resolution limit) θ_s of an optical telescope: $\theta_s \sim 1''$ for optimal ground based observations and ~0.03'' for observations with an LST, i.e., a large space telescope (Bahcall and Wolf, 1976). The conservative criterion established by Bahcall and Wolf (1976) for believing that a black hole is present in a cluster (i.e., the number of stars within a projected angular radius θ_s from the cluster center is at least F times the unperturbed value for the core, where $F \simeq 3$–10) yields for the minimum detectable black hole mass the value

$$M_{(\mathrm{detectable})} \simeq 5\times 10^3 M_\odot \left(\frac{F}{10}\right)^{4/7}\left(\frac{\theta_c}{5''}\right)^{4/7}\left(\frac{\theta_s}{1''}\right)^{3/7}\frac{v_m^2}{10^2\ \mathrm{km^2\ s^{-2}}}, \tag{6.55}$$

where θ_c is the angular radius of the cluster core. Equation (6.55) is obtained by comparing the total number of stars within θ_s for an unperturbed (~ constant) core density profile n_c with an approximate representation of the stellar density profile for a cluster core containing a massive black hole

$$n(r) \simeq n_c[1+(r_a/r)^{7/4}]\,. \tag{6.56}$$

Apparently, ground based observations are only sensitive to black hole masses greater than $5\times 10^3 M_\odot$ while LST observations can detect masses greater than $10^3 M_\odot$.

Recently, optical determinations of the central surface density profiles of several globular clusters containing x-ray sources indicate that if a central black hole is present, its mass must be less than $\sim 10^4 M_\odot$. This conclusion is generally consistent with the results of Bahcall *et al.* (1975) in the case of NGC 7078 (M15), of Bahcall (1976) in the case of NGC 6624, and of Bahcall and Hausman (1976) in the case of NGC 6440 and 6441. It is not clear whether the brightness excess observed in M15 [and also found in other x-ray globular clusters (Bahcall and Hausman, 1976)] represents a concentration of stars at the center or some other source of optical light (gas?).

As mentioned above, the analysis leading to Eq. (6.50) explicitly ignores the removal of high-energy ($E \gg E_t \equiv -GM/r_t$) low angular momentum stars, satisfying $J \lesssim J_{\min}(E) \equiv [2(E+GM/r_t)]^{1/2} r_t \simeq (GMr_t)^{1/2}$, which move in highly eccentric orbits with large apocenter distances $r \gg r_t$ but which move within r_t at pericenter. The removal of these stars which enter the so-called "loss-cone" in J space is significant and indicates the two-dimensional nature of the problem, i.e., $f=f(E,J)$. Recently, Lightman and Shapiro (1977) presented an approximate, analytic analysis of the two-dimensional Fokker–Planck equation describing diffusion in energy E and angular momentum J for bound stars in the cusp, i.e., Eq. (3.14). This two-dimensional equation has been examined more recently by Ipser (1978), using numerical integrations, valid for $r < r_{\mathrm{crit}}$ (see below), and by Shapiro and Marchant (1978), using more exact Monte Carlo techniques. The orbital period $P(E)$ in Eq. (3.14) is now given by $P(E) = 2\pi GM/(-2E)^{3/2}$. Equation (3.14) is subject to the boundary conditions that (i) $f=0$ for $J > J_{\max}(E) \equiv GM/(-2E)^{1/2}$, where $J_{\max}$ is the angular momentum of a circular orbit at energy E, (ii) no stars cross the "loss cone" at $J \equiv J_{\min}(E)$ from *lower* J, and (iii) the unbound core stars satisfy a Maxwell–Boltzmann distribution with rms velocity v_m.

The basic results of the above analyses are as follows: (i) A self-consistent solution exists for which the distribution function is essentially isotropic for large $J[J_{\min} \ll J \lesssim J_{\max}(E)]$, and decreases only logarithmically with J for smaller J, due to capture at $J_{\min}(E)$. (ii) Loss-cone effects are significant inside the radius r_{crit} at which j_2, the rms angular momentum trans-

ferred to a star in one orbital period, equals $J_{\min}$. (iii) The total consumption rate of stars, F, is roughly the total number of stars inside $r_{\rm crit}$ divided by the relaxation time at $r_{\rm crit}$. In some cases $r_{\rm crit} > r_a$ and the dominant contribution to F comes from unbound stars (see below). (iv) The stellar density distribution in the region $r \gg r_t$ satisfies $n(r) \simeq n_c[1+(r_a/r)^{p+3/2}]$, where n_c is the ambient density of unbound stars in the core and p is $\frac{1}{4}$ for $r \gg r_{\rm crit}$ [cf. Eq. (6.60)], and decreases inside $r_{\rm crit}$. A modification of the simple scaling argument of Eq. (5.12b) to allow for a sink term due to loss-cone consumption on the right-hand side, in the region $r \ll r_{\rm crit}$, yields the result (Ipser, 1978):

$$\frac{d}{dr}\left(\frac{nr^2}{t_e}\right) = \frac{nr}{\beta t_e}\ , \quad r \ll r_{\rm crit}\ , \tag{6.57}$$

where β is the ratio of (the effective) loss-cone diffusion timescale to energy diffusion timescale. Equation (6.57) indicates that p must decrease somewhat as r decreases and that the value of p is sensitive to the value of β unless $\beta \gg 1$. However, the detailed Monte Carlo computations of Shapiro and Marchant (1978) indicate that $\beta \gg 1$ and that the results of Lightman and Shapiro (1977), which give p logarithmically decreasing below $\frac{1}{4}$ with increasing $|E|$, are substantially correct. Here and above, we can associate a mean radius $r \sim GM/|E|$, with each energy E. Frank and Rees (1976) have independently obtained results consistent with conclusions (i)–(iii) above. Conclusion (iv) agrees with more exact earlier calculations of Bahcall and Wolf (1976) in the region $r \gg r_{\rm crit}$.

2. Consumption rate of stars by a massive black hole

As mentioned in conclusion (iii) above, the consumption rate of bound stars in the cusp, F, is given approximately by (Frank and Rees, 1976; Lightman and Shapiro, 1977)

$$F \simeq \frac{9.0}{\ln(E_t/4E_{\rm crit})}\left(\frac{r_t}{r_a}\right)(n_c r_a^3)\left(\frac{GM}{r_a^3}\right)^{1/2}\left|\frac{E_{\rm crit}}{E_a}\right|^{5/4}$$

$$\sim \frac{N_r}{t_r}\bigg|_{r=r_{\rm crit}} \quad (r_a > r_{\rm crit})\ , \tag{6.58a}$$

$$\sim 0.6\times 10^{-9} M_3^{61/27} n_{c*}^{-7/6} R_{c*}^{-49/9} \text{ stars yr}^{-1}\ . \tag{6.58b}$$

In Eqs. (6.58), $N_r \sim n(r)r^3$ is the total number of stars within r, t_r is the local relaxation time at r, and $r_{\rm crit} \equiv -GM/E_{\rm crit}$ is the critical radius corresponding to the critical energy $E_{\rm crit}$ at which $j_2(E)$ [cf. Eq. (6.22)], the rms angular momentum transferred to a star in one orbital period via stellar encounters, equals $J_{\min}(E)$.

The radius $r_{\rm crit}$ is located where $q \equiv (j_2/J_{\min})^2 = 1$. For $q \ll 1$ stars can diffuse into the loss cone $J \leq J_{\min}$. For $q \gg 1$ the step size of the random walk in J space, j_2, is larger than the cone size, and only a fraction $\sim q^{-1}$ of the stars in the ring $J_{\min} < J < J_{\min} + j_2$ can jump into the cone each orbital period (cf. Fig. 21). Setting $q = 1$ gives $E = E_{\rm crit}$:

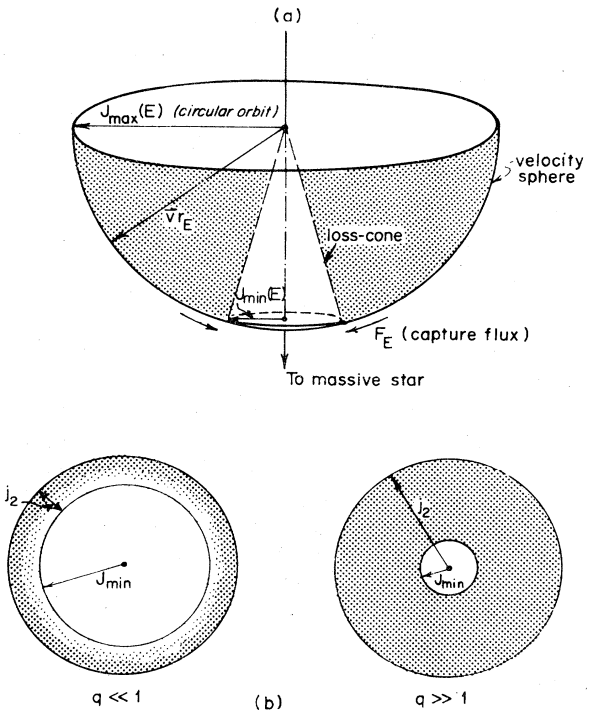

FIG. 21. (a) Velocity distribution for ingoing stars with fixed energy E, radius $r_E \equiv GM/2|E|$, and speed $v = (2|E|)^{1/2}$. Stars with angular momentum J in the range $J_{\min}(E) \ll J \leq J_{\max}(E)$ are distributed nearly uniformly on the velocity sphere, where $J_{\min}(E) \equiv [2(E + GM/r_t)]^{1/2} r_t$ and $J_{\max}(E) \equiv GM/(2|E|)^{1/2}$. Stars scattered into the loss cone with $J \leq J_{\min}(E)$ may be removed from the system in an orbital period. (b) The velocity sphere viewed from below. The quantity j_2 represents the dispersion in ΔJ suffered by a star in one orbital period due to stellar encounters; $q(E) \equiv j_2^2/J_{\min}^2(E)$. The phase space density of stars outside the loss cone falls rapidly with J as $J \to J_{\min}$ when $q \ll 1$ (the "diffusion" limit), but the density remains nearly uniform when $q \gg 1$ (the "pinhole" limit). In each dynamical time only stars in the ring $J_{\min} < J \lesssim J_{\min} + j_2$ may enter the loss cone. From Lightman and Shapiro (1977).

$$-E_{\rm crit} \simeq \frac{GM}{r_a}\left[7\ln\left(\frac{6}{11}\frac{M}{m}\right)\left(\frac{m}{M}\right)^2 n_c r_a^3 \frac{r_a}{r_t}\right]^{4/9}\ , \tag{6.59a}$$

$$\simeq -E_a(0.3 M_3^{20/27} n_{c*}^{-4/3} R_{c*}^{-32/9})\ , \tag{6.59b}$$

or, equivalently,

$$r_{\rm crit} \simeq 0.04 M_3^{7/27} n_{c*}^{1/3} R_{c*}^{14/9}\ . \tag{6.60}$$

The above expressions for $E_{\rm crit}$ and $r_{\rm crit}$ can be obtained approximately from Eqs. (6.22), (6.46), (6.50), and (6.53) together with the definitions of $J_{\min}(E)$, $\langle J\rangle \sim J_{\max}(E)$ and $P(E)$ given above. In Eqs. (6.58), (6.59), and (6.60) we have employed a dimensionless core density $n_{c*} \equiv n_c/(5\times 10^4\ \text{pc}^{-3})$ and a dimensionless core radius $R_{c*} \equiv R_c/(1\ \text{pc})$. For typical compact globular clusters $r_{\rm crit}/r_a \lesssim 0.1$.

On dimensional grounds alone, the ratio $N_r/t_r \equiv F_{\max}$, evaluated at any radius (or corresponding energy) in the cusp, is the maximum possible net inward flux of stars

in that radial interval r to $2r$, since no physical quantity can be transported on a timescale shorter than the local relaxation time in a large N-body system. Defining $F_E d|E|$ to be the net consumption rate of stars with energy between E and $E+|dE|$, then the total consumption rate for bound stars in the cusp is

$$F=\int_0^{|E_t|} F_E d|E| \ , \tag{6.61}$$

where $-E_t=GM/r_t$. One finds that F is determined at the radius $r_{\rm crit}$ (i.e., $F\sim F_{|E_{\rm crit}|}\cdot|E_{\rm crit}|\sim F_{\rm max}[E_{\rm crit}]$) since for $|E|>|E_{\rm crit}|$, F_E *increases* with decreasing $|E|$ according to the relation $F_E\sim F_{\rm max}(E)/|E|\propto|E|^{-2}$, while for $|E|<|E_{\rm crit}|$, F_E *decreases* with decreasing $|E|$ according to $F_E\sim|E|^{1/4}$. Qualitatively, at small radii $r\ll r_{\rm crit}$ (i.e., $|E|\gg|E_{\rm crit}|$) there are too few stars in the cusp to contribute significantly to the consumption rate, while at large radii $r\gg r_{\rm crit}$ (i.e., $|E|\ll|E_{\rm crit}|$) the condition that $j_2(E)\gg J_{\rm min}(E)$ effectively causes all but a small fraction $\sim q^{-1}(E)\propto|E|^{9/4}$ of the bound stars originally moving in the loss cone at apocenter to be scattered out of the loss cone by the time they reach the tidal radius near pericenter. The manner in which bound stars of a given energy E enter the loss cone $J\leq J_{\rm min}(E)$ is illustrated by the velocity phase space diagram in Fig. 21(b).

Occasionally, the ratio $r_{\rm crit}/r_a$ may exceed unity in an N-body system, and then the consumption of *unbound* core stars moving in hyperbolic orbits with constant rms velocity v_m about the black hole will dominate F. To lowest order it is adequate to analyze the capture of approximately isotropic, positive-energy, core stars in the collisionless gas approximation, originally considered by Zel'dovich and Novikov (1971) for noninteracting gas particles accreting onto black holes and by Hills (1975c) for stars tidally consumed by massive black holes in galactic nuclei. The consumption rate in this limit is given roughly by

$$F\sim\sigma n_c v_m\sim\pi r_t r_a n_c v_m, \quad r_{\rm crit}>r_a \tag{6.62}$$

where $\sigma\sim\pi b_{\rm min}^2$ is the cross section and $b_{\rm min}\sim J_{\rm min}/v_m\sim(GMr_t)^{1/2}/v_m$ is the impact parameter for capture at r_t. Numerically, the above rate gives

$$F\sim 5\times10^{-9}M_3^{4/3}n_{c_*}^{1/2}R_{c_*}^{-1}\ \text{stars yr}^{-1} \tag{6.63}$$

(Frank and Rees, 1976).

F. Dissolution of clusters with central singularities: The final state

The dynamical evolution of a large N-body system leads invariably to core contraction and collapse, which probably ends in the formation of a "singularity" at the center of the cluster. It is not possible at the present time to predict the exact nature of the final, dynamical "singularity" which forms at the cluster center; only the timescale of ~ 3–$20\ t_{rh}$ required for its appearance can be estimated with any confidence. It is possible that the final state following core collapse will be dominated by either a central, tight binary system or by a central, massive black hole. In either of these cases, the remaining cluster remnant will be "heated" by the central singularity, expand to large core radii, and eventually dissolve in the galactic tidal field, as discussed below.

If the central core forms a tight binary system, then the N-body simulation experiments indicate that the binary will grow tighter by absorbing a growing fraction of the total negative energy of the system. Through encounters with third bodies, the binary emits a continuous flow of (positive) energy to the ambient core, causing it to expand in compliance with the virial theorem (Hénon, 1961). A Monte Carlo calculation involving a large N-body system containing an artificial energy source at the center, representing a binary star system, has been performed by Hénon (1975). The calculation indicates that, following initial contraction and the onset of catastrophic core collapse, the collapse of the core is halted after a finite time and is eventually reversed. The entire stellar system then undergoes steady expansion, which proceeds indefinitely as more and more of the binding energy of the cluster is absorbed by the central singularity. Although the expansion decelerates with time as the cluster relaxation timescale steadily increases with the expansion, it appears that the cluster will ultimately dissolve completely, since tidal forces can remove the outermost, loosely bound stars with increasing ease (Wielen, 1971). The above considerations may be modified somewhat by the decreasing efficiency of the central binary (Sec. VI.B.4).

If a massive black hole forms at the cluster center following catastrophic core collapse, the dynamical fate of the cluster may be similar, since the massive black hole also acts as a source of (positive) energy for the ambient core stars. These core stars are heated via the consumption of bound, negative-energy stars in the cusp (assuming $r_{\rm crit}<r_a$; see Sec. VI.E). The outward flux of energy is achieved by small-angle, two-body encounters in the cusp: in these encounters, some stars lose energy, move closer to the black hole, and are eventually consumed, while the neighboring stars with which they interact gain energy and move outward from the cusp and into the ambient core (see Sec. IV.C). Two-body encounters in the ambient core thermalize this energy in a (central) core relaxation timescale t_{rc}, eventually causing the core to expand and the core density and velocity dispersion to decrease. For purposes of illustration we shall assume that the massive hole resides at the center of a moderately large $N(N>10^3)$ system.

Since the distribution and consumption of stars in the cusp proceeds on the local relaxation time in the cusp, $t_r=t_{rc}(r/r_a)^{1/4}$, which is more rapid than t_{rc} inside r_a, the steady-state cusp solution presented in Sec. VI.E applies at every moment during the quasisteady, reexpansion phase of the ambient core. Accordingly, the rate of energy deposited in the core by the central black hole, $\mathcal{E}$, may be determined from Eq. (6.61) and the discussion following it, yielding

$$\mathcal{E}=m\int_0^{|E_t|}F_E|E|d|E|\cong mF|E_{\rm crit}|\ln|E_t/E_{\rm crit}| \tag{6.64a}$$

or, substituting Eqs. (6.58) and (6.59),

$$\mathcal{E}\simeq(0.9\times10^{-9})\frac{GN_c m^2}{R_c}M_3^3 n_{c_*}^{-5/2}R_{c_*}^{-9}\ \text{yr}^{-1}\ . \tag{6.64b}$$

In deriving Eqs. (6.64) we assume that $r_{crit}/r_a \ll 1$ and that the dominant capture rate of stars by the black hole is due to bound stars in the cusp. The response of the ambient core to this outward flux of energy from the center can be evaluated by a simple homology model (Shapiro, 1977). The model represents a straightforward extension of Eqs. (5.38)–(5.42) in Sec. V.A, employed to analyze secular core contraction via stellar evaporation in the absence of a central black hole. Modifying these equations to account for the consumption of bound stars by the black hole, we may write

$$\dot{N}_c = \dot{N}_{esc} + F = -0.0074\frac{N_c}{t_{rc}} - F \ , \tag{6.65}$$

where $\dot{N}_{esc}$ is the escape rate of core stars due to evaporation, t_{rc} is the core relaxation time, and F is the rate of consumption by the black hole, and we have used Eq. (5.9) for the effective value of ν and t_{rc} as a representative relaxation time in the homogeneous core. With a massive black hole present in the cluster center, the total energy E_c of the core constantly increases, according to Eqs. (6.64), $\dot{E}_c = \mathcal{E}$. The instantaneous magnitude of E_c is not influenced by the black hole provided $M \ll N_c m$. Using Eq. (6.19) and substituting Eqs. (6.64) and (6.65) yield

$$\frac{\dot{R}_c}{R_c} = \frac{2\dot{N}_c}{N_c} + 0.5\frac{F}{N_c}\ln\left(\frac{r_{crit}}{r_t}\right)(M_3^{20/27} n_{c*}^{-4/3} R_{c*}^{-32/9}) \ . \tag{6.66}$$

The first term in Eq. (6.66) drives the secular contraction of the core in the absence of the black hole ($F=0$), resulting in total core collapse in a time $t \sim 40 t_{rc}$ (see Sec. V.A). The second term causes core contraction to cease and reexpansion to occur. The mass of the central black hole will increase somewhat with time due to the consumption of stars and/or gas. If, for example, the total consumption rate by the black hole originates from tidally disrupted stars, we may write

$$\dot{M}_3 = 10^{-3}\left(\frac{m}{M_\odot}\right) F \ . \tag{6.67}$$

The three differential equations, Eqs. (6.65)–(6.67), have been solved numerically (Shapiro, 1977) and the results are illustrated in Fig. 22. In the figure we plot R_{c*} as a function of time (in units of the initial core relaxation time $t_{rc0} = 6\times10^6$ yr) for different initial values of M_3 between 0.1 and 1.0, assuming $n_{c*0} = 0.2$ and $R_{c*0} = 0.5$ at $t=0$ and $m = M_\odot$. As demonstrated in the figure, for sufficiently small black holes, stellar evaporation dominates initially, driving core contraction for a time $t \sim 40\ t_{rc0}$, at which time the contraction is halted and reversed. In this circumstance, contraction terminates when the core radius falls to a value $R_{c_{min}}$ determined by setting $\dot{R}_c$ equal to zero. The result is

$$\frac{R_{c_{min}}}{R_{c_0}} \cong 0.9\times10^{-2}\left\{\frac{M_3^2 n_{c*0}^{-2} R_{c*0}^{-6}}{[\ln(N_{c_0}/2)]^{2/3}}\right\} \ , \tag{6.68}$$

after which reexpansion proceeds asymptotically to infinity according to

$$\frac{R_c}{R_{c_{min}}} \simeq [1 + 2.8\times10^{-14}(M_3^3 n_{c*,min}^{-7/2} R_{c*,min}^{-12})t]^{2/3} \rightarrow t^{2/3} \ \text{as} \ t\rightarrow\infty \ . \tag{6.69}$$

For sufficiently massive black holes, stellar consumption dominates from the onset and the core expands according to Eq. (6.69), with $R_{c_0} = R_{c_{min}}$, etc. In all cases examined, the central black hole grows by less than 15% in mass during the entire lifetime of the cluster. During reexpansion, the number of core stars N_c decreases very slowly with time so that n_c varies almost as R_c^{-3} and $\langle v^2\rangle$ varies as R_c^{-1}. Apparently, stellar consumption functions as a self-regulating, dynamical dynamo whereby the core is driven outward to keep the consumption rate from destroying the cluster too rapidly. The ratio r_{crit}/r_a decreases with increasing time, insuring the validity of Eq. (6.58) for the capture rate F.

The end-point evolutionary state of a globular cluster containing a massive central black hole is thus quite similar to the final state of a cluster containing a tight binary system in its core—namely, cluster reexpansion and, presumably, total dissolution. The situation is analogous to that pertaining in a stellar interior, where the

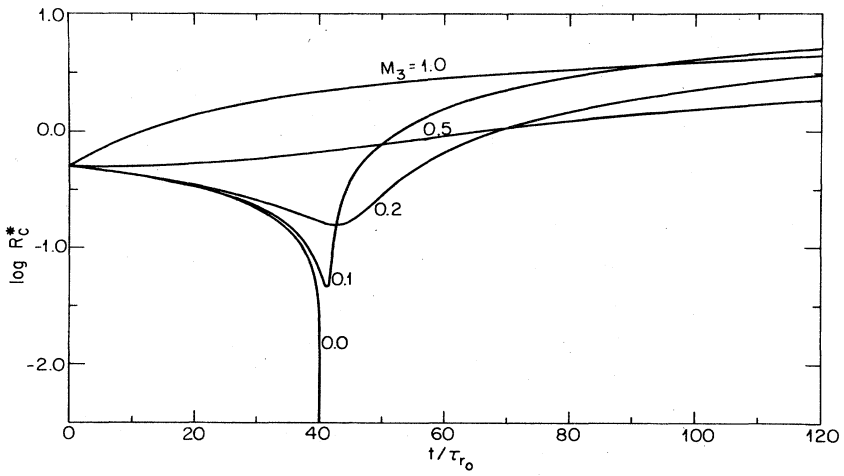

FIG. 22. The core radius R_c^* as a function of time t (in units of the initial relaxation time $\tau_{r\,0} = 6.2\times10^6$ yr) for a cluster with an initial core density $n_{c\,0}^* = 0.2$, radius $R_{c\,0}^* = 0.5$, and black hole mass M_3 between 0 and 1. Core parameters are expressed in the following nondimensional units: $n_c^* = n_c/(5\times10^4 \text{pc}^{-3})$, $R_c^* = R_c/(1\ \text{pc})$, $M_3 = M/(10^3 M_\odot)$. Massive central black holes invariably halt and reverse core collapse. From Shapiro (1977).

ignition of a new energy source at the center halts the contraction of the star. In the case of a massive, central black hole, the dissolving cluster will eventually leave behind a massive collapsed remnant, comparable in mass to the initial black hole. An important issue is whether the expanding cluster core can, in fact, "reabsorb" and dissolve (by evaporation) the residual halo, part of which was "frozen out" of the collapsing core prior to the formation of the central singularity (cf. Sec. VI.C). This question, raised again in Sec. VII.B following a statistical analysis of globular cluster relaxation timescales, can be answered definitively only by detailed numerical calculations of advanced cluster evolution with a central singularity.

VII. OBSERVATIONAL EVIDENCE FOR THE EVOLUTION AND DEATH OF GLOBULAR CLUSTERS

A. Globular cluster x-ray sources

The recent discovery that x-ray sources may be associated with globular clusters (Giacconi *et al.*, 1974; Clark, Markert, and Li 1975; Markert, 1975; Grindlay *et al.*, 1976; Clark *et al.*, 1976) has stimulated new interest in the final dynamical evolution of globular clusters. The globular cluster x-ray sources appear to be different from the other known galactic x-ray sources: the cluster x-ray sources occur ~100 times more frequently per unit mass (Katz, 1975; Clark, 1975) and, in contrast to previously identified sources associated with luminous, young, Population I stars or with recent supernovae remnants, the cluster sources are optically related to the oldest (age $\sim 10^{10}$ yr), Population II stellar component in our galaxy. Their origin may thus be associated with late evolutionary or dynamical processes unique to old, globular cluster stellar systems.

At the present time there are seven "steady" x-ray sources identified with globular clusters (the clusters are NGC 1851; 6440; 6441; 6624; 6712; 7078; and Liller 1). At least two (probably more) of the $\gtrsim 30$ "bursting" x-ray sources are located in globular clusters. A detailed summary of the x-ray and optical data of the cluster x-ray sources has recently been presented elsewhere by Grindlay (1977); the data for the known x-ray burst sources have been compiled and reviewed by Lewin (1976) and by Lewin and Joss (1977). We therefore confine our comments here to several qualitative remarks. The spectra of the steady sources are similar and well-represented by exponentials with $kT \simeq 5$–8 keV. The x-ray luminosities in the energy band from ~2 to 10 keV all are in the range $\lesssim 8\times10^{35}$–3×10^{37} erg s^{-1}. The emission from the "steady" sources varies by factors of 3–10 over timescales of minutes to months. The x-ray burst sources emit at more or less regular intervals of hours to tens of hours; the intervals change by factors of ~2 or more. Typically, the x-ray burst sources have rise times $\lesssim 1$ sec, last several seconds to tens of seconds, and have luminosity factors of $\lesssim 2$ to 150 times the associated "steady" luminosity (for eight cases in which the latter has been measured). The majority of the known burst sources with positions determined to better than a few degrees are distributed along the galactic equator in a wide arc ($\lesssim 35°$) about the galactic center less than ~8° from the galactic plane. The known sources do not exhibit a globular cluster spatial distribution about the galaxy, and it has been argued that most burst sources cannot be located in globulars (Lewin, 1976). Very recently Johnson (1976) and Terzian and Conklin (1977) have reported the detection of several weak radio sources from the direction ($\lesssim 2'$) of 10 globular clusters, three of which are x-ray globulars.

Two classes of models have been proposed to explain x-ray emission from globular clusters: binary star systems, in which a normal primary transfers mass into a compact secondary, thereby generating x-ray emission (Katz, 1975; Clark, 1975), and supermassive black holes (~100–1000 $M_\odot$), which may reside at the centers of globular clusters and accrete gas ejected from old, late-type stars (Bahcall and Ostriker, 1975; Silk and Arons, 1975). In the binary star model, x-ray bursts may be associated with instabilities in the magnetosphere of accreting neutron stars (Lamb *et al.*, 1976) or with time-varying mass flow due to the preheating of the infalling gas by the emergent x-rays, which suppresses accretion, (Ostriker *et al.*, 1976; Sunyaev, 1976). In the supermassive black hole model, x-ray bursts may again be associated with x-ray preheating of infalling matter (Ostriker *et al.*, 1976; Grindlay, 1978) or with secular or thermal instabilities occurring in the main, innermost radiating regions of the gaseous accretion disk near the black hole. At the present time both classes of models appear generally consistent with the data, although both the dynamical considerations of the last section and the statistical analysis below suggest ~100 $M_\odot$ as the upper limit to the mass of a black hole which can be formed in globular clusters. The HEAO B x-ray satellite, scheduled for launch in 1979 and possessing a positional accuracy of 1″, may be able to rule out the massive black hole hypothesis if it locates the source far from the center of the core.

B. Death rate of globular clusters and evidence for evaporation and dissolution

Some remarkable conclusions about the evolution, collapse, and dissolution of globular clusters, supporting much of the theory, result from combining simple cosmological assumptions with a statistical analysis of the observational data on cluster relaxation times. As has been shown above, the theory (cf. Secs. V.E and VI) indicates that globular clusters evolve by relaxation and collapse to some sort of "singular state" in a finite time. When the finite radii of stars are taken into account, the singular state is probably one in which stellar collisions dominate the subsequent evolution and form one or more massive stars, unless there is a large population of initial binaries. If the end-point evolution is dominated by either the formation of a massive black hole or a central binary, the subsequent evolution may be much the same: ultimate and possibly rapid expansion of the cluster core (cf. Sec. VI.F). As suggested in Sec. VI.F, the expansion of the cluster core may, in fact, dissolve the entire cluster. In any

case, in a finite time the cluster may evolve into a regime in which it is no longer recognizable as a globular cluster, and we will say the cluster has then "died." We can test this hypothesis by examining the relationship between the death rate and existing cluster data. We closely follow here the work of Lightman *et al.* (1978).

At any given time t the remaining lifetime of the cluster, t', is taken to be some constant multiple of the current central relaxation time $t_{rc}(t)$ (cf. Sec. V.E),

$$t' = \eta t_{rc}(t) , \tag{7.1}$$

with t_{rc} decreasing in time to zero. In one-component systems Eq. (7.1) is (1) observed in the numerical experiments and (2) a consequence of the evaporation theory of core collapse. In systems with a continuous mass distribution, it may be true in some average sense, since t_{rc} is the only natural timescale. The remaining lifetime is more conveniently expressed in terms of t_{rc} than in terms of the mean relaxation time t_{rh} because observational data is more readily available for the former. After the initial violent relaxation (cf. Sec. IV) t_{rc} is some 10 times shorter than t_{rh}. The numerical experiments (cf. Sec. V.E) then indicate that η is expected to be approximately 100.

When clusters were formed long ago at cosmological time t_b (cf. Sec. II), the distribution in initial relaxation times (determined by the primordial masses and binding energies) determined a distribution of times at which each cluster was fated to die [cf. Eq. (7.1)]. One may define a globular cluster death function $q(t)$ such that $q(t)dt$ is the number of clusters destined to die between time t and $t+dt$, where t is measured from the "Big Bang". At times $t \gg t_b$, it is reasonable to assume that $q(t)$ evolved into a smooth functional form. In particular, $q(t)$ should contain no structure which distinguishes the present epoch, $t = t_0 \gg t_b$. The simplest hypothesis for the form of $q(t)$ at $t \gg t_b$ is a power law

$$q(t) \propto t^{-\alpha-1} \quad \text{for } t \gg t_b . \tag{7.2}$$

The number of clusters which will die in intervals around t in the future may be related to the number of clusters with current relaxation times in the interval t_{rc} to $t_{rc}+dt_{rc}$, $n(t_{rc})dt_{rc}$. Then, since $t = t_0 + t'$ (by definition of the remaining lifetime at the current epoch), one has the relation

$$n(t_{rc}) = \eta q(t_0 + \eta t_{rc}) . \tag{7.3}$$

Integrating Eq. (7.3) to obtain a cumulative distribution and using Eq. (7.2), one obtains

$$N(t_{rc}) = N_0 [1 - (1 + \frac{\eta}{t_0} t_{rc})^{-\alpha}] . \tag{7.4}$$

Here $N(t_{rc})$ is the number of clusters with central relaxation times $\leq t_{rc}$ and N_0 is the total number of clusters in a data sample, plus one to ensure a finite value for the longest observed relaxation time. The observed cumulative distribution $N^*(t_{rc})$ is obtained by simply ranking the observed clusters in order of increasing relaxation time. Parameters α and η/t_0 which best fit the data are then obtained by fitting $N(t_{rc})$ to $N^*(t_{rc})$.

Figure 23 from Lightman *et al.* (1978), gives the data

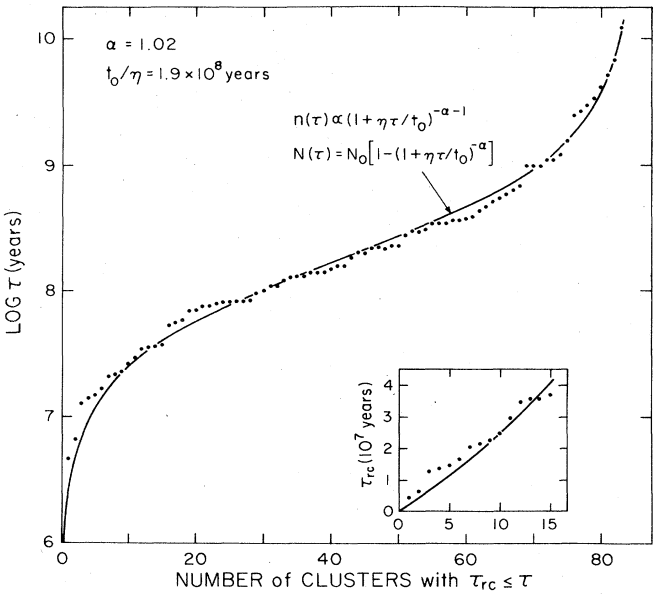

FIG. 23. Data (one dot per cluster) for 83 globular clusters for which central relaxation timescales are available. Clusters are sequentially ranked in order of increasing relaxation time. The theoretical cumulative distribution $N(\tau)$ for a pure power-law model has been fit to the data and is indicated by the solid curve. The inset shows the 15 clusters of shortest relaxation time plotted on a linear scale. The good fit for these clusters to an almost-straight line suggests that no new processes accelerate or retard the final stages of the evolution. From Lightman, Press, and Odenwald (1977).

for 83 clusters for which data are available, together with the best fitting theoretical curve for the data set,

$$\alpha_D = 1.02 , \tag{7.5a}$$

$$\eta_D = 79 \left(\frac{t_0}{1.5 \times 10^{10} \text{ yr}} \right) , \tag{7.5b}$$

where we have adopted a value $\sim 1.5 \times 10^{10}$ yr for the age of the universe, t_0. Monte Carlo simulations of a large number of independent sets of 83 clusters each, with each set an independent stochastic realization of the theoretical distribution, Eq. (7.4), indicate that the observed data set fits the theoretical distribution as well as ~50% of the Monte Carlo simulations. From these simulations one may also estimate the probable range of values of α and η/t_0 in the underlying theoretical distribution which could have yielded the observed values α_D and $(\eta/t_0)_D$ [cf. Eq. (7.5)]. The ranges containing $\frac{2}{3}$ of the likelihood are

$$0.7 \lesssim \alpha \lesssim 1.3 , \tag{7.6a}$$

$$54 \left(\frac{t_0}{1.5 \times 10^{10} \text{ yr}} \right) \lesssim \eta \lesssim 132 \left(\frac{t_0}{1.5 \times 10^{10} \text{ yr}} \right) . \tag{7.6b}$$

Additional Monte Carlo simulations indicate that an exponential function form for $q(t)$ fits the data set very poorly compared to the well-fitting power law form.

It is possible that the measured central relaxation timescales have little connection with the evolution of the cluster and that the above fit of the theory with the data (cf. Fig. 23) is merely a coincidence. However,

the high statistical significance of the fit, as indicated by the Monte Carlo simulations, plus the agreement between the fitted and theoretical values of η, suggest that the above theory of cluster deaths be seriously considered. The following implications and questions then follow: (i) Figure 23 implies that existing clusters are collapsing smoothly to some state in which they are no longer recognizable as globular clusters. There is no evidence for a class of sufficiently evolved postcollapse clusters (cf. Sec. VI.F) in the set of observed globular clusters. It is highly unlikely that such objects could mock up a distribution merging smoothly with that of Fig. 23. As suggested by the numerical calculations of cluster cores with central singularities (e.g., massive black holes and tight binary systems), postcollapse clusters evolve with entirely different homological reexpansion laws (see Sec. VI.F). In fact, a reanalysis which tests the possibility that a fraction of observed clusters could be in an expansion phase following core collapse shows that the data are inconsistent with this possibility, unless we live in a preferred epoch. In light of the numerical calculations the above analysis of the observational results has the following implication: assuming that we do *not* live in a preferred epoch, the likely cluster reexpansion and dissolution must presumably occur on sufficiently rapid timescales (much less than typical observed values of ηt_{rc} $\sim 10^9$–10^{10} yr) that reexpanding stellar systems quickly become too diffuse to be detected optically and hence do not contaminate Fig. 23 in significant numbers.

A serious challenge to this interpretation of the data is to explain, in detail, how the entire cluster can be dissolved after core collapse. It is conceivable that an expanding core, heated by a central singularity, could reabsorb and evaporate the residual ambient halo. If the central singularity is a massive black hole, the discussion in Sec. VI.F and Fig. 22 indicate that the cluster core could expand sufficiently rapidly to explain the data if $M_{\rm hole} \lesssim 100 M_\odot$, an upper limit also suggested by dynamical considerations of black hole formation (cf. Secs. VI.B and VI.D). In any case, detailed numerical calculations are required to settle this issue. (ii) If any singularities reside in observed clusters, formed, for example, from the early collapse of a small subsystem of heavy stars (cf. Secs. V.B, V.E, and VI.D), such small singularities have little effect on the evaporative evolution of the cluster during its observable lifetime. (iii) There is no evidence for clusters "hanging up" on the edge of collapse, as was the initial interpretation of Fig. 5. Such objects would produce a horizontal edge in the lower left corner of Fig. 23, which is not observed.

(iv) The number of clusters which have died between time $t < t_0$ and now, $\mathfrak{N}(t)$, can be estimated by integrating $q(t)$:

$$\mathfrak{N}(t) = N_0 \left[\left(\frac{t_0}{t} \right)^{\alpha} - 1 \right] . \tag{7.7}$$

If t is pushed back to a few t_b, then the total number of clusters which have died is a few to $\sim 10^3$ times the number of existing clusters, depending on the unknown value of t_b (see Sec. II).

ACKNOWLEDGMENTS

We are grateful to S. M. Fall, B. Flannery, A. Marchant, W. H. Press, G. Rybicki, E. E. Salpeter, and L. Spitzer, Jr. for useful discussions and helpful criticism. This work was supported in part by National Science Foundation Grant AST-75-21153.

REFERENCES

Aarseth, S. J., 1966, Mon. Not. R. Astron. Soc. **132**, 35.
Aarseth, S. J., 1974, Astron. Astrophys. **35**, 237.
Aarseth, S. J., 1975, in *Dynamics of Stellar Systems* (I.A.U. Symposium No. 69), edited by A. Hayli (Reidel, Dordrecht).
Aarseth, S. J., and D. Heggie, 1976, Astron. Astrophys. **53**, 259.
Aarseth, S. J., M. Hénon, and R. Wielen, 1974, Astron. Astrophys. **37**, 183.
Aarseth, S. J., and M. L. Lecar, 1975, Annu. Rev. Astron. Astrophys. **13**, 1.
Aarseth, S. J., and W. C. Saslaw, 1972, Astrophys. J. **172**, 17.
Aarseth, S. J., and N. J. Woolf, 1972, Astrophys. Lett. **12**, 159.
Agekian, T. A., 1958, Soviet Astron.–AJ **2**, 22 [Astron. Zh. **35**, 26 (1957)].
Allen, C. W., 1974, *Astrophysical Quantities* (Athlone, London).
Ambartsumian, V. A., 1938, Ann. Leningrad State Univ., No. 22.
Antonov, V. A., 1962, Vestn. Leningr. Gros. Univ. **7**, 135.
Arp, H. C., 1965, in *Galactic Structure*, edited by A. Blaauw and M. Schmidt (University of Chicago, Chicago).
Arp, H. C., and F. D. A. Hartwick, 1971, Astrophys. J. **167**, 499.
Bahcall, J. N., N. A. Bahcall, and D. Weistrop, 1975, Astrophys. Lett. **16**, 159.
Bahcall, J. N., and J. P. Ostriker, 1975, Nature **256**, 23.
Bahcall, J. N., and R. A. Wolf, 1976, Astrophys. J. **209**, 214.
Bahcall, N. A., 1976, Astrophys. J. Lett. **204**, L83.
Bahcall, N. A., and M. A. Hausman, 1976, Astrophys. J. Lett. **207**, L181.
Baker, N. H., 1965, Bamberger Veroff **4**, 122.
Bouvier, J., and G. Janin, 1970, Astron. Astrophys. **5**, 127.
Butler, D., 1975, Astrophys. J. **200**, 68.
Cantera, R., 1975, Astrophys. J. Lett. **200**, L63.
Chandrasekhar, S., 1942, *Principles of Stellar Dynamics* (Dover, New York).
Chandrasekhar, S., 1969, *Ellipsoidal Figures of Equilibrium* (Yale University, New Haven).
Christy, R. F., 1966, Astrophys. J., **144**, 108.
Clark, G. W., 1975, Astrophys. J. Lett. **199**, L143.
Clark, G. W., T. H. Markert, and F. K. Li, 1975, Astrophys. J. Lett. **199**, L93.
Clark, G. W., F. K. Li, C. Canizares, G. Jernigan, and W. H. G. Lewin, 1977, Astrophys. J., in press.
Clayton, D. D., 1968, *Principles of Stellar Evolution and Nucleosynthesis* (McGraw-Hill, New York).
Colgate, S. A., 1967, Astrophys. J. **150**, 163.
Cox, J. P., and T. R. Giuli, 1968, *Principles of Stellar Structure*, Vol. 2 (Gordon and Breach, New York).
Cuperman, S., S. Goldstein, and M. Lecar, 1969, Mon. Not. R. Astron. Soc. **146**, 161.
Da Costa, G. S., and K. C. Freeman, 1976, Astrophys. J. **206**, 128.
Demarque, P., J. G. Mengel, and M. L. Aizenman, 1971, Astrophys. J. **163**, 37.
Eggen, O. J., D. Lynden-Bell, and A. R. Sandage, 1962, Astrophys. J. **136**, 748.
Emden, R., 1907, *Gaskugeln* (Leipzig).

Fabian, A. C., J. E. Pringle, and M. J. Rees, 1975, Mon. Not. R. Astron. Soc. **172**, 15P.
Fall, S. M., and A. P. Lightman, 1977, unpublished.
Fall, S. M. and M. J. Rees, 1977, Mon. Not. R. Astron. Soc. **181**, 37P.
Faulkner, J., 1972, Nature **235**, 27.
Field, G., 1975, in *Galaxies and the Universe*, edited by A. Sandage, M. Sandage, and J. Kristian (University of Chicago, Chicago).
Flannery, B., 1977, private communication.
Frank, J., and M. J. Rees, 1976, Mon. Not. R. Astron. Soc. **176**, 633.
Giacconi, R., S. Murray, H. Gursky, E. M. Kellogg, E. Schreier, T. Matilsky, D. Koch, and H. Tananbaum, 1974, Astrophys. J. Suppl. Ser. No. 237, **27**, 37.
Gold, T., W. I. Axford, and E. C. Ray. 1965, in *Quasi-Stellar Sources and Gravitational Collapse*. edited by I. Robinson, A. Schild, and E. Schucking (University of Chicago, Chicago), p. 93.
Gott, J. R., III, 1973, Astrophys. J. **186**, 481.
Grindlay, J. E., 1977, *Highlights of Astronomy*, Vol. 4.
Grindlay, J. E., 1978, Astrophys. J., in press.
Grindlay, J. E., H. Gursky, H. Schnopper, D. Parsignault, J. Heise, A. Brinkman, and J. Schrijver, 1976, Astrophys. J. Lett. **205**, L127.
Haggerty, M. J., and G. Severne, 1976, Adv. Chem. Phys. **35**, 119.
Harris, H. G., and R. Canterna, 1977, Astron. J. **82**, 798.
Harris, W. E., and M. G. Smith, 1976, Astrophys. J. **207**, 1036.
Harris, W. E., 1976, Astron. J. **81**, 1095.
Hayli, A., 1975, Editor, *Dynamics of Stellar Systems* (I.A.U. Symposium No. 69), (Reidel, Dordrecht).
Heggie, D. C., 1975a, Mon. Not. R. Astron. Soc. **173**, 729.
Heggie, D. C., 1975b, in *Dynamics of Stellar Systems* (I.A.U. Symposium No. 69), edited by A. Hayli (Reidel, Dordrecht).
Hénon, M., 1961, Ann. Astrophys. **24**, 369.
Hénon, M., 1964, Ann. Astrophys. **27**, 83.
Hénon, M., 1967, Bull. Astron. Ser. 3, **2**, 91.
Hénon, M., 1971, Astrophys. Space Sci. **13**, 284; **14**, 151.
Hénon, M., 1973, in *Dynamical Structure and Evolution of Stellar Systems*, edited by L. Martinet and L. Mayor (Geneva: Observatory).
Hénon, M., 1975, in *Dynamics of Stellar Systems* (I.A.U. Symposium No. 69), edited by A. Hayli (Reidel, Dordrecht).
Hills, J. G., 1975a, Astron. J., **80**, 809.
Hills, J. G., 1975b, Astron. J., **80**, 1075.
Hills, J. G., 1975c, Nature **254**, 295.
Hills, J. G., and C. A. Day, 1976, Astrophys. Lett. **17**, 87.
Hills, J. G., and M. J. Klein, 1973, Astrophys. Lett. **13**, 65.
Hohl, F., and J. W. Campbell, 1968, Astron. J. **73**, 611.
Huang, K., 1963, *Statistical Mechanics* (Wiley, New York).
Iben, I., Jr., and R. T. Rood, 1970, Astrophys. J. **159**, 605.
Ipser, J. R., 1978, Astrophys. J., in press.
Jeans, J., 1902, Philos. Trans. Soc. Lond. **199A**, 49.
Johnson, H., 1976, Astrophys. J. **208**, 706.
Kadomtsev, B. B., and O. P. Pogutse, 1970, Phys. Rev. Lett. **225**, 1155.
Katz, J. I., 1975, Nature **253**, 698.
King, I. R., 1958, Astron. J. **63**, 114.
King, I. R., 1961, Astron. J. **66**, 68.
King, I. R., 1962, Astron. J. **67**, 471.
King, I. R., 1965, Astron. J. **70**, 376.
King, I. R., 1966, Astron. J. **70**, 376.
Knapp, G. R., W. K. Rose, and F. J. Kerr, 1973, Astrophys. J. **186**, 831.
Kustaanheimo, P., and E. J. Stiefel, 1965, J. Math. **218**, 204.
Larson, R. B., 1970a, Mon. Not. R. Astron. Soc. **147**, 323.
Larson, R. B., 1970b, Mon. Not. R. Astron. Soc. **150**, 93.
Lecar, M., 1976, unpublished.
Lecar, M., and L. Cohen, 1971, Astrophys. Space Sci. **13**, 397.
Lewin, W. H. G., 1977, Mon. Not. R. Astron. Soc., **179**, 43..
Lewin, W. H. G., and P. C. Joss, 1977, Nature, **270**, 211.
Lightman, A. P., 1977, Astrophys. J. **215**, 914.
Lightman, A. P., and S. M. Fall, 1978, Astrophys. J., **223**, in press.
Lightman, A. P., W. H. Press, and S. Odenwald, 1978, Astrophys. J., **219**, 629.
Lightman, A. P., and S. L. Shapiro, 1977, Astrophys. J. **211**, 244.
Lynden-Bell, D., 1967, Mon. Not. R. Astron. Soc. **136**, 101.
Lynden-Bell, D., 1975, in *Dynamics of Stellar Systems* (I.A.U. Symposium No. 69), edited by A. Hayli (Reidel, Dordrecht).
Lynden-Bell, D., and R. Wood, 1968, Mon. Not. R. Astron. Soc. **138**, 495.
Markert, T. H., D. E. Backman, C. R. Canizares, G. W. Clark, and A. M. Levine, 1975, Nature **257**, 32.
Michie, R. W., 1963, Mon. Not. R. Astron. Soc. **126**, 499.
Milgrom, M., and S. L. Shapiro, 1978, Astrophys. J., in press.
Miller, R. H., and E. N. Parker, 1964, Astrophys. J. **140**, 50.
Ogorodnikov, K. F., 1958, *Dynamics of Stellar Systems* (Pergamon, New York).
Oort, J. H., 1958, in *Proceedings of the Solvay Conference on the Structure and Evolution of the Universe* (Stoops, Brussels), p. 163.
Oort, J. H., 1965, in *Stars and Stellar Systems*, Vol. V, *Galactic Structure*, edited by A. Blaauw and M. Schmidt (University of Chicago, Chicago), p. 455.
Ostriker, J. P., R. McCray, R. Weaver, and A. Yahil, 1976, Astrophys. J. Lett. **208**, L61.
Ostriker, J. P., L. Spitzer, and R. A. Chevalier, 1972, Astrophys. J. Lett. **176**, L51.
Peebles, P. J. E., 1969, Astrophys. J. **155**, 393.
Peebles, P. J. E., 1970, Astron. J. **75**, 13.
Peebles, P. J. E., 1971, *Physical Cosmology* (Princeton University, Princeton, N. J.).
Peebles, P. J. E., 1972a, Gen. Rel. Grav. **3**, 63.
Peebles, P. J. E., 1972b, Astrophys. J. **178**, 371.
Peebles, P. J. E., and R. H. Dicke, 1968, Astrophys. J. **154**, 891.
Peterson, C. J., 1974, Astrophys. J. Lett. **190**, L17.
Peterson, C. J., 1976, Astron. J. **81**, 617.
Peterson, C. J., and I. R. King, 1975, Astron. J. **80**, 427.
Press, W. H., 1976, private communication.
Press, W. H., and A. P. Lightman, 1978, Astrophys. J. Lett., **219**, L73.
Press, W. H., and S. A. Teukolsky, 1977, Astrophys. J. **213**, 183.
Preston, G., 1959, Astrophys. J. **130**, 507.
Rosenbluth, M. N., W. MacDonald, and D. Judd, 1957, Phys. Rev. **107**, 1.
Saito, M., and M. Yoshizawa, 1976, Astrophys. Space Sci. **41**, 63.
Salpeter, E. E., 1955, Astrophys. J. **121**, 161.
Sandage, A., 1970, Astrophys. J. **162**, 841.
Sanders, R. H., 1970, Astrophys. J. **162**, 791.
Saslaw, W. C., 1969, Mon. Not. R. Astron. Soc. **143**, 437.
Saslaw, W. C., 1973, Publ. Astron. Soc. Pac. **85**, 5.
Seidl, F. G. P., and A. G. W. Cameron, 1972, Astrophys. Space Sci. **15**, 44.
Shapiro, S. L., 1977, Astrophys. J., **217**, 218.
Shapiro, S. L., and A. P. Lightman, 1976, Nature **262**, 743.
Shapiro, S. L., and A. B. Marchant, 1976, Astrophys. J. **210**, 757.
Shapiro, S. L. and A. B. Marchant, 1978, Astrophys. J., in press.
Shapley, H., 1918, Astrophys. J. **48**, 89.
Shapley, H., 1930, *Star Clusters* (McGraw-Hill, New York).
Silk, J., 1968, Astrophys. J. **151**, 459.
Silk, J., and J. Arons, 1975, Astrophys. J. Lett. **200**, L131.
Spitzer, L., 1940, Mon. Not. R. Astron. Soc. **100**, 396.
Spitzer, L., 1971, in *Nuclei of Galaxies*, edited by D. J. L.

O'Connell (North-Holland, Amsterdam).
Spitzer, L., 1962, *Physics of Fully Ionized Gases* (Wiley, New York).
Spitzer, L., 1969, Astrophys. J. Lett. **158**, L139.
Spitzer, L., 1975, in *Dynamics of Stellar Systems* (I.A.U. Symposium No. 69), edited by A. Hayli (Reidel, Dordrecht).
Spitzer, L., and R. A. Chevalier, 1973, Astrophys. J. **183**, 565.
Spitzer, L., and R. Harm, 1958, Astrophys. J. **127**, 544.
Spitzer, L., and M. H. Hart, 1971a, Astrophys. J. **164**, 399.
Spitzer, L., and M. H. Hart, 1971b, Astrophys. J. **166**, 483.
Spitzer, L., and W. C. Saslaw, 1966, Astrophys. J. **143**, 400.
Spitzer, L., and S. L. Shapiro, 1972, Astrophys. J. **173**, 529.
Spitzer, L., and J. M. Shull, 1975, Astrophys. J. **201**, 773.
Spitzer, L., and T. X. Thuan, 1972, Astrophys. J. **175**, 31.
Sunyaev, R. A., 1976, private communication.
Terzian, Y., and E. K. Conklin, 1977, Astron. J., **82**, 468.
Thanert, W., 1971, Astron. Nachr. **292**, 251.
Thuan, T. X., and J. R. Gott, III, 1975, Nature **257**, 774.
Tremaine, S. D., J. P. Ostriker, and L. Spitzer, 1975, Astrophys. J. **196**, 407.
Ulam, S. M., and W. E. Walden, 1964, Nature **201**, 1202.
van den Bergh, S., 1975, Astron. Astrophys. **44**, 231.
Vishniac, E., 1978, Astrophys. J., in press.
von Hoerner, S., 1958, Z. Astrophys. **44**, 17.
von Hoerner, S., 1960, Z. Astrophys. **50**, 184.
von Weizsacker, C. F., 1955, Z. Astrophys. **35**, 252.
Wallerstein, G., and H. L. Hefner, 1966, Astron. J. **71**, 350.
Weinberg, S., 1971, Astrophys. J. **168**, 175.
Weinberg, S., 1972, *Gravitation and Cosmology* (Wiley, New York).
Wielen, R., 1968, Bull. Astron. Ser. 3, **3**, 127.
Wielen, R., 1971, Astron. Astrophys. **13**, 309.
Wielen, R., 1975, in *Dynamics of Stellar Systems* (I.A.U. Symposium No. 69), edited by A. Hayli (Reidel, Dordrecht).
Zel'dovich, Ya. B., and I. D. Novikov, 1971, *Relativistic Astrophysics*, Vol. 1, (University of Chicago, Chicago).
Zwicky, F., 1957, *Morphological Astronomy* (Springer, Berlin), p. 142.

FIG. 1. The globular cluster Omega Centauri (NGC 5139), taken with the 1-m Yale reflector at Cerro Tololo Inter-American Observatory, La Serena, Chile. Date: May 20, 1974; 15-min exposure on blue sensitive emulsion. From Kitt Peak National Observatory.